Shearzone related talc mineralizations; evidences from a multi-analytical approach

Dissertation

Anke Wölfler

Montanuniversität Leoben
Department of Applied Geosciences and Geophysics
Chair of Geology and Economic Geology

Supervisors
Ao.Univ.-Prof. Dr.phil. Walter Prochaska
Ao.Univ.-Prof. Dr.phil. Harald Fritz

November 2014

Affidavit

I declare in lieu of oath, that I wrote this thesis and performed the associated research myself, using only the literature cited in this volume.

Anke Wölfler

Abstract

Shear zones are zones of enhanced fluid flow and may act as pathways for mineralizing fluids. The occurrence of talc may be related to such shear zones. To discerne the mechanism and characteristics of these shear zone related talc mineralization, several talc deposits related to major fault zones were chosen: the magnesite and talc deposits of the Eastern Greywacke Zone, in the Eastern Alps in Austria i.e. Veitsch, Wald am Schoberpass and Lassing, further the Gemerska Poloma talc deposit in Slovakia and the Sardinian talc deposits Sa Matta and Su Venosu.

In the investigated deposits talc mineralization occurrs within Mg-carbonate hostrocks. Geochemical analysis, stable isotopes and fluid inclusion study were performed to yield indications on kind, origin, temperature and timing of the talc minerlalizing fluid. In addition, (U-Th)/He measurements were applied at the Sa Matta talc deposit to yield information on the age of the talc formation. The study of the deposits of the Eastern Greywacke Zone shows how temperature and deformation features increase with growing proximity to the fault zones and that these features can be related here to the formation of talc. Investigations of the Gemerska Poloma talc deposit show the transfer of stress and fluids that were activated during fault slip affected the magnesite body and induced talc mineralization. The (U-Th)/He dating of the talc-chlorite event indicates that the hydrothermal event that led to the mineralization is at least 75 Ma. This is an important indicator that the talc mineralization took place before the activiation of the alpine Nuoro-fault.

This study has given insights on the role of fault zones as fluid pathways and the enrichment of talc resulting from deformation along fault zones.

Zusammenfassung

Scherzonen sind Zonen erhöhter Fluidtätigkeit und bilden als Bahnen fr das mineralisierende Fluid. Talk-Vorkommen können an solche Scherzonen gebunden sein. Um den Mechanismus und die Eigenschaften solcher Scherzonen gebundenen Talk-Mineralisation besser zu verstehen, wurden mehrere Talk-Lagerstätten entlang bedeutender Störungen ausgewhlt: Die Magnesite- und Talk-Lagerstätten der östlichen Grauwackenzone in den Ostalpen, Österreich, d.h. Veitsch, Wald am Schoberpass und Lassing, ferner die Talk-Lagerstätte Gemerska Poloma, Slowakei und die Talk-Lagerstätten Sa Matta und Su Venosu, Sardinien.

In den untersuchten Lagerstätten ist die Talk-Mineralisation an Mg-Karbonate gebunden. Geochemische Analysen, die Untersuchung von stabilen Isotope und Flüssigkeitseinschlüssen wurden durchgeführt, um Hinweise auf Art, Herkunft, Temperatur und Abfolge der Talk-Mineralisation zu erhalbten. Zusätzlich wurde mit Hilfe der (U-Th)/He-Methode der Versuch unternommen die Talkformation der Lagerstätte Sa Matta zu datieren. Die Studie der Lagerstätten der östlichen Grauwackenzone zeigt, die Abhängigkeit von Temperatur und Deformation mit Nähe zur Störung und deren Einfluss auf die Bildung von Talk. Untersuchungen anhand der Lagerstätte von Gemerska Poloma zeigt, wie Spannung und Fluide welche während des Störungsbewegung aktiviert wurden auf den Magnesitkörper übertragen wurden und dort zur Talk-Bildung führten. Die (U-Th)/He Datierungs-Methode des Talk-Chlorit bildenden Ereignisses mindestens 75 Ma ist. Dieses Ergebnis ist ein entscheidener Hinweis, dass die Talk-Mineralisation vor der Aktivierung der alpidisch geprägten Nuoro-Störung statt fand.

Die Studie hat wichtige Einblicke in the Rolle von Störungen as Fluid-Wege gewährt und zeigt wie Talk entlang von Störungen angereichert wird.

Acknowledgments

I am grateful for the opportunity to write this thesis. First I want to thank my supervisor Walter Prochaska for his support and the framework he provided so I could do my research and work on this project. Thank you for your discussions, time during field trips and help with the laboratory work. I also want to thank my co-supervisor Harald Fritz for his support during the field work and the fruitful discussions we had.
I also extend my thank you to my colleagues, past and present at the chair of geology and economic geology: Fritz Ebner, Sabine Feuchter (thank you for countless thin-sections), Klaus Lassnig, Heinrich Mali, Brigitte Mang, Frank Melcher, Gerd Rantitsch and Thomas Unterweissacher.
For their assistance with the analytical work I thank R. Gratzer, Ronald Bakker, Sylvain Richoz (Univ. Graz), Benita Putlitz (Univ. Lausanne) and Eva Enkelmann (Univ. Tübingen).
My closest friends that supported me during the work at this thesis deserve their acknowledement well: Anett Weisheit (how many moves did you manage for us?), Marlen and Roman Sander (you helped me survive the six month I stayed all by myself in Graz), Helga Klinger, Christine Latal and Christian Steidler, Borgny Ollendorff, Karin and Bernd Scheuch, Inge Kober, Hanni und Engelbert Morschhauser, Judith Heidler, Lisa Mitte. You helped in many ways that this project was sucessful! And not to forget the people who made us feel welcome at our new destination in Hannover.
Last but not least I express my deep gratitude for my family for always being there for me and for their trust that I could finish my dissertation. Giving birth to two children during that time sure didn't make it easy. But with the help of my best friend and husband, Andreas, I knew I could make it. Thank you for diving with me through this adventurous journey.

Contents

Chapter 1

Introduction

Talc is a mineral that is of great commerical value. However its petrogenesis, occurrence and timing of formation are still a matter of discussion. Talc occurs most abundantly in metamorphosed ultramafic rocks and the environments of talc formation have been described in detail by *Evans & Guggenheim* (1991) and references therein. Further Mg-carbonates such as siliceous dolomitic limestone and magnesite serve as hostrocks. In such rock suits talc may form under prograde as well as retrograde metamorphic conditions. These carbonate hostrocks may be subject to hydrothermal alteration (*Moine et al.* (1989)) with Si-rich fluids reacting with the Mg-carbonates:

$$3\mathrm{CaMg}\left(\mathrm{CO_3}\right)_2 + 4\mathrm{SiO_2} + \mathrm{H_2O} \longrightarrow \mathrm{Mg_3Si_4O_{10}}\left(\mathrm{OH}\right)_2 + 3\mathrm{CaCO_3} + 3\mathrm{CO_2} \quad (1.1)$$

in the case of dolomitic hostrock and:

$$3\mathrm{MgCO_3} + 4\mathrm{SiO_2} + 2\mathrm{H_2O} \longrightarrow \mathrm{Mg_3Si_4O_{10}}\left(\mathrm{OH}\right)_2 + 3\mathrm{CO_2} \quad (1.2)$$

in the case of magnesite hostrock. In addition, zones of intense deformation, where fluid flow is elevated, are prone to the formation of talc (e.g. *Moore & Rymer* (2007), *Collettini et al.* (2009)) . Examples for such talc deposits are Trimouns

in the french Pyrenees (*Moine et al.* (1989) and *Boulvais et al.* (2006)), Puebla de Lillo in the Cantabrian zone of Northern Spain (*Tornos & Spiro* (2000)), Rabenwald and Lassing in the Eastern Alps *Prochaska* (1989), *Prochaska* (2000), *Neubauer* (2001) and Göpfersgrün in the Fichtelgebirge (*Hecht et al.* (1999)) to name some. To a smaller extend talc forms in hydrothermal and surface environments and in high pressure rocks (*Spandler et al.* (2008)).

1.1 Aims of research

In this study the focus of research is on fault zone related talc mineralizations with Mg-carbonate hostrocks. Talc forms dissolving Mg from its hostrocks and forms with SiO_2-rich fluids that percolate the hostrocks. In the case of magnesite and dolomite hostrocks the origin of Mg seems to be obvious. However the source of the SiO_2-rich fluids is more a matter of discussion. It is also an issue to deciper the conditions under which talc is formed and to understand the role during fault deformation. Faults may act as pathways for fluids and concentrate stress that may be accomodated by a weak mineral phase such as talc. The timing of a hydrothermal event that triggered the formation of talc may be determined by temperature sensitive dating techniques.
For this purpose suitable methods are applied in order to yield results on the origin and characteristics of the ore forming fluid as well as the mechanism and timing of the mineralization and the role of the related fault zone.

1.2 Investigated deposits

The Lassing talc deposit in the eastern Greywacke Zone, the Gemerksa Poloma talc deposit and the talc deposits of Sa Matta and Su Venosu are all deposits were talc was produced in the past (Lassing), is currently produced (Sa Matta and Su Venosu) or is still under prospection for talc production (Gemerska Poloma). The deposits investigated in this study were chosen due to their linkage to their mutuality of the geological and tectonic setting. They are all bound to fault zones and have carbonate hostrocks. The magnesite deposits Veitsch and Wald

am Schoberpass were added to the study to investigate the changing conditions between the deposits within the same geological nappe system (i.e. the Eastern Greywacke Zone). A brief summary of the investigated deposits is given in table 1.1.

deposit	hostrock	talc content	shearzone
Eastern Greywacke Zone			
Veitsch	magnesite	no	Mur-Mürz-Fault
Wald am Schoberpass	magnesite	minor	PLF
Lassing	dolomite	talc deposit	SEMP, PLF
Gemericum			
Gemerska Poloma	magnesite	talc deposit	shearzone in footwall position of the steatitized magnesite body
Corsica-Sardinia Batolith			
Sa Matta	dolomite	talc deposit	Nuoro Fault
Su Venosu	dolomite	talc deposit	Nuoro Fault

Table 1.1: *Summary of the investigated deposits. PLF = Paltental-Liesingtal-Fault SEMP = Salzach-Ennstal-Mariazell-Puchberg-Fault*

The chosen deposits have been subject to previous research and detailed studies have been carried out on the deposits of the Eastern Greywacke Zone (*Prochaska* (1989), *Prochaska* (1997), *Prochaska* (2000), *Neubauer* (2001), *Polgári et al.* (2010) and references therein), Gemerska Poloma (*Malachovský et al.* (1992), *Kilík* (1997), *Turanová et al.* (1997), *Radvanec et al.* (2004), *Petrasová et al.* (2007), *Hurai et al.* (2011) and references therein) and the Sardinian deposits (*Fiori & Grillo* (2002), *Grillo & Prochaska* (2007) and references therein).

1.3 Methodology

1.3.1 Geochemical Analysis

In geochemical analysis the distribution pattern of rare earth elements (REE) are of great importance for the interpretation of rock forming minerals. The term

REE refers to a group of elements also called lanthanides, i.e. the elements from Lanthan to Lutetium. These are characterized by equal ionic charge (3^+) and similar ionic radii. The small differences in ionic radii that do exist account for fractional processes that make the REE so suitable for interpretation of geological processes. They are further subcatagorized into light REE (elements La to Sm) and heavy REE (elements Gd to Lu). Their distribution is presented in so called spider diagrams. As the absolute amount of REE may vary greatly a reference system is used. They are normalized to the composition of chondrites (C1 chondrite, values tabled according to *Anders & Grevesse* (1989) steht in White Geochemistry) according to the equation:

$$\mathrm{REE}_x = \frac{\mathrm{REE}_x^{sample}}{\mathrm{REE}_x^{chondrite}} \tag{1.3}$$

where REE_x refers to the respective REE element.

The elements Eu^{3+}, Yb^{3+} and Ce^{3+} may change their oxidation state and be reduced in the case of Eu and Yb to Eu^{2+} and Yb^{2+} or oxidized in the case of Ce to Ce^{4+}. Eu and Ce form then anomalies that are used for interpretational purposes as they give hints on redox environments and rock forming conditions. The redox equilibrium is a function of pressure, temperature and chemical composition of the fluid including pH. According to *Bau* (1991) the Eu^{3+}/Eu^{2+} redox potential increases strongly with inceasing temperature. A negative Eu anomaly is a strong indicator for high temperature (+200°C, *Bau & Möller* (1992)).

The study of *Möller* (1989) on magnesite states that the amounts and fractionation of REE are an indicator of the composition of the fluid from which the mineral derives and the chemical composition of the magnesite precursor rock. Purely marine magnesites tend to have very low REE concentration but become increased if magnesitization is induced by hydrothermal fluids during diagnesis (*Franz et al.* (1979))

1.3.2 Stable Isotopes

Theoretical considerations

The principles of Stable Isotope geochemistry are well constraint. A summary of the method described in this chapter are according to *Hoefs* (2009) and *Faure & Mensing* (2005):

Isotopes are defined as atoms that contain the same number of protons but different numbers of neutrons. This results in differing atomic masses and thus differences in chemical and physical properties.
The strength of a covalent bond of a molecule is the result of energy reduction while two atoms decrease their distance by forming a molecule. The energy of a molecule is restricted to discrete energy levels with the minimum level being

$$\frac{1}{2}h\nu \tag{1.4}$$

where h is the Planck's constant ($6.626176 * 10^{-34}$ J/Hz) and ν is the vibrational frequency. As a result molecules always have a vibrational energy. Even at absolute 0 K molecules vibrate with their fundamental energy. The vibrational energy depends on the mass of the molecules. Thus molecules with different isotopes posess different masses and as a result different vibrational energy. As heavy isotopes have a lower vibrational frequency they also have a lower vibrational energy resulting in a stronger covalent bond. Thus such molecules are of greater stabibility than molecules with lighter isotopes.

The dissociation of molecules (e.g. phase A and B) due to their masses can be described with the fractionation factor α.

$$\alpha = \frac{R_{\mathrm{A}}}{R_{\mathrm{B}}} \tag{1.5}$$

where R is the ratio of the heavier and the lighter isotope of phase A and B (e.g. $^{18}O/^{16}O$). But as it is difficult to determine the absolute frequencies of isotopes the relation of the individual isotope compared to an international standard is used and denoted as δ-value. For phases A and B the δ-value are

$$\delta_{\mathrm{A}} = \left(\frac{R_{\mathrm{A}} - R_{\mathrm{St}}}{R_{\mathrm{St}}} \right) * 10^3 \tag{1.6}$$

$$\delta_{\mathrm{B}} = \left(\frac{R_{\mathrm{B}} - R_{\mathrm{St}}}{R_{\mathrm{St}}} \right) * 10^3 \tag{1.7}$$

where R_{A} and R_{B} are the respective isotope ratios measured in the laboratory for phases A and B and R_{St} is the defined isotope ratio of a standard sample. The δ-value is always denoted in ‰. In the case of oxygen isotopes measured in phase A the δ-value would be

$$\delta^{18}\mathrm{O} = \frac{\left(\frac{^{18}\mathrm{O}}{^{16}\mathrm{O}}\right)_{\mathrm{A}} - \left(\frac{^{18}\mathrm{O}}{^{16}\mathrm{O}}\right)_{\mathrm{St}}}{\left(\frac{^{18}\mathrm{O}}{^{16}\mathrm{O}}\right)_{\mathrm{St}}} * 10^3 \tag{1.8}$$

For oxygen isotopes the Vienna standard mean ocean water (VSMOW) is used as a reference standard. For carbon isotopes the Vienna PeeDee Belemnite (VPDB) is used. The δ-value can be positive, negative and 0 which indicates that the measured $^{18}\mathrm{O}/^{16}\mathrm{O}$ is enriched, depleted or equal relative to the seawater standard. It is always the heavier isotope that is compared to the standard.

The δ-value and α are related by

$$\delta_A - \delta_B = \Delta_{AB} \approx 10^3 \ln \alpha_{AB} \tag{1.9}$$

Fluid reconstruction

Through Stable Isotope measurements it is possible to yield reasonable predictions on the origin of the mineralization and the mineralizing fluid.

With increasing temperature light oxygen isotopes dominate over heavier isotopes. In conclusion $\delta^{18}\mathrm{O}$ decreases with increasing temperature. However $\delta^{18}\mathrm{O}$-values should not be stricktly considered as temperature values because diffusion and the amount of fluid that filtrates the rockbody affects fractionation.

Figure 1.1 shows certain carbonate species and their typical composition of $\delta^{18}\mathrm{O}$

and δ^{13}C. Sparry magnesite of the Veitsch type generally occupies the same compositional field as marine carbonates as far as δ^{13}C-values but tends towards much lighter δ^{18}O-values (*Kralik et al.* (1989)). This is especially true for magnesite affected by diagenetic or metamorphic processes (*Schroll* (2002)) The reason can be found in either the equilibration of the magnesite rock with metamorphic water (*Kralik et al.* (1989)) or in the rising of hot basinal brines of connate origin (*Aharon* (1988)). In fact four factors controll the isotope composition of metamorphic rocks: the temperature of exchance, the composition of the precursor rock, the effects of volatilization with increasing temperature and the exchange with infiltrating fluids or melts. The latter can be assumed if the change of stable isotope composition is greater than 5–10 ‰(*Baumgartner & Valley* (2001)) and coupled C-O depletion seems evident. Fluids can either percolate the rock independently of structural and lithological control or be channelized in individual beds or units without homogenizing the complete rock. Especially marbles may act as fluid barriers and are impermeable during metamorphism (*Nabelek et al.* (1984)). The fluids are then channelized through silicate layers and the carbonate rock does not homogenize and keeps its original sedimentary signature (*Valley et al.* (1990)). In shearzones fluid flow is concentrated in narrow zones.

1.3.3 Ion-chromatography

Theoretical considerations

The crush leach method has been described in detail by *Bottrell et al.* (1988). *Prochaska* (1997) added some minor modifications and *Gleeson* (2003) gave an additional detailed summary of calculations applied to the method.

The crush leach method is a bulk analysis of electrolytes in fluid inclusions to determine the major cation (e.g. Li, Na^+, K^+, Mg^{2+}, Ca^{2+}) and anion (F^-, Cl^-, Br^-, I^-, SO_4^{2-}) composition. It may indicate the origin and the evolution of the fluid. The charge balance is calculated to assess the quality of the data. The following equation is applied according to *Shepherd* (1985):

$$\frac{Q^+}{Q^-} = \frac{\Sigma Charge * (Concentration/AtomicMass)_{cation}}{\Sigma Charge * (Concentration/AtomicMass)_{antion}} \tag{1.10}$$

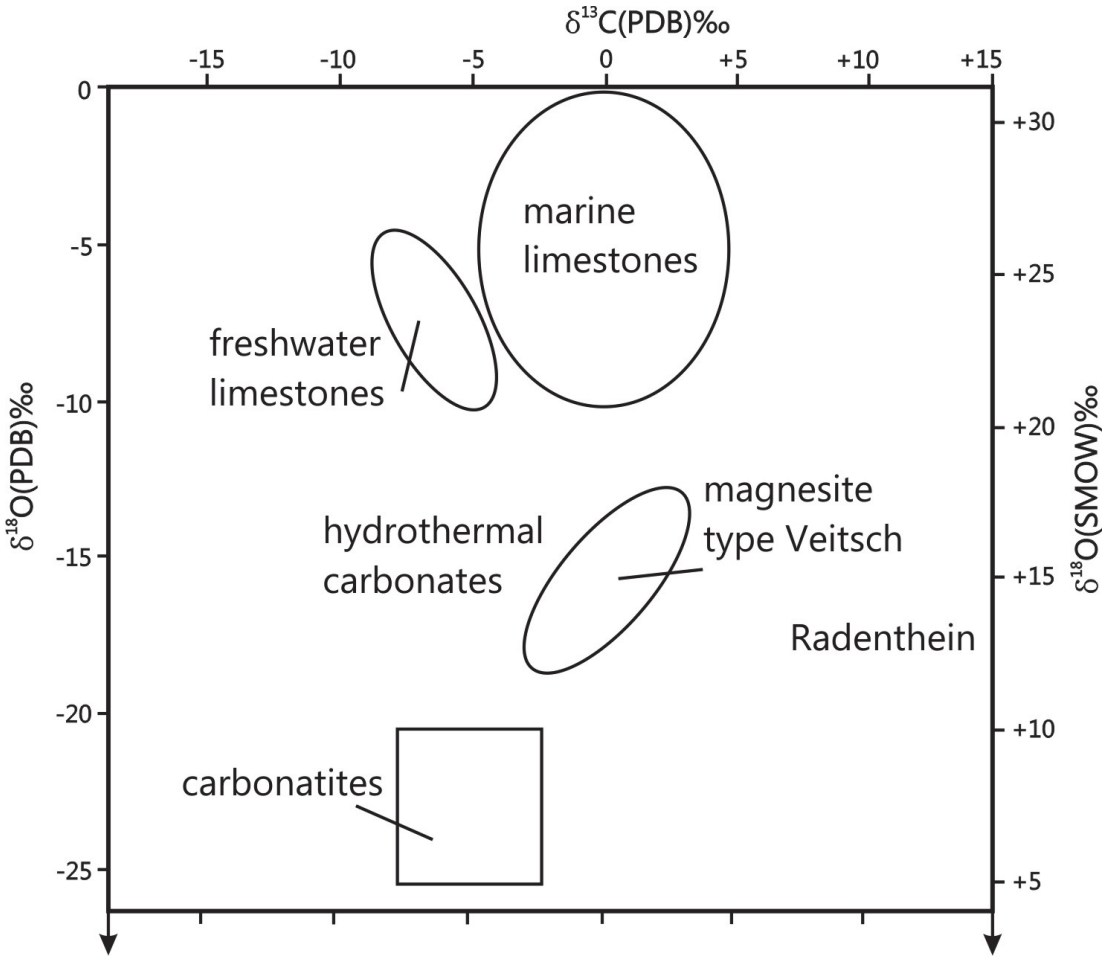

Figure 1.1: *Diagram of $\delta^{18}O$ vs $\delta^{13}C$ of certain carbonate species and the typical isotope composition of Veitsch type sparry magnesite. Modified after* Schroll *(1997)*

Deviations from perfect charge balance ($Q^+/Q^- = 1$) can be due to contaminations or lost of volatile phases (e.g. CO_2) during crushing (*Hafellner* (1995)). Also concentrations of H^+, CO_3^{2-} and OH^- may cause imperfect charge balance.

Of special interest in the crush leach analysis are chloride and bromide. Both have very similar ion radii (Cl=1,81Å, Br=1,96Å) but have a very distinct fractionation behavior during evaporation. With beginning evaporation Cl and Br concentration are equal but Cl starts to precipitate and form halite (NaCl) with an evaporation index >10. As Br is not (or rather at a very slow rate) incorporated into the crystal lattice, it is enriched in the residual solution. With ongoing evaporation Na and Cl are continously depleted from the solution and Br is enriched. At an evaporation index of 70 Mg-salts and later K-salts start to precipitate (*McCaffrey et al.* (1987)). To reconstruct the origin of salinity of palaeofluids Na-Br-Cl diagrams are used. Fluids that yield their salinity during evaporation have Na/Br and Cl/Br contents along the "seawater evaporation line"(fig. 1.2). In contrary fluids that yield their salinity by the dissolution of salt during crustal migration are along the "halite dissolution line". Non-fractionated seawater has a Cl/Br ratio of 658 (*Gleeson* (2003)). With the very high evaporation index during Mg-salt and K-salt precipitation the Cl/Br ratio drops to ∼100 and even 90, respectively.

Temperature approximation

In order to estimate the temperature of the palaeofluid geothermometers can be applied. They are based on temperature-dependent fluid-rock reactions that will controll the chemical composition of the fluid. The crush leach method is a bulk method that irregards the distinct possible compositions of primary, secondary and pseudo-secondary fluid inclusions. Temperatures can be estimated from the chemical composition of the fluid inclusions. The Na/K method of *Can* (2002) is applied in this study:

$$t = \frac{1052}{1 + \exp\left(1.714\log\left(\frac{Na}{K}\right) + 0.252\right)} + 76\,(^\circ\mathrm{C}) \tag{1.11}$$

The formula is empirical and based on the observation that low Na/K ratios were indicative of high temperatures at depth. Further details are given in *Can* (2002).

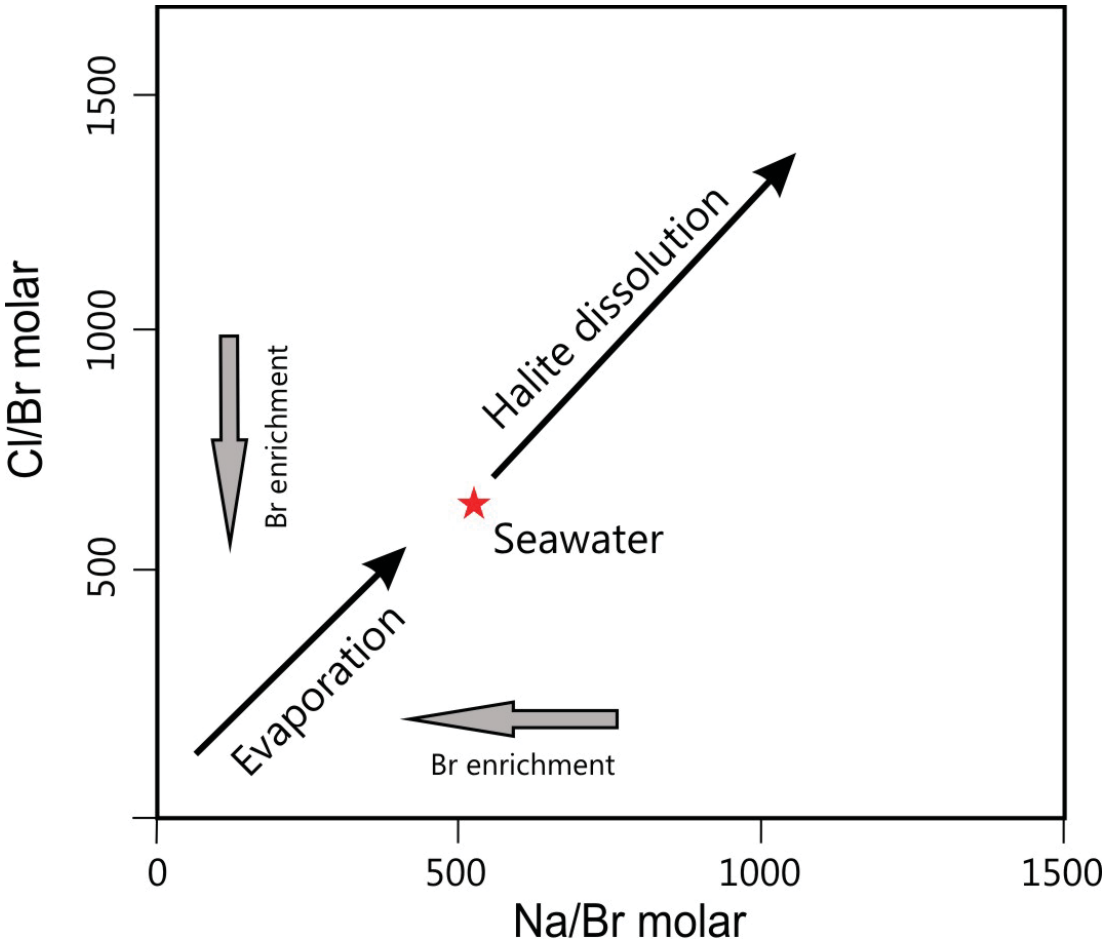

Figure 1.2: *Na/Br-Cl/Br diagram displaying seawater evaporation trend and halite dissolution trend.*

1.3.4 (U-Th)/He dating

Theoretical considerations

The (U-Th)/He method is used to date processes in the uppermost part of the crust. It is based on the decay of ^{235}U, ^{238}U, ^{232}Th and ^{147}Sm by α emission (^{4}He nucleus). The He apparent age can be calculated by measuring U, Th, Sm and He and applying the following formula:

$$^4\mathrm{He} = 8^{238}\mathrm{U}\left(\exp\left(\lambda_{^{238}U}t\right)-1\right)+7\left(^{238}U/137.88\right)\left(\exp\left(\lambda_{^{235}U}t\right)-1\right)+6^{232}Th\left(\exp\left(\lambda_{^{232}Th}t\right)-1\right) \quad (1.12)$$

where ^{4}He, U and Th are the present-day amounts, t is the accumulation time or He age and λ is the decay constant. The constants preceeding U and Th account for the multiple α particles emitted within each decay serie and the factor (1/137.88) is the present day (^{235}U/^{238}U) ratio. It is assumed that the initial ^{4}He present in the crystal is zero and that air-derived He is unlikely to be present. The last assumption is based on that fact that the concentration of ^{4}He in the atmosphere is very low (5 ppm). However excess Helium in fluid or mineral inclusions need to be taken into consideration. Therefore visual screening for inclusions is important to eliminate possible excess helium.

The characteristic engergy and characteristic stopping distance for each α decay within the U and Th series are well known (*Ziegler* (1977)). Therefore an α particle will come to stop on the surface of a sphere centered on the site of its parent nucleus and with a radium equivalent to the stopping distance. *Farley et al.* (1996) proposed a quantative model for correcting He ages. The model is based on the measured geometry and size of crytstals to be dated. Three assumptions are made (i) U and Th are homogenously distributed within the crystal, (ii) implantation of α particles from outside the crystal are insignificant and (iii) the dated crystals are a hexagonal prism or have a spherical geometry. The two variables that control the total fraction of α particles in a surface are (a) the surface to volume ratio ($\beta = (2.31\mathrm{L} + 2\mathrm{R})/\mathrm{RL}$, where R is the radius and L is the lenght of a prism and (b) the α stopping distance. The total amount of

α particles retained in the crystal is then described by the F_t correction factor (*Farley et al.* (1996)):

$$F_t = 1 + a_1\beta + a_2\beta \tag{1.13}$$

where a_1 and a_2 are fit parameter incorporating the stopping distance and density of the stopping medium. For a hexagonal prism this is according to *Farley* (2002): $a_1 = -5.13$ and $a_2 = 6.78$ for the ^{238}U series and $a_1 = -5.9$ and $a_2 = 8.99$ for the ^{235}U and ^{232}Th series. Given that stopping distances of parent nuclides are slightly different, the mean F_t factor is:

$$^{mean}F_t = a_{238}F_t + (1 - a_{238})^{Th232}F_t \tag{1.14}$$

where F_t are the respective correction factors for each corresponding parent nuclide, a_{238} is the fraction derived from ^{238}U that can be approximated from the measured Th/U ratio for an integration period of $<\sim$200 Ma as:

$$a_{238} = (1.04 + 0.245\,(Th/U))^{-1} \tag{1.15}$$

Finally the α corrected He age is then calculated as

$$\text{Corrected age} = \frac{\text{Measured age}}{\text{mean}\,F_t} \tag{1.16}$$

Applications of the (U-Th)/He method

Because of its very low closing temperature of about 100°C (*Wolf et al.* (1996)) the (U-Th)/He method is an important method to yield information about processes in the uppermost crust. Between ~85°C and ~40°C He in apatite crystals is neither completely lost nor completely retained within the mineral crystal (*Farley* (2002)). For zircon crystals the temperature range is between ~200°C and ~180°C (*Reiners et al.* (2003)). This zone is denoted as the partial retention zone (APRZ and ZPRZ for apatites and zircons respectively) and definded as the temperature range where 5 to 95% of the He is retained in the crystal (*Wolf et al.*

(1998)). Therefore at depths corresponding to temperatures below 40°C He in apatite crystals is retained and He ages track time. At temperature above 80°C He is lost and He ages remain zero. The same applies to He in zircons in respect to the temperature of the ZPRZ.

During the last years low-temperature thermochronology (including (U-Th)/He and Fission Track) has been applied to date the deformation of fault zones (e.g. *D'Alessio et al.* (2003), *Yamada et al.* (2007), *Siebel et al.* (2010), *Wölfler et al.* (2010), *Kurz et al.* (2011), *Emmel et al.* (2012), *Tagami* (2012)) and to determine the timing of fluid flow within fault zones (e.g. *Yamada et al.* (2007), *Wölfler et al.* (2010), *Emmel et al.* (2012)). Heating effects during hydrothermal fluid flow are expected to be detected by the low temperature ranges of the APRZ and ZPRZ.

Chapter 2

Analytical Procedures

2.1 Geochemical analysis

Whole rock geochemical analysis of major, minor and trace elements were performed at Act Labs, Canada. Prior to analyzing, samples were prepared at the University of Leoben by crushing and grinding. Analytical procedures of the treatment are described by Act Labs as follows: Samples are analyzed in a batch system, wherein each batch contains a method reagent blank, certified reference material and 17% replicates. Samples are then mixed with a flux of lithium metaborate and lithium tetraborate and fused in an induction furnace. The molten melt is immediately poured into a solution of 5% nitric acid containing an internal standard and mixed continuously until completely dissloved. The samples are run for major oxides and selceted trace elements (including REE) on a combination simultaneous/sequential Thermo Jarrel-Ash ENVIRO II ICP or a Varian Vista 735 ICP. Calibration is performed using 7 prepared USGS and CANMET certified reference materials. One of the 7 standards is used during the analysis for every group of ten samples. Totals must be between 98,5% and 101%.

2.2 Stable Isotopes

δ^{18}O and δ^{13}C of carbonates

Analysis of carbon and oxygen isotope ratios of carbonates were performed at the Stable Isotope lab at the University of Leoben. Samples were prepared by using a dentist drill. 0.2 – 0.3 mg of rockpowder was drilled and transferred into autosampler vials (Labco Exetainer vials) and sealed with butyl-rubber septa. The analyses were performed on a Thermo Fisher Delta V mass sprectrometer employing a Finnigan Gas Bench II according to *Spötl & Vennemann* (2003). The samples were dissolved with anhydrous H_3PO_4 (density $1.91\frac{g}{cm^3}$) in a pressurised helium atmosphere at 70°C for 8 hours. Multiple measurements of in-house calcite reference material were used and precision of δ^{18}O and δ^{13}C measurement were yielded with $\pm 0.07\,‰$ and $\pm\ 0.05\,‰$ (1s, n=180), respectively. Oxygen isotope data are reported relative to Vienna Mean Ocean Water (VSMOW) and carbon isotopes realtive to Vienna PeeDee Belemnite (VPDB).

δ^{18}O of quartz

Analysis of oxygen isotope ratios of quartz were performed at the Stable isotope lab at the University of Lausanne. Quartz samples were prepared by crushing and handpicking to yield grains free of impurities. Each aliquot (1-2 mg) was washed with distilled water and dilute HCl (10%) to remove calcite residuals. Oxygen was then extracted using a CO_2 laser-line and fluorine reagent (method according to *Kasemann et al.* (2001)). Isotopic compositionn of extracted oxygen was measured using a ThermoFinnigan MAT 253 mass spectrometer. Results were normalized against an in-house quartz standard (LS-1, 20-50 mesh, δ^{18}O=18.1 ‰ calibrated against NBS-28 of δ^{18}O=9.64 ‰). The standard reproduced to within an error of $\pm 0.1\,‰$. Oxygen isotope data are reported relative to Vienna Mean Ocean Water (VSMOW).

2.3 Ion-chromatography

Crush leach analysis on fluid inclusions in quartz and carbonates was performed using ion-chromatography. The samples were crushed, thoroughly washed and

handpicked. In addition quartz samples were treated with HNO_3 in a sand bath to remove possible contaminations. Sample size was 1.00 g given the dependency of the ion concentration from the number of fluid inclusion in one sample. The leaching process was performed with minor modifications according to *Bottrell et al.* (1988) and *Prochaska* (1997): Samples were ground with 5 ml double distilled water in an agate mortar, filtered and transfered into suitable vials. Halogens and anions (F^-, Br^-, Cl^-, I^-, SO_4^{2-}) were measured using a DIONEX DX- 500 system at Leoben University. Cations (Li^+, Na^+, K^+, Mg^{2+}, Ca^{2+}) were analysed in the aliquots of the same solution.

2.4 (U-Th)/He

Clear and complete apatite and zircon grains without cracks were selected using a binocular microscope. The grain dimensions were measured for the calculation of the alpha-correction factor after *Farley et al.* (1996). Afterwards the single grains were packed in Nb-tubes for U-Th/He analysis. 2-3 aliquots per sample were analyzed in the Patterson helium-extraction line at the University of Tübingen, which is equipped with a 960nm diode laser to extract the helium gas. Zircon grains were heated for 10 minutes at 20 Amps. Each grain was heated again and analyzed to make sure that the grain was degassed entirely in the first step. The re-extracts generally showed <1% of the first signal. After Helium analysis the grain packages were sent to the University of Arizona at Tucson for U, Th, and Sm measurements using an ICP-MS.

The analytical error of the mass spectrometer measurements are generally very low and do not exceed 2%. In contrast, the reproducibility of the sample age constitutes a much larger error. Therefore the mean U-Th/He age and the standard deviation of the measured aliquots are reported as the sample error. For single grain ages a 5% 2 sigma error is applied based on the reproducibility of standard measurements in the lab.

Chapter 3

Deposits

3.1 Eastern Greywacke Zone

The contents of this chapter were submitted for publication to Austrian Journal of Earth Science.

In the eastern Greywacke Zone talc occurs within Mg-carbonate rocks of the Veitsch nappe, such as dolomites and magnesites. The Lassing talc deposit has been one of the largest talc deposits in Austria until its closure in 1998 due to a cave accident. The deposits Wald am Schoberpass and Veitsch are primarily magnesite deposits partly with talc impurities as it is the case for Wald am Schoberpass. The three deposits were chosen because of their common geological position and similar hostrock composition. It is the aim of the study to develop a model for the conditions, the mechanism and timing of talc formation. Additionally the relationship of talc mineralization with the regional tectonic regime will be discussed. For this purpose geochemical analysis of major, minor and trace elements, stable isotopes on carbonates and quartz as well as fluid inclusion measurements were performed.

3.1.1 Geology

3.1.1.1 Tectonic evolution of the Eastern Alps

Geographically the Alps can be subdivided into Western-, Central- and Eastern Alps and are composed of four major geological units: the southalpine, austroalpine, penninic and helvetic unit. The austroalpine (AA) consists of a precarboniferous basement – in fact protolith ages date back until the Proterozoic (*Schulz et al.* (2004)) or even the Archean (*Neubauer et al.* (2002)) – and a Permomesozoic cover (such as the Northern Calcareous Alps (NCA), fig. 3.1). Today's prealpine units were accreted to Laurussia during several episodes between the late Precambrian (Cadomian) to the Variscan orogeny (*Stampfli et al.* (2002)). After the attachment of Avalonia (originally located at the northern rim of Gondwana) to form Laurussia in Ordovician, the Hun superterrane rifted off the Gondwana margin and travelled northwards during Silurian. The attachment to previously consolidated Laurussia evolved in distinct phases and led to the closure of oceanic domains during Variscan orogeny between Devonian and Carboniferous times. Final collision was completed in Visean.

Following the Carboniferous episode of mountain building Permian extension and subsidence signaled the breakup of the Pangea. A Triassic carbonate platform with proximal and distal facies elements (Hauptdolomit-, Dachstein- and Hallstatt-facies) evolved and documents position of the Austroalpine close to the Tethys shelf, i.e. shelf of the Meliata-Hallstatt ocean. The opening of the Central Atlantic during Jurassic induced the opening of the Southpenninic ocean (*Laubscher* (1987)) and the closure of the Meliata-Hallstadt ocean (which initialed nappe stacking of the former passive continental margin). At ca. 90 Ma the main metamorphic imprint within the Eastern Alps occured. With the ongoing opening of the Atlantic ocean the Northpenninic ocean opended and seperated the Briançonnais from the European continent. The continents in the south (adriatic indenter) experienced anticlockwise rotation (due to the opening of the south atlantic) and initialized nappe stacking within the Lower Austroalpine and Penninc units. Thrusting was followed by subsidence due to subduction tectonic erosion (*Faupl* (1991), *Wagreich* (1993)) and the formation of strike-slip basin that were filled with accretionary wedge sediments – the Gosau basins (*Wagreich* (1995)).

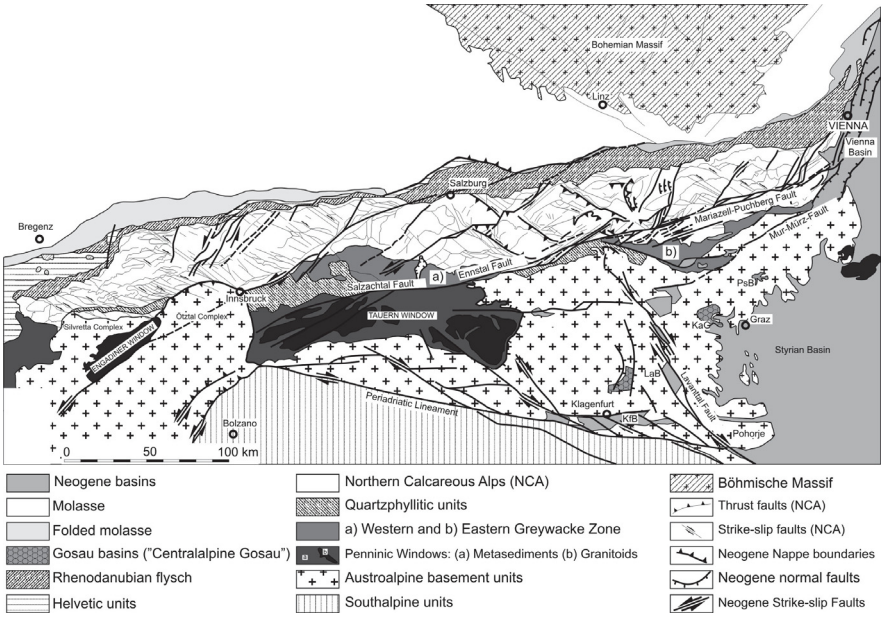

Figure 3.1: *Geological Sketch of the Eastern Alps. Modified after* Linzer et al. *(2002)*

Closure of all Penninic oceanic domains induced the final episode of the alpine orogeny (*Frisch* (1976)). The continuous north drift of the adriatic indenter and simultaneous retreat of the Carpathian subduction zone enabled the exhumation of the Tauern Window. Both processes coupled with the slab breakoff of the northpenninic ocean (*Blanckenburg & Davies* (1995)) led to the uplift of the ductile penninic units and causes the brittle overlying Austro Alpine to break along reactivated and newly formed faults (*Frisch et al.* (2000)). Normal faults east (Katschberg normal fault) and west (Brenner normal fault) of the Tauern Window (*Genser & Neubauer* (1989) and *Selverstone* (1988)) as well as numerous other arguments (*Frisch et al.* (1998), *Spiegel et al.* (2000), *Kuhlemann et al.* (2001), *Spiegel et al.* (2004)) confirm the tectonic nature of the exhumation of the Tauern Window. Lateral faults north (Salzach-Ennstal-Mariazell-Puchberg-Fault (SEMP)) and south (Defereggen-Antholz-Vals-Fault (DAV)) of the Tauern Window and their continuation (Mur-Mürz-Fault (MMF) and Paltental-Liesingtal-Fault (PLF)) flank the Tauern Window and are related to its formation.

3.1.1.2 Geology of the Eastern Greywacke Zone

According to their former position with respect to the Meliata-Hallstatt ocean (Tethys ocean) *Tollmann* (1977) subdivided the Austroalpine Nappe stack into Lower and Upper Austroalpine Nappe Complex. By contrast *Schuster & Frank* (1999) and *Schmid et al.* (2004) divide the Austroalpine nappe stack according to their position with respect to the 90 Ma old high pressure wedge represented by the Koralpe Wölz nappe sytsem. In both interpretations the Greywacke Zone (Noric nappe) and overlying Tirolic Juvaic nappe system of the NCA occupy a high tectonic position (Upper Austroalpine nappes). The basement of the Upper Austroalpine is formed generally by low grade Palaeozoic metasedimenary units (*Handler et al.* (1997)). These low grade Palaeozoic metasedimentary units are the Graz Nappe complex, the Gurktal Nappe complex and the Greywacke Zone. They are the oldest sedimentary units of the Upper Austroalpine units in the Eastern Alps with Ordovician to Carboniferous depositional ages.

The Greywacke Zone is generally divided into a western and an eastern part. The latter reaches from the eastern end of the Tauern Window to the Vienna basin (fig. 3.2). The rock series comprises Paleozoic carbonates, metapelites and acid volcanics and are of Ordovician ages. Parts of the Greywacke Zone, namely the Noric Nappe System has been interpreted as sedimentary sequence deposited on the northern margin of Gondwana.

The eastern Greywackezone comprises four nappe sheets from footwall to hangingwall: Veitsch nappe, Silbersberg nappe, Kaintaleck nappe and Noric nappe (*Neubauer et al.* (1993), fig. 3.3). Each nappe unit exhibits very distinct tectonothermal ages. These ages were constraint using the detrital white mica method that reveals the age of the source rock. The detrital white mica ages reflect the distinct source area of each nappe. (*Handler et al.* (1997)). Thus the Noric nappe (detrital white mica Ar/Ar age 600–500 Ma) being the one closest to the Gondwana north rim still showing affects of the Cadomian tectonothermal event. It is constituted of Ordocivian to Lower Carboniferous sediments i.e. arkosic phyllites (Gerichtsgrabenformation) at the base and overlain by the Blasseneck porphyroid and the Rad Phyllite made of slates and phyllites and is concluded with an angular unconformity that forms the boundary to the Prebichl and Wer-

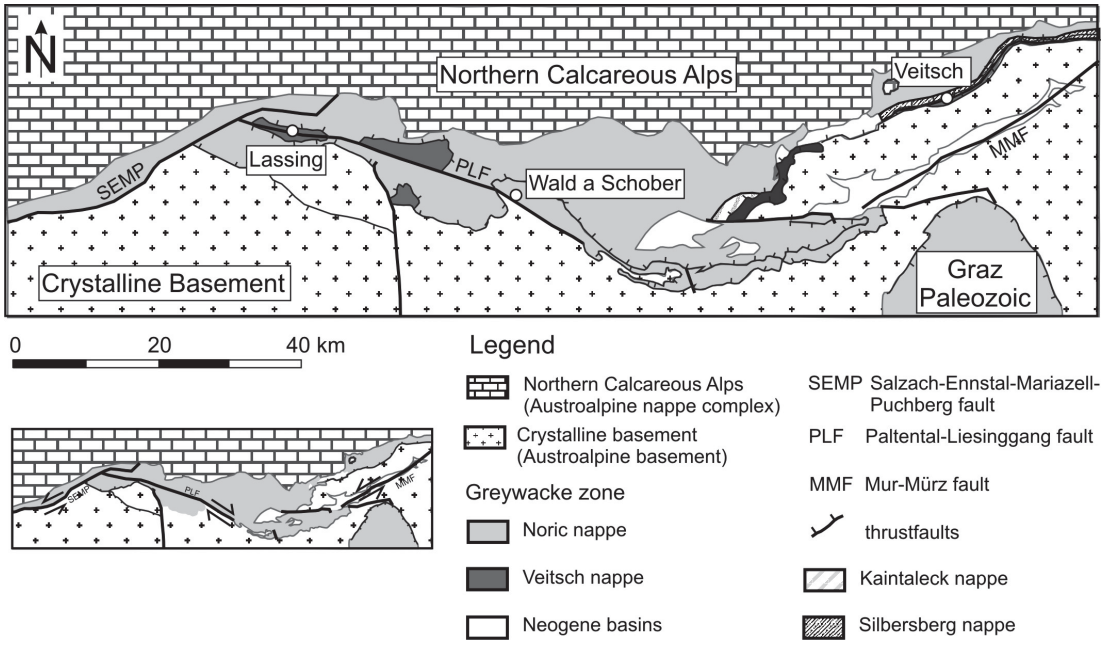

Figure 3.2: *Geological Sketch of the Eastern Greywacke Zone. Modified after* Rantitsch et al. *(2004)*

fen fromation (*Neubauer et al.* (1993)). The Prebichl formation has detrital mica ages of around 303 Ma (*Handler et al.* (1997)).

Both Silbersberg and Kaintaleck nappe have similar detrital ages (400–360 Ma and 383.8±1.1). These areas were affected by Devonian tectonothermal activity (early Variscan event). The Silberberg nappe consists of chlorite-carbonate schists and quartzphyllite with intercalated lenses of foliated volcanics at the base of the nappe. Above a fine-grained mylonitic gneiss (Gloggnitz Riebeckite Gneiss) forms the boundary to the Silbersberg Conglomerate containing light-colored greenish quartzitic phyllites with thin layers of acidic tuffs (*Neubauer et al.* (1993)).

The hangingwall Kaintaleck nappe is made of two lithological units: the Kaintaleck Metamorphic complex at the base of the nappe with amphibolites, paragneiss and micaschist as well as thin marble layers and lenses. The overlaying Kalwang Conglomerate contains basement fragments as amphibolites and serpentinites but is mostly dominated by orthogneiss clasts.

The lowest tectonic unit, the Veitsch nappe has a detrital age of 310 Ma. *Ratschbacher* (1987) already classifies the carboniferous marine to deltaic carbonate

and clastic sediments as molasse-type sediments. (Rb-Sr and Ar/Ar cooling ages of *Handler et al.* (1999) and *Neubauer et al.* (2002) support this theory.) Yet the source area of the Veitsch nappe still remains unknown (*Schoenlaub* (1981), *Ratschbacher* (1987), *Ratschbacher & Frisch* (1993), *Handler et al.* (1997), *Neubauer et al.* (2002)). The Veitsch nappe is subdivided into three formations from footwall to hangingwall: Steilbachgraben formation with clastics and minor carbonates, the Triebenstein formation mainly composed of carbonates and to a lesser degree of greenschists, and the Sunk formation containing quartz conglomerates and anthracite/graphite deposits (*Neubauer et al.* (1994)). Lenses of magnesite are bound to marine carbonates of Visean age.

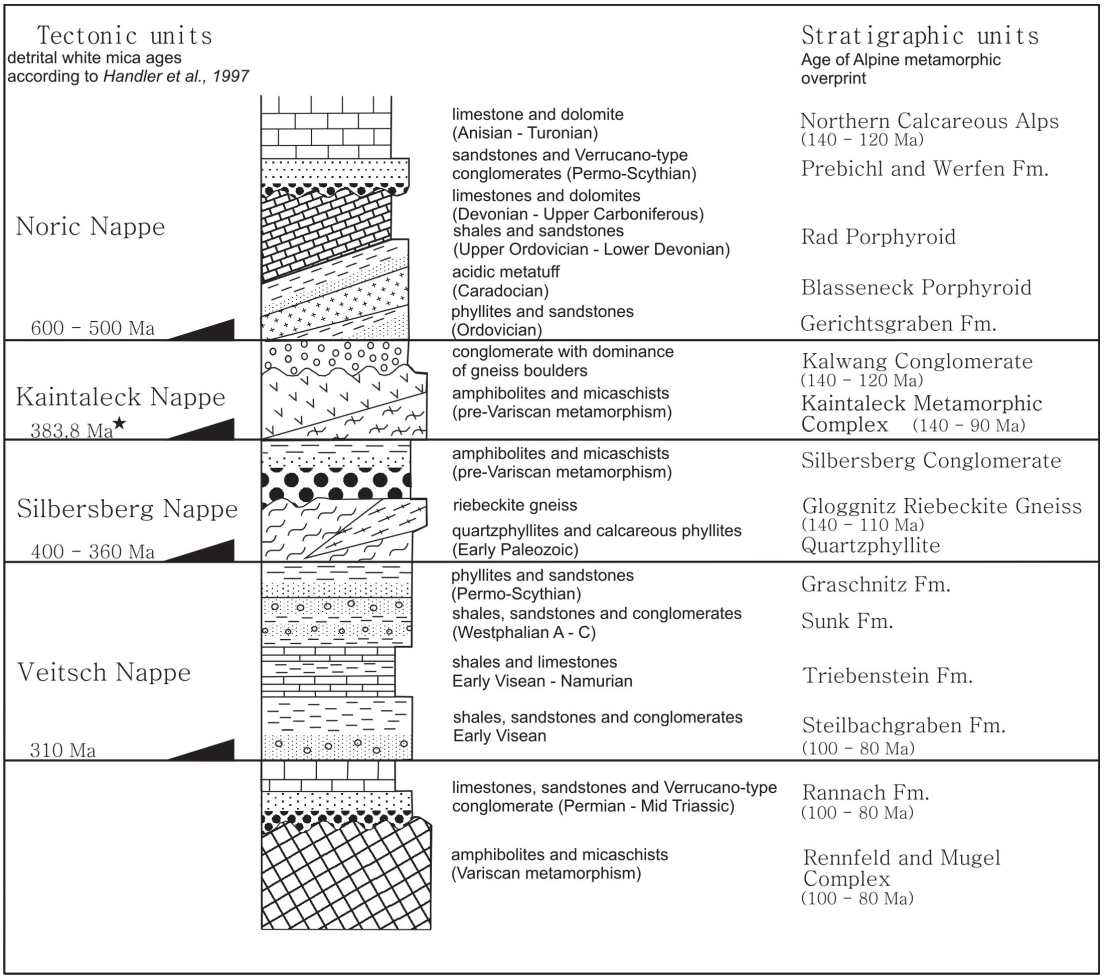

Figure 3.3: *Stratigraphy of the Eastern Greywacke Zone.* ⋆ *data from* Handler et al. *(1992). Modified after* Neubauer et al. *(1994)*

3.1.1.3 Geology of specific deposits of the Eastern Greywacke Zone

Veitsch

The magnesite deposit in Veitsch represents the type locality for sparry magnesite. It is situated north of the village Veitsch in Styria and approximatly 7 km from the valley floor of the Mürztal (MMF). The magnesite body of the Veitsch deposit is hosted by dolomitic carbonates of Carboniferous age of the Veitsch nappe and also by Carboniferous limestones, schists, conglomerates, quarzites and greywackes (*Prochaska* (2000)). The lense shaped magnesite bodies seem to evolve from the dolomitic carbonate. The carbonate bodies are embeded into Carboniferous phyllites and overlain by Silurian Quartz-porphyry and schists (fig. 3.4). Within the magnesite bodies horsetooth dolomite occurs as well as abundant quartz veins that crosscut both the dolomitic carbonate and the magnesite. The magnesite body itself is coarsley grained with pinolitic and rosulate textures.

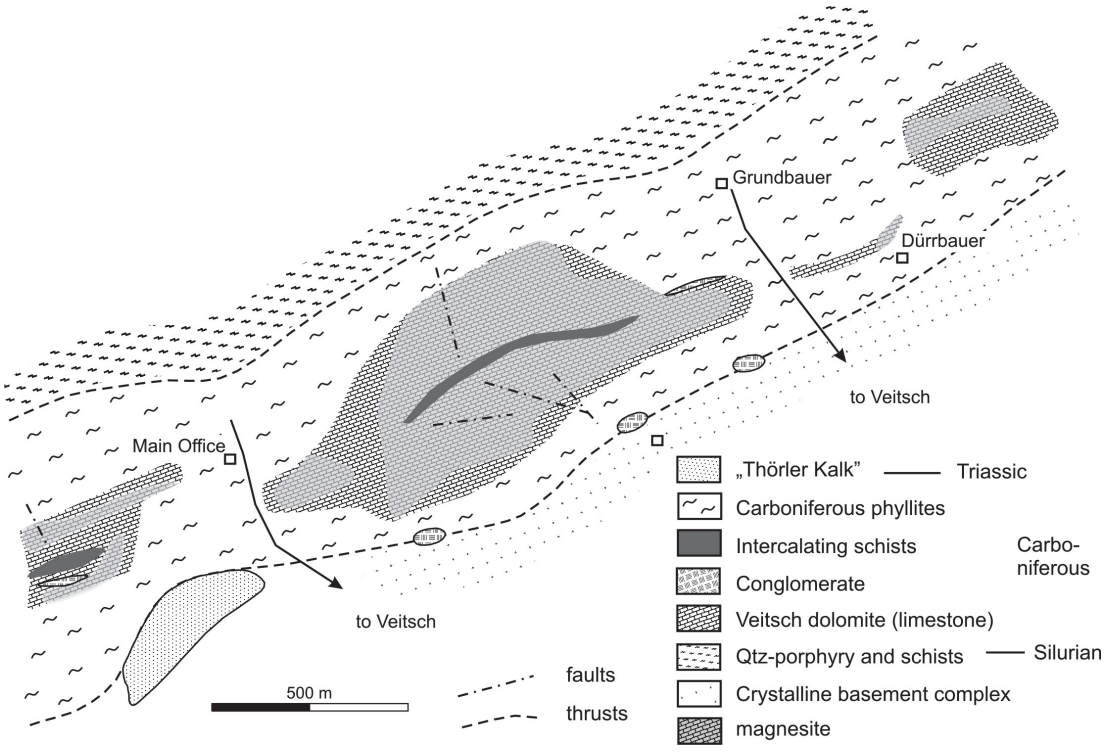

Figure 3.4: *Geological sketch of the Veitsch magnesite deposit. Modified after* Polgári et al. *(2010)*

Wald am Schoberpass

The magnesite deposit Wald am Schoberpass is situated between Wald am Schoberpass and Tregelwang in Styria. It is only a couple of meters to the southwest above the valley floor of the Paltental and thus in close proximity to the Paltental-Liesingtal-Fault. The deposit is embeded in Carboniferous limestones (*Felser* (1977)) as part of the Veitsch nappe. The magnesite body is bordered by a broad rim of dolomite that transists smoothly into the magnesite body. At the bottom of the deposit bedded and massive limestones of Visean age occur. The magnesite body itself ranges from fine grained to coarsly grained magnesite and pinolitic sparry magnesite. Also horsetooth dolomite occurs within the magnesite body. An important feature of the Wald am Schoberpass magnesite deposit is the occurrence of small to several cm-dm broad shear zones with talc and chlorite mineralization. In addition talc mineralizations also occur dispersely distributed within the magnesite body. The magnesite body is overlain by dolomite as well as slates and sandstone.

Lassing

The talc deposit of Lassing has been abandoned since the cave accident in 1998. It is situated at the junction of the Ennstal and Paltental. The vein type talc mineralization is hosted by dolomitic carbonates of the Veitsch nappe. The rock suits of the deposit consist of limestones, dolomites, magnesite, clastic metasediments and subordinate basic metavolcanics of upper Visean and Namurian age (*Prochaska* (1989)). The Paltental-Liesingtal-Fault is a fault zone in this area with dextral sense of shear (*Linzer et al.* (2002)). The talc deposit is situated north of an E-W striking anticline of Carboniferous rocks. It is flanked to the south by the Paltental-Liesing fault and to the north by the SEMP (fig. 3.5).

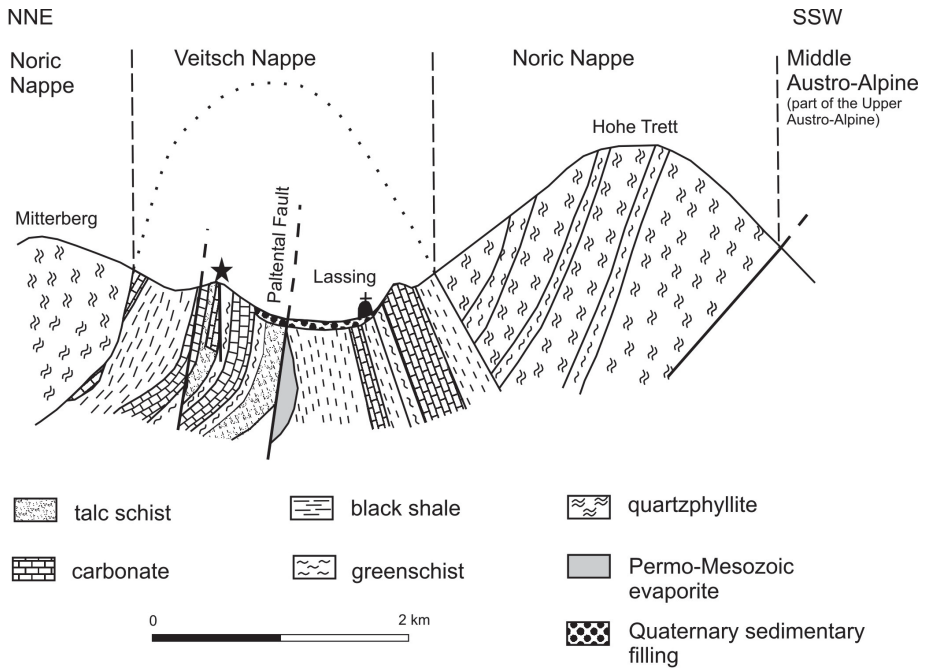

Figure 3.5: *Geological sketch of the Lassing talc deposit. Modified after* Prochaska *(1989)*

3.1.2 Results

3.1.2.1 Sample description

The chosen deposits of the Eastern Greywacke Zone are hosted in different lithologies of varying talc content. Only in the Lassing talc mine talc was produced and occurs within dolomite hostrocks. The magnesite deposits of Veitsch and Wald am Schoberpass produce magnesite while Wald am Schoberpass contains talc impurities on a cm to dm scale within shear zones and dispersely accumulated within magnesite rocks.

The sparry magnesite body of the ***Veitsch*** deposit is generally of massive nature and contains mostly brittle deformation structures such as brittle faults or feather joints. The magnesite samples are of reddish color and coarsely grained. They evolve from a greyish dolomite hostrock. Both are part of the Veitsch nappe. The states of formation – the beginning of magnesite formation and the final state with an almost completely mineralized magnesite and only leftover dolomite –

can be observed in the deposit (fig. 3.6) and in hand specimen (fig. 3.7). Post-magnesite-formation veins of quartz and dolomite penetrate the dolomite and magnesite bodies. A sketch of the order of mineralization is shown in fig. 3.8. Minor components of ore minerals as fahlore and malchite can be observed as well. Thus the evolution of the deposit can be reconstructed as the following: greyish precursor dolomite which evolves into a reddish sparry magnesite. Both are later penetrated by quartz and dolomite veins. The dolomite and quartz veins dip NNE with approx. 020/70 and NNW with approx. 340/45. A younger set of veins dips NE with approx. 305/80.

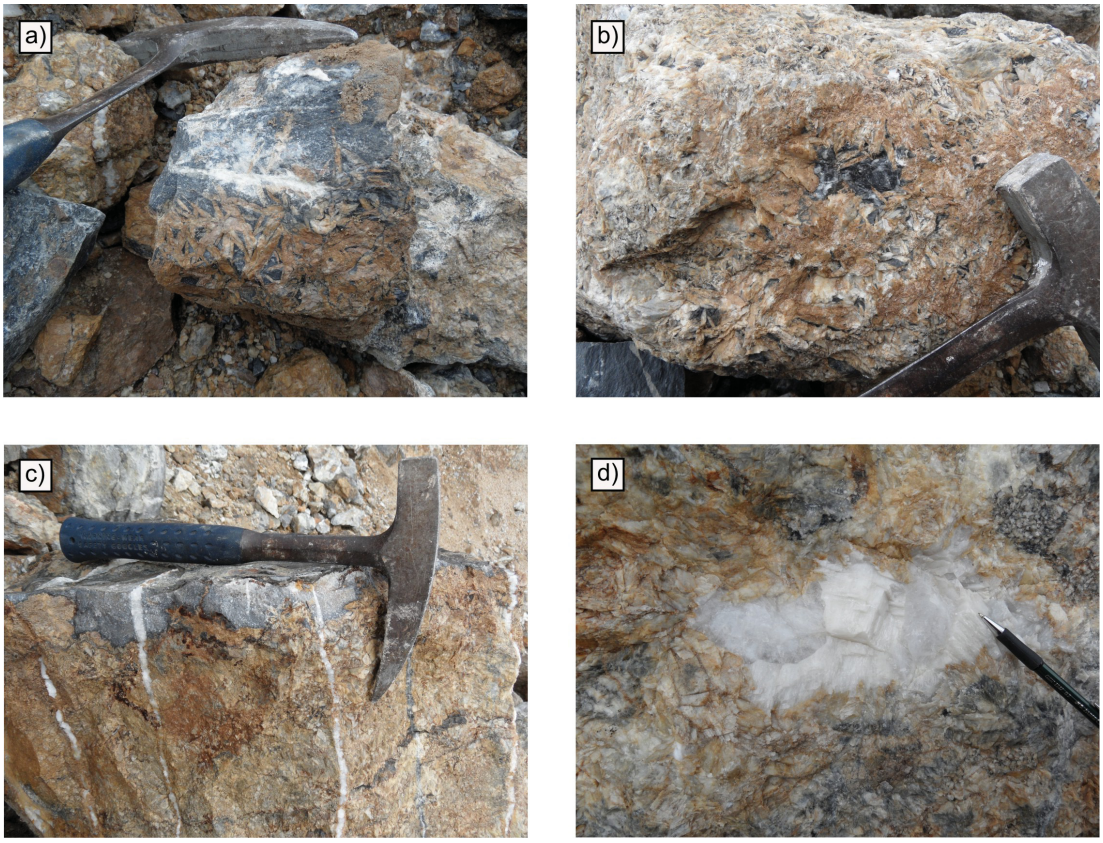

Figure 3.6: *Field observations from the Veitsch magnesite deposit: a) Early state of magnesite formation from greyish precursor dolomite, b) Late state of magnesite formation with small residual precursor dolomite, c) Late dolomite veins penetrating magnesite and dolomite body, d) Late dolomite and quartz formation within magnesite*

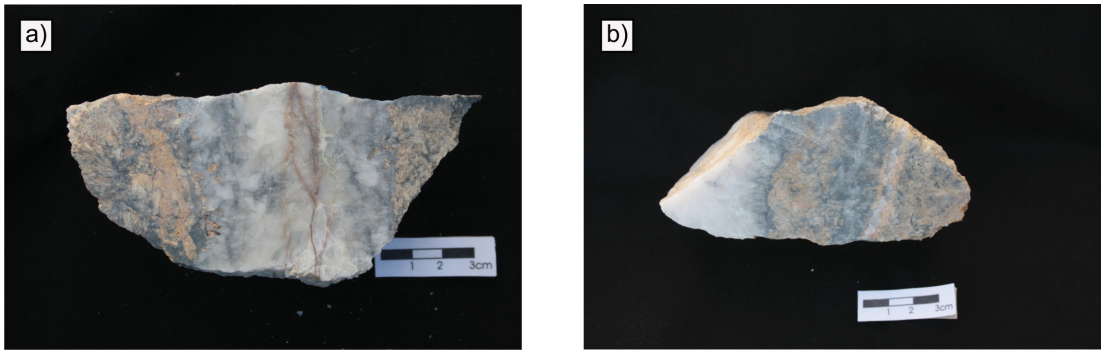

Figure 3.7: *Hand specimen of magnesite from the Veitsch magnesite deposit: a) VE1 – magnesite with residual dolomite and late quartz vein, b) VE2b – magnesite with residual dolomite and late dolomite vein*

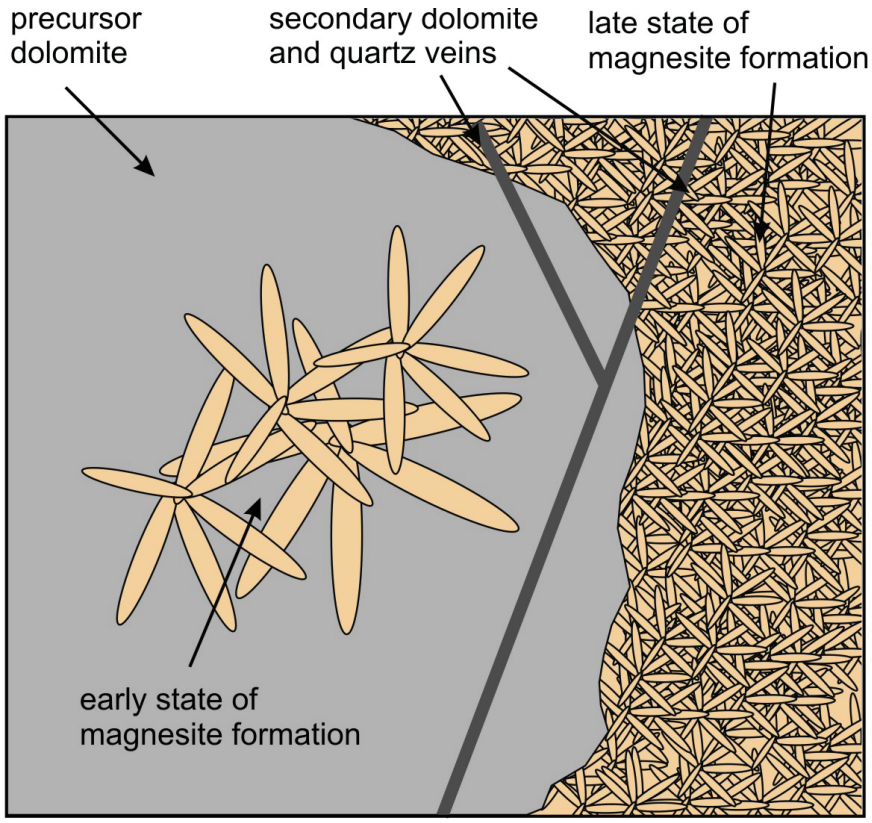

Figure 3.8: *Sketch of mineralization phases at the Veitsch magnesite deposit*

The magnesite deposit of ***Wald am Schoberpass*** is clearly penetrated by ductile deformation. Structures as SC-textures (fig. 3.9c), shearzones (fig. 3.9 a, b) and boundinages (fig. 3.9 d) can be found. Shearzones are filled with talc mineralizations. Talc accumulations can be concentrated in the fault core of a shearzone (fig. 3.9 f) or dispersely distributed within the magnesite body (fig. 3.9 e). The sparry magnesite body itself is mostly of whitish or greyish color and coarsley grained and is part of the Veitsch nappe. Towards the shear zones it takes a reddish color and marks a seam along the shear zone. Talc mineralization within the shearzones are mostly of greyish and whitish color. More massive talc bodies (up to dm scale) are of milky whitish and yellowish color. Secondary carbonates such as horse tooth dolomite also occur within the magnesite body. A sketch of the mineralization phases is shown in fig. 3.10.
Thin-sections confirm dispersely accumulated talc concentrations within the magnesite body (fig. 3.11a). Shear zones are composed of a fine grained hyaline matrix of gouge material and fragments of carbonate rocks (fig. 3.11b & fig. 3.11c & fig. 3.11d). The transition zone towards the hostrock magnesite body is marked by fractured carbonate rocks filled with a fine grained matrix (fig. 3.11b).

The deposit is characterized by ductile deformation structures such as SC-textures, shearzones and boundinages. Talc accumulations can be concentrated in the fault core of shearzones. These talc shearzones have a general dip of ESE with approx. 100/35 and WNW with approx. 330/20. Slickensides show normal faulting with approx. 100/35 and 330/20. A prominent fault approx. parallel to the Paltental-Liesingtal-fault dips NNE with approx. 010/60 and reveals two generations of slickenside with dexral sense of shear and 308/15 for the younger one and 020/60 for the older one with a normal faulting component.

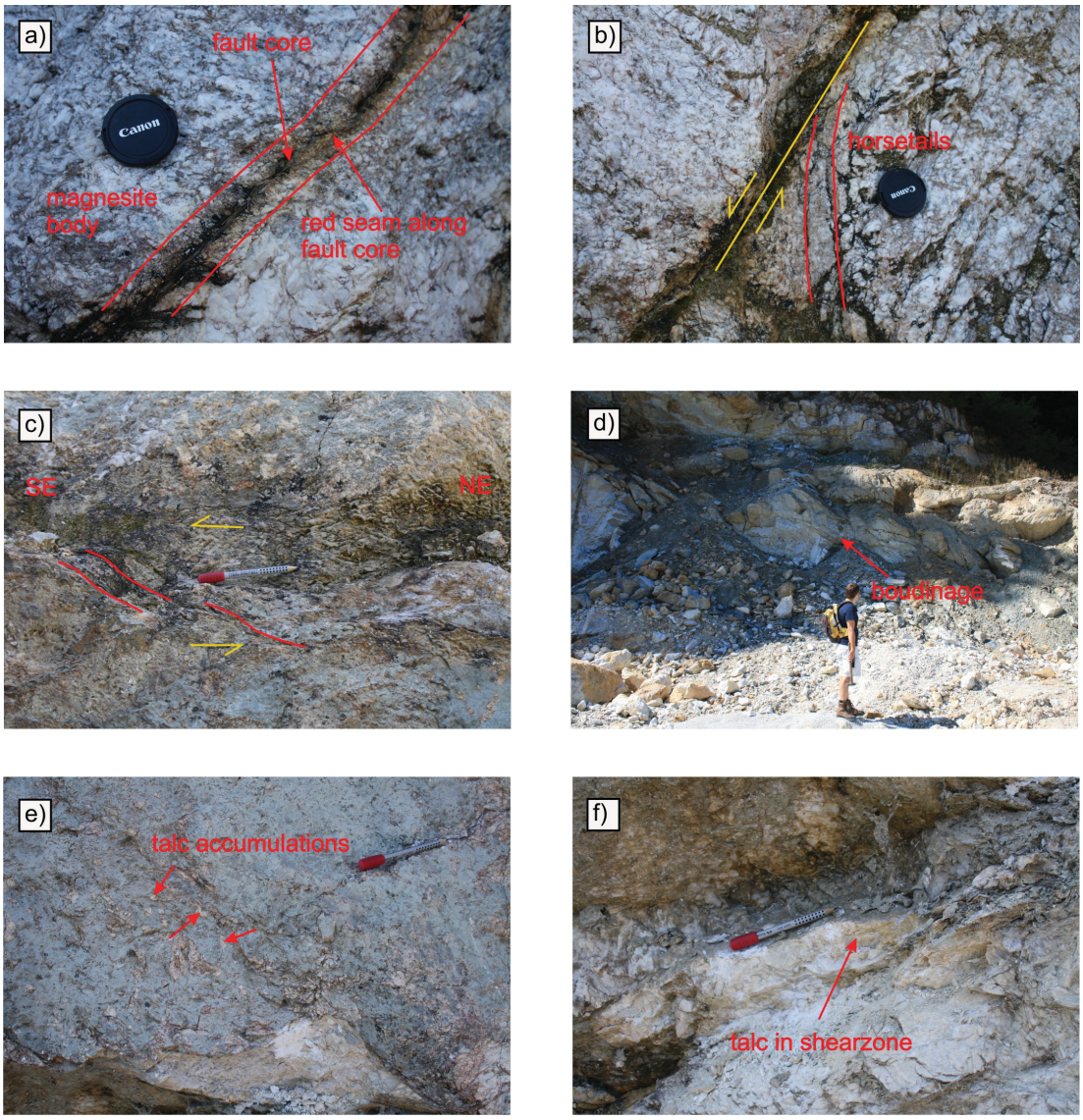

Figure 3.9: *Field observations from the Wald am Schoberpass magnesite deposit: a) shear zone with talc fault core and reddish seam along the fault core within magnesite body, b) shear zone with horsetails indicating normal sense of shear, c) shear zone with SC texture indicating sinistral sense of shear, d) boudinage, e) dispersely distributed talc accumulations within magnesite body, f) larger talc accumulation in shearzone*

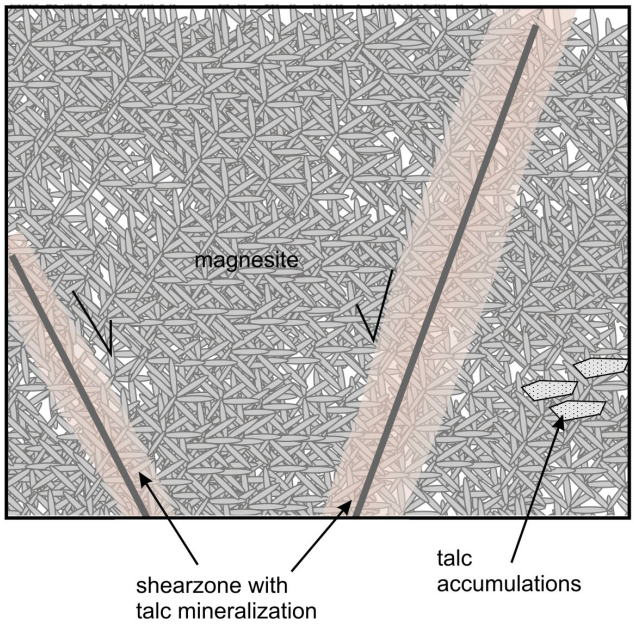

Figure 3.10: *Sketch of the mineralization phases at the Wald am Schoberpass magnesite deposit*

The talc deposit of ***Lassing*** has been closed since the mining disaster in 1998. Hence samples could only be taken from surface exposures. Some handspecimen from the deposit were available at the University of Leoben and could be used for analysis. The massive talc mineralization lies within a dolomite body that is part of the Veitsch nappe.

Thinn-sections from the surroundings of the Lassing talc mine reveal multiple deformation events that overprinted the carbonate rocks (fig. 3.12a). Younger quartz veins within these rocks show also signs of deformation such as undulose extinction and bulging (fig. 3.12b) . A late state post tectonic deformation phase is recognizable in statically grown quartz grains (features are triple junctions, equigranular grain boundaries and lack of undulose extinction, fig. 3.12c).

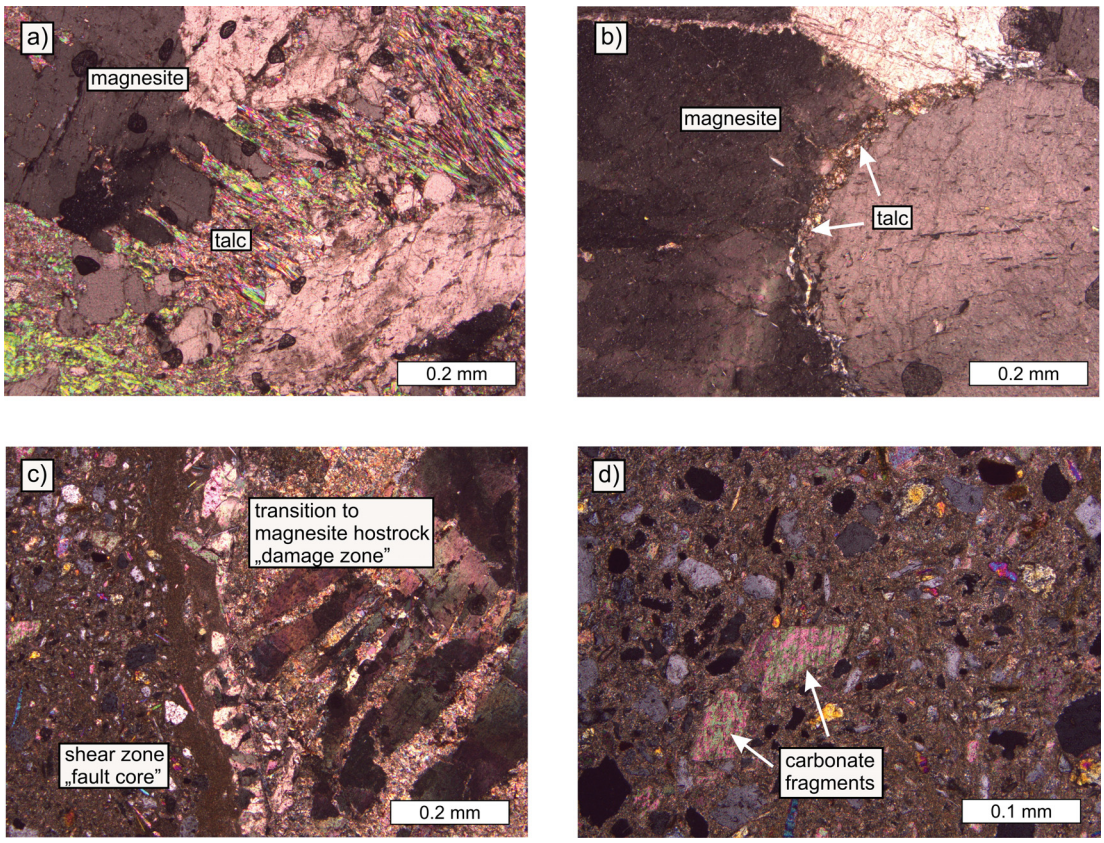

Figure 3.11: *Thinn-sections of the Wald am Schoberpass magnesite deposit: a) and b) the magnesite body is penetrated by disperse talc accumulations (WS 11 and WS 20), c) the shear zones of the deposit consist of a fined grained hyaline matrix of gouge material with fragments of carbonate – "fault zone"; the transition zone towards the magnesite hostrock body shows broken carbonate grains filled with a fine grained matrix – "damage zone" (WS 35), d) detail of carbonate fragments within a hyaline matrix of gouge material – "fault core" (WS 35)*

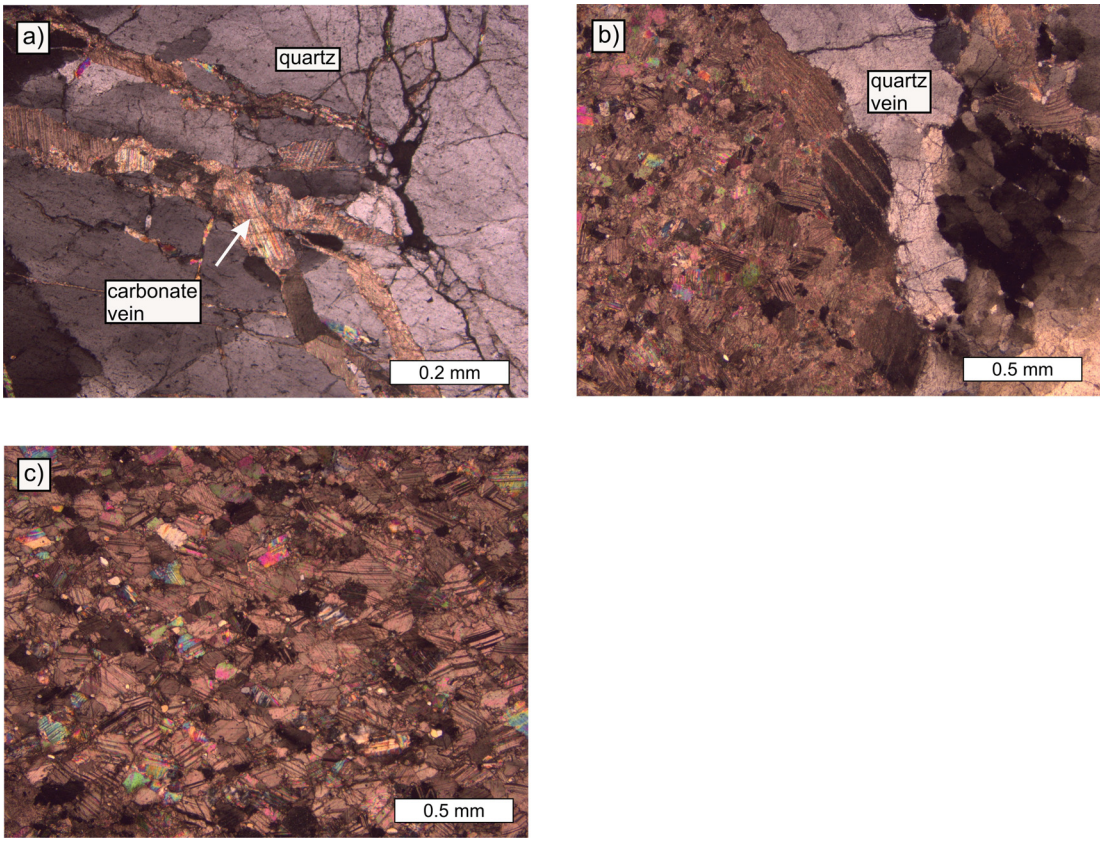

Figure 3.12: *Thinn-sections from the surroundings of the Lassing talc deposit: a) fractured quartz vein with calcitic vein filling (LA 1b) , b) quartz vein within calcitic marble (LA 4) c) Calcitic marble shows multiple deformation events (LA 20)*

3.1.2.2 Major, minor, trace elements

Rock samples from each deposit were analyzed with regard to the tectonic structures in the respective deposits.

In the ***Veitsch*** deposit samples from the magnesite, the precursor dolomite and the vein mineralizations were analyzed.
Magnesite samples (VE5a, VE14b) are slightly depleted in MgO (36.77–43.22 wt%) (compared to values of magnesite from *Deer et al.* (1992)) and elevated in CaO (2.24–8.17 wt%), FeO (3.55–4.82 wt%) and Sr (27–63 ppm). Other minor and trace elements analyzed do not give hints on significant elevation or depletion of the magnesite. The dolomites of the deposit seem to be dividable into two groups. Such grey dolomites with no intermediate contact to magnesite (VE7, VE9, VE14a) have partly a different geochemical composition than dolomites that are in direct contact with magnesite (VE2a, VE2b, VE5b, VE5c, VE5d). The latter represent more the late state of magnesite minerallization. Major and minor element composition of both dolomite groups are comparable and do not deviate from typical samples as the ones analyzed in *Deer et al.* (1992) except for a higher content of FeO (0.98–3.00 wt%). However the early state magnesite samples have low Sr (32–77 ppm) and Y (1.2–5 ppm) contents – more similar to the respective contents in the magnesite samples.

In the ***Wald am Schoberpass*** magnesite deposit the majority of the magnesite samples represent the typical signature of major elements: MgO (38.58–46.90 wt%), CaO (0.44–5.02 wt%), MnO (0.07–0.10 wt%). FeO is slightly elevated (1.23–2.20 wt%). SiO_2 contents are generally low (1.09–2.89 wt%) but elevated in certain magnesite samples (WS2, WS11, WS12, WS20) (4.94– 14.05 wt%) A similar trend is detectable in the Sr content of certain samples. Most samples have expectably low Sr contents (2–6 ppm), but samples WS 9ca, WS9cb and WS 20 have significantly higher Sr contents (19–46 ppm). Other major, minor and trace elements do not show any significant variations or trends. Dolomite samples follow the general geochemical composition of dolomites with MgO (20.22–21.28 wt%), CaO (28.98–30.03 wt%), FeO (0.12–0.54 wt%) and MnO (0.02–0.04 wt%). Sr contents are between 65 ppm (WS1) and 116 and 119 (WS7 and WS8 respectively).

The samples taken outside the ***Lassing*** talc deposit are calcite marble with MgO (0.68–5.19 wt%), CaO (49.1–53.51 wt%), FeO (0.11–0.51 wt%) and MnO (0.01–0.08 wt%). The handspecimen from inside the deposit are dolomite with MgO (13.73–22.39 wt%), CaO (24.67–33.1 wt%), FeO (0.36–0.8 wt%) and Mn (0.02–0.07 wt%).

3.1.2.3 REE pattern

REE patterns of carbonates from the ***Veitsch*** magnesite deposit show some distinct features according to their type and generation. The so called "early state" grey dolomite (VE 9 & VE 7) shows a downward pattern of REE with lower values of HREE and a moderate positive Eu anomly (fig. 3.13a). Sample VE 14a is an exception with a roof-shaped REE pattern. The red magnesite of samples VE 14b and VE 5a shows a similar roof-shaped pattern with slightly lower HREE (fig. 3.13b). The REE pattern of the "late state" dolomite are distinct from earlier carbonate generations of the Veitsch deposit. They show a general downward directed REE pattern with lower values of HREE but with a prominent positive (VE 2a, 2b,& 5c) and negative (VE 5b & d) Eu anomaly (fig. 3.13c). REE contents of carbonates with contents of SiO_2 and Al_2O_3 show no positive correlation.

The magnesite samples from the ***Wald am Schoberpass*** deposit show no significant distinction in their REE pattern. All samples (whether free of talc or with disperse talc accumulations) have a roof shaped REE pattern. Only two samples show a more prominent Eu anomaly (fig. 3.14b) . However samples in contact with the talc bearing shear zones have a very prominent negative Eu anomaly with a general roof shaped REE pattern. The late state "horse tooth dolomite" is very enriched in REE compared to other samples from the deposit with a roof shaped REE pattern. And the hostrock (dolomite marble) has a downward directed REE pattern with low HREE values (fig. 3.14a).

The REE patterns at the ***Lassing*** talc deposit show a lot more variation in their respective groups than the samples at the other deposits. Calcitic marbles from outside the deposit are depleted in HREE and have a downward REE trend with partly positive and negative Eu anomaly (fig. 3.15a). A similar pattern can be ob-

served from the dolomite marble inside the deposit with partly more pronounced negative and positive Eu anomalies (fig. 3.15b). Eu anomalies can be an important indicator for temperature estimations and the origin of the mineralizing fluid.

3.1.2.4 Stable Isotopes

Carbon isotope values at the ***Veitsch*** magnesite deposit range from $\delta^{13}C$ = -7.00 to -1.68 ‰ (VPDB) and oxygene isotope values range from $\delta^{18}O$ = 13.04 to 20.16 ‰ (VSMOW) (fig. 3.16). The different genetic rock groups show distinct trends. The early state grey dolomite has lowest values of $\delta^{13}C$ and $\delta^{18}O$. Also the late state dolomite veins are depleted in $\delta^{18}O$ compared to magnesite samples. The magnesite samples from the deposit spread in a much broughter range but have a tendency to higher $\delta^{13}C$ and $\delta^{18}O$ values. Generally all carbonate samples are depleted in their $\delta^{13}C$ and $\delta^{18}O$ values compared to seawater.
Oxygene isotope values of quartz are in the range of $\delta^{18}O$ = 14.7 to 15.42 ‰ (VSMOW).

At the ***Wald am Schoberpass*** magnesite deposit carbon isotope values range from $\delta^{13}C$ = -3.92 to -0.17 ‰ (VPDB) and oxygene isotope values are in the range of $\delta^{18}O$ = 11.64 to 20.46 ‰ (VSMOW) (fig. 3.16). Magnesite samples have generally a tendency to lower $\delta^{18}O$ values compared to the magnesite samples from the Veitsch deposit. Distinction between the different magnesite groups are not as obvious as at the Veitsch deposit where magnesites show a much clearer distinction from the late state dolomite veins. The hostrock dolomite marble represents another group with a tendency to higher $\delta^{13}C$ and $\delta^{18}O$ values than the magnesite from the deposit.

Samples of dolomite from the Lassing talc deposit have carbon isotope values in the range of δ^{13}C = -1.24 to 1.57 ‰ (VPDB) and oxygen isotope values in the range of δ^{18}O = 13.66 to 20.42 ‰ (VSMOW, 3.16).

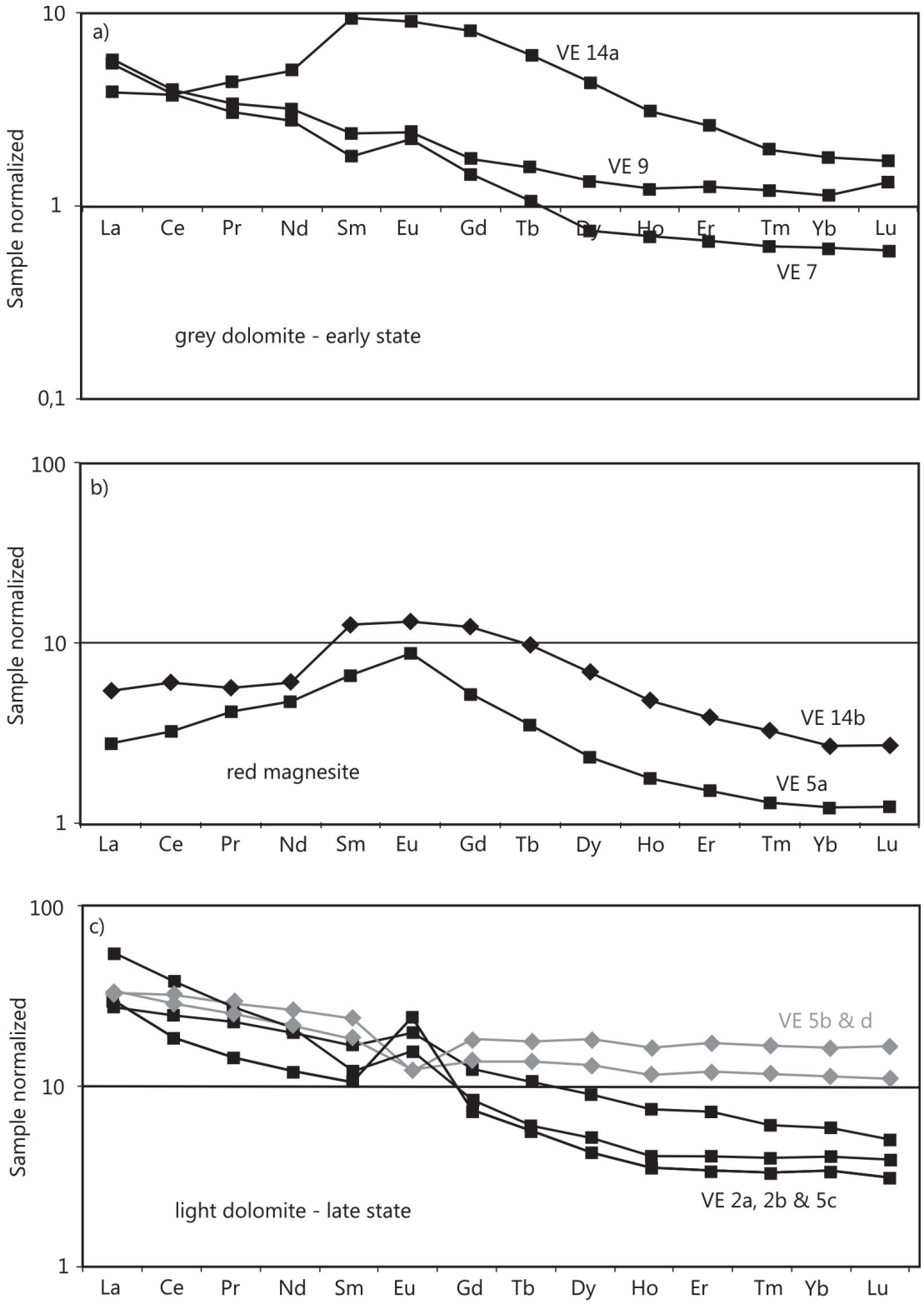

Figure 3.13: *Chondrite-normalized REE patterns of different carbonate generations form the Veitsch magnesite deposit: a) "early state" grey dolomite, b) red magnesite, c) "late state" light dolomite*

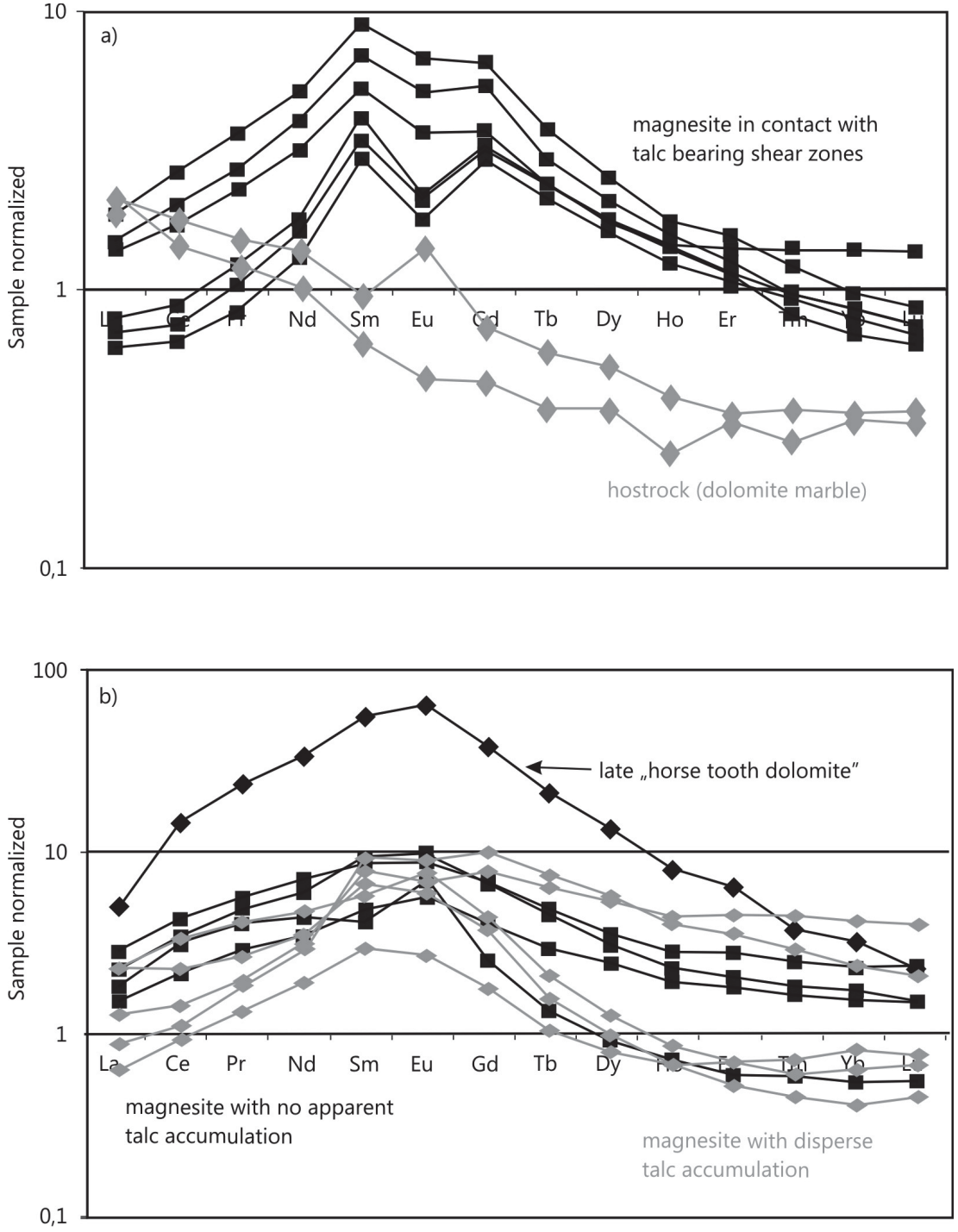

Figure 3.14: *Chondrite-normalized REE patterns of different carbonate generations form the Wald am Schoberpass magnesite deposit: a) magnesite in contact with talc bearing shear zones and hostrock dolomite marble b) magnesite with disperse talc accumulation and magnesite with no apparent talc accumulation, late state "horse tooth dolomite"*

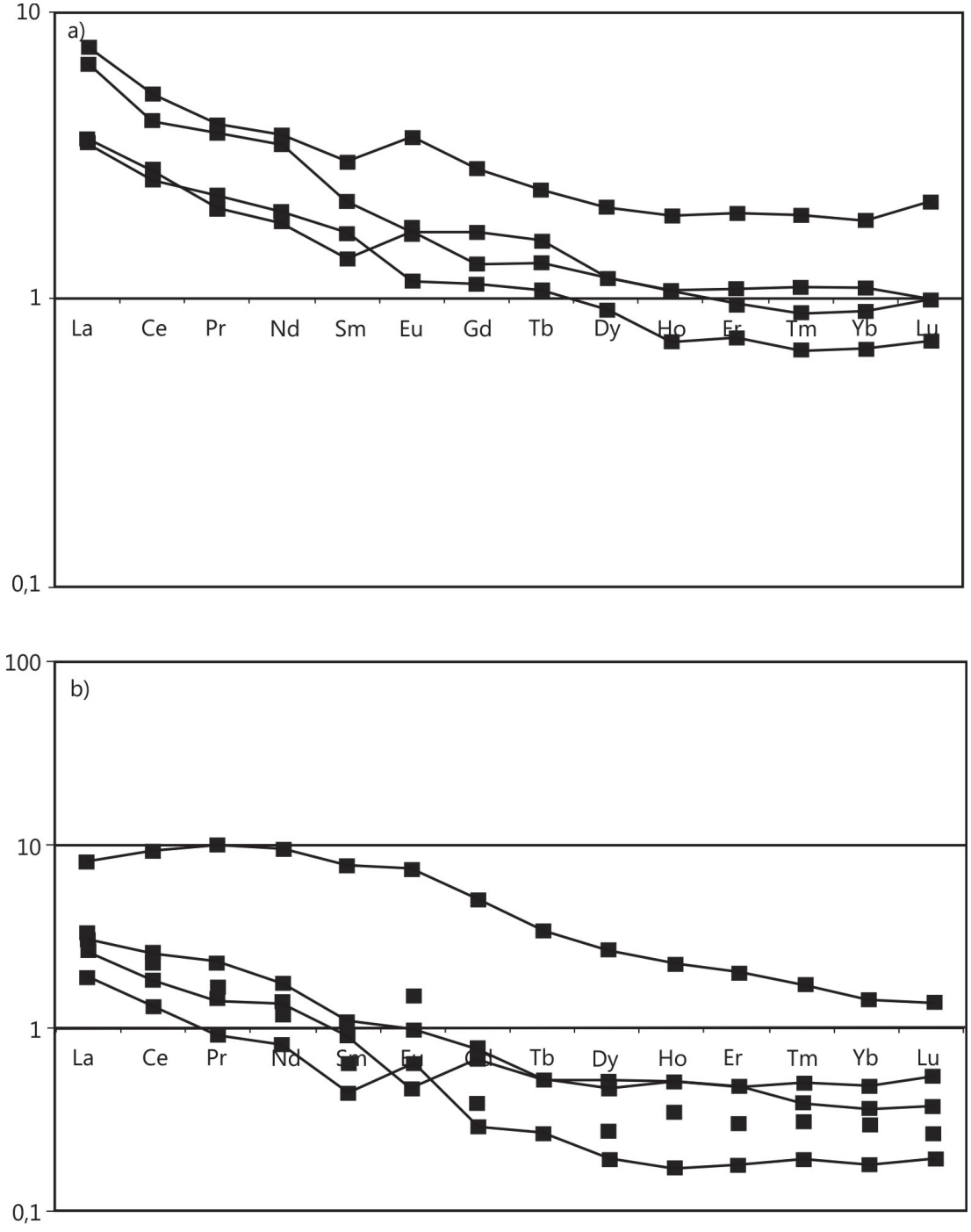

Figure 3.15: *Chondrite-normalized REE patterns of different carbonate generations form the Lassing talc deposit: a) Calcitic marble from outside the deposit, b) dolomite marble from inside the deposit*

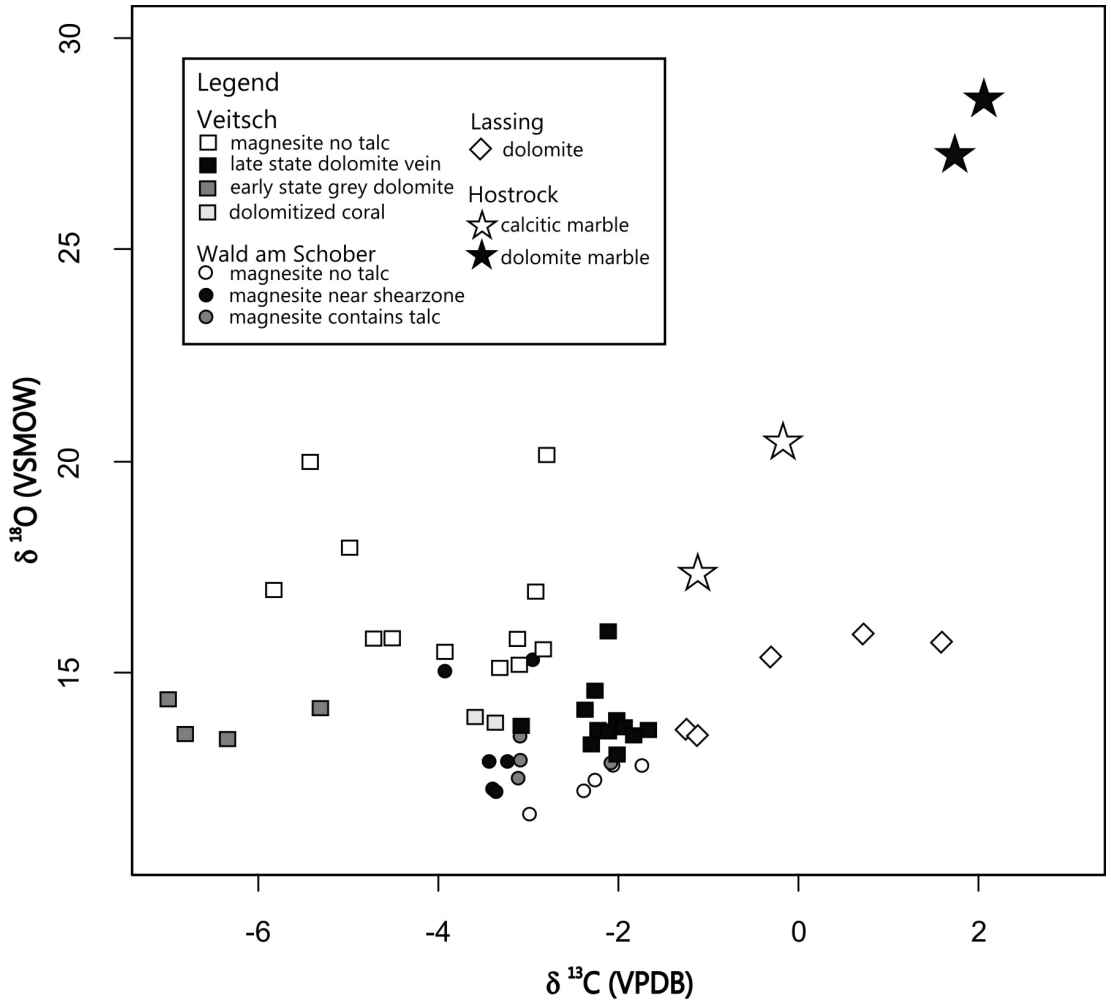

Fig. 15

Figure 3.16: *Stable isotopes from Veitsch, Wald am Schoberpass, Lassing and hostrocks*

3.1.2.5 Ion-chromatography

At the ***Veitsch*** magnesite deposit fluid inclusions magnesite, early and late state dolomite and secondary quartz were analysed (fig. 3.17). All samples have low Na/Br (< 405) and Cl/Br (< 513) ratios compared to modern seawater. Samples from early state dolomite have especially low values (Na/Br < 78 and Cl/Br < 123). Li/Na ratios are also low (< 0.0135) with no apparent trend.
Na-K-temperatures for carbonates calculated according to *Can* (2002) are low at around 180°C. Na-K-temperatures are significantly higher at 340°C for secondary quartz.
Charge balance ($Q^+/Q^- = 1$) for carbonates is imperfect with values between 4 and 5 but comes close to 1 for the quartz samples with around 1.4. The imperfect charge balance within the carbonate samples might be due to volatile phases lost during the crushing process.

At the ***Wald am Schoberpass*** magnesite deposit samples are also generally lower than modern seawater (with Na/Br < 290 and Cl/Br < 350) and lower than samples from the Veitsch deposit. Only samples VE7 & VE8 (hostrock from outside the deposit) come close to the values of modern seawater. Li/Na ratios are low (with $< 0{,}0058$) (fig. 3.17).
Na-K-temperatures are at 248°C for magnesite from the deposit and at 184°C for samples VE7 & VE8.
Charge balance ($Q^+/Q^- = 1$) for carbonates is also imperfect with values between 4 and 8.

The ***Lassing*** talc deposit shows low Na/Br and Cl/Br ratios for samples from inside the deposit (Na/Br < 440 and Cl/Br < 500). Samples from outside the deposit vary greatly from values below the values of modern seawater and values well beyond the values of modern seawater (fig. 3.17).
Na-K-temperatures of carbonate samples from inside the deposit are at around 140°C. Temperatures of carbonate samples from outside are higher with 200°C and quartz temperatures are even as high as 360°C.
Charge balance ($Q^+/Q^- = 1$) for carbonates are again imperfect and vary for samples from outside the deposit between 2 and 3 and for samples from inside the deposit between 3 and 9. However quartz samples from outside are close to

perfect charge balance with values between 1.2 and 1.4.

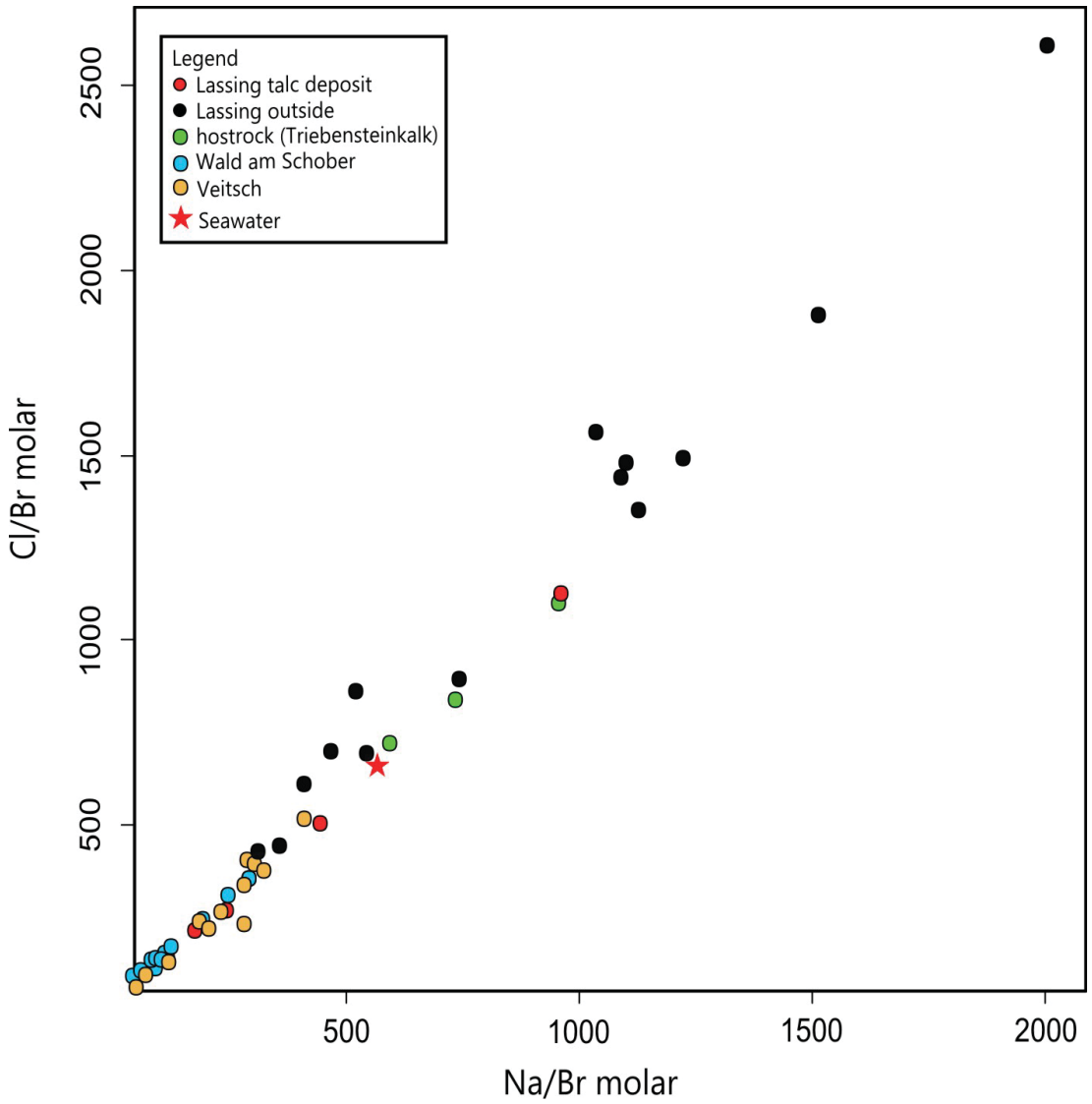

Figure 3.17: *Crush leach data of deposits from the Eastern Greywacke Zone (Veitsch, Wald am Schoberpass and Lassing)*

3.1.3 Discussion

The deposits discussed in this paper are bound to the tectonic evolution of the Eastern Alps. The Veitsch magnesite deposit is about 7 km from the Mur- Mrz-Fault and at the nappe boundaries of Silbersberg nappe and Veitsch nappe, the Wald am Schoberpass magnesite deposit is in direct connection to the Palental-Liesingtal-Fault and the Lassing talc deposit is situated at the junction of the Paltental-Liesingtal-Fault and the SEMP (fig. 3.2).

Veitsch

The brittle tectonic features of the Veitsch deposit propose that deformation took place under low temperature conditions. Field observerations suggest several geological events: The greyish dolomite can be regarded as a precursor rock. It is consumed to a large extent by reddish coarsely grained sparry magnesite. Residuals of the precursor dolomite are present throughout the deposit. Partly, it can be seen that very distinct grains of magnesite have evolved from the dolomite. In other parts magnesitization has progressed further and only very small residuals of dolomite are left. Due to its low Na/Br and Cl/Br (typically Cl/Br = 658 according to *Gleeson* (2003)) ratios that indicate an evaporitic origin of the mineralizing fluid. *Prochaska* (2000) explains the magnesite formation with residual evaporitic brines that percolated through the crust during Permoskythian rifting. High heatflow during rifting (*Schuster et al.* (1999)) induced hydrothermal convection systems and allowed highly evaporated seawater to percolate the crust and mineralize the dolomite rocks to magnesite. Temperatures of fluid inclusion study of the non-steatitized magnesite is estimated to be at approx. 180°C. With increasing metamorphism the δ^{13}C and δ^{18}O change towards lighter values (*Schroll* (2002)) which can be attributed to equilibration of the carbonates with metamorphic fluids (*Kralik et al.* (1989) and *Schroll* (2002)) or due to rising hot basinal brines of connate origin (*Aharon* (1988)). Precursor dolomite from the Veitsch deposit differs significantly in their δ^{13}C values from late state dolomite veins and magnesite. This can indicate the occurrence of multiple hydrothermal events or different precipitation mechanisms within the hydrothermal system (*Hurai et al.* (2011)). The REE pattern of the dolomitic precursor rock and the magnesite are comparable in their general trend and their amount of REE. The characteristics

of REE patterns are controlled by the composition of the migrating fluid, the mineralogical features of the hostrock and the physico-chemical conditions during precipitation (*Bau & Möller* (1992)). According to *Möller* (1989) the REE concentration of purely marine magnesites are very low and become considerably higher if magnesite formation is caused by hydrothermal fluids during diagnesis. The similarity of the REE pattern of the magnesite and the dolomitic host rock reflects the genetic link between both rocks indicating that the magnesites formation can be attributed to Mg^{2+} metasomatism of the hostrock. The late state dolomite of the Veitsch deposit is depleted in HREE compared to LREE. This is a hint for remobilised fluids (*Schroll* (1997)) that led to the precipitation of the late state dolomite. The varying positive and negative Eu anomaly supports that. The redox potential of Eu strongly depends on temperature, slightly on pH and is almost unaffected by pressure (*Bau* (1991)). At temperatures above 200°C Eu^{2+} dominates over Eu^{3+} and a positive Eu anomaly is formed (*Bau & Möller* (1992)). Field evidences and analytical study from Veitsch support the model of *Koch* (1893) and *Redlich* (1909) of the epigenetic nature of magnesite formation. Carbonate samples that represent the non-steatitized country rock "Triebensteinkalk" of the Sunk formation (carbonate samples from outside the Lassing deposit, SU1, SU2, WS7, WS8) plot above the seawater ratio along the (halite-dissolution trend). However quartz samples of veins within the Triebensteinkalk country rock have lower Na/Br and Cl/Br ratios as seawater indicating a relation of the fluids from within the deposit and the quartz veins. Na/K temperatures of the "Triebensteinkalk" country rock are equally low as temperatures from the Veitsch deposit. Also clearly higher $\delta^{18}O$ and $\delta^{13}C$ values are closer to that of marine carbonates.

Wald am Schoberpass

At the magnesite deposit Wald am Schoberpass talc occurs as impurities within the carbonate hostrock body. The deposit is clearly marked by ductile deformation indicating higher temperature conditions. Precursor rocks were not found within the boundaries of the deposit. It can be assumed that the magnesite formed under similar conditions during Permoskythian rifting as the magnesite body at the Veitsch deposit. The coarsely grained greyish to whitish magnesite body is penetrated by shear zones. The fault core is composed of talc and a fine

grained hyaline matrix of gouge material. Towards the magnesite hostrock fragments of carbonate rocks occur in a fine grained matrix. This indicates differing strength of deformation with a concentration of deformation in the fault core. The talc shear zones are dominantly normal faults. The circulation of a silica-rich fluid through these faults may lead to dissolution of the magnesite hostrock and the precipitation of talc. The talc formation may have started to develop along fractures or as isolated patches within the hostrock and form interconnected networks as strain increases (*Collettini et al.* (2009)). Na/Br and Cl/Br values of the carbonate rocks are again well below the corresponding ratios of seawater (typically Cl/Br = 658 according to *Gleeson* (2003)). Na-K temperatures of fluid inclusions however are significantly higher (approx. 250°C) than at the Veitsch deposit. Also δ^{18}O values from the Wald am Schoberpass deposit compared to values from the Veitsch deposit are depleted but still in the range of the typical signature of metamorphic fluids. The moderate depletion of δ^{18}O indicates higher fluid temperatures that penetrated the magnesite hostrock. Generally the similarity of the δ^{18}O values of the magnesite of Veitsch and Wald am Schoberpass is an indicator for a common source of the mineralizing fluids. The group of magnesite samples close to talc shear zones with lighter δ^{13}C may indicate an increase of temperature towards the shear zones. Again the slight but significant decrease of δ^{13}C indicates a common origin of the magnesite body but a tendency of higher tempertated fluids that migrated through the shear zones and led to the alteration in the vicinity of the shear zones and the formation of talc. The magnesite samples also show the roof-shaped pattern very similar to the magnesites from the Veitsch deposit also indicating the formation of the magnesite by metamorphogenic hydrothermal fluids (*Bau & Möller* (1992)). However magnesite samples in close contact with the talc bearing shear zones at Wald am Schoberpass have a very pronounced negative Eu anomaly.

Tectonic events may have induced enough stress to dissolute Mg from the magnesite hostrocks and to enrich talc in the existing fractures through circulating SiO_2-rich fluids. Ductile tectonic features of Wald am Schoberpass clearly postdate the magnesite formation. Also the higher temperatures compared to magnesite samples from Veitsch and the "Triebensteinkalk" country rock indicates that after magnesite formation a hydrothermal event took place that led to the formation

of the talc within shear zones. According to *Willingshofer et al.* (1999a), *Willingshofer et al.* (1999b), *Kurz & Fritz* (2003) and *Rantitsch et al.* (2005) subsidence movements after Eoalpine orogeny yielded tectonic structures and temperatures that are in agreement with the features at Wald am Schoberpass. In that case nappe boundaries may act as fluid circuits and transport SiO_2-rich fluids. The position of the Wald am Schoberpass deposit at the Paltental-Liesingtal-Fault also need some consideration. However not much is known about the Paltental-Liesingtal-Fault except for its dextral sense of shear (*Linzer et al.* (2002)), its position within the Miocence escape tectonic fault system of the eastern Alps and its brittle nature (*Brosch & Kurz* (2008)). These arguments of temperature and deformation structures may outrule a possible link of the talk shear zones at Wald am Schoberpass and the Miocence Paltental-Liesingtal-Fault.

Lassing

The carbonates surrounding the Lassing talc mine show multiple deformational events as well as a post tectonic phase. The talc mine is situated at the junction of two fault zones (Paltental-Liesingtal-Fault and SEMP). Structural data from the Lassing talc mine from *Neubauer* (2001) confirms the multiphase deformation phases and reveals some insights on the geology of the mine: Talc forms lenses and bodies confined by anastomosing fault planes. Lenses of talc represent the fault core while hostrocks constitute shear lenses or even boudins. The structures are related to NNE-SSW shortening and subvertical extension. The formation of such large talc bodies can be related to the activity of the fault zone with hot Si-bearing fluids concentrated within shear zones that formed networks of shear zones dissoluting Mg from the hostrock. After all Mg was used and abundant Si reactant was left over veins of quartz formed. Quartz samples from Lassing are posttectonic and have high Na-K temperatures (340°C). The large formation of talc was possible due to a rich occurrence of Mg carbonates and large amounts of Si bearing fluids. However such bodies are not seen in the Wald am Schoberpass deposit which is also related to the Paltental-Liesingtal-Fault. *Jordan* (1987) and *Handy* (1990) describe experiments and modelling that show the importance of rheology difference of materials for the formation of such bodies. The weak mineral phase is enriched with increasing strain and forms large bodies while the stronger mineral phase remains as lenses. The Na/Br and Cl/Br ratios

from Lassing are as well below the ratio of seawater and plot along the seawater evaporation line. Na/K temperatures are approx. 140-200°C. The carbonate samples from the Lassing talc deposit have a tendency to reflect the signature of marine carbonates with δ^{13}C values around 0. The reason can be found in the impermeability of marbles during metamorphism (*Nabelek et al.* (1984)). As a barrier they impede fluid flow and thus homogenization with the metamorphic fluid and keep their original sedimentary isotopic signature (*Valley et al.* (1990)) The carbonates from the Lassing deposit do not show a clear roof shaped REE pattern as the carbonates from Veitsch and Wald am Schoberpass. The Lassing samples have a tendency of depleted HREE and enrichment of LREE indicating remobilisation.

3.1.4 Conclusion

The study shows the significance of fault zones to the formation of talc. Even though talc mineralization is not exclusively linked to fault zone (*Evans & Guggenheim* (1991)), it did play an important role for its formation in the eastern Greywacke zone. The deposits investigated in this study are of similar hostrocks but differ in their distance to the fault zone. The Veitsch deposit is furthest away from the Mur-Mürz-Fault and no talc occurrence is reported. In addition geochemical analysis and field study supports the low deformation and low temperature metamorphism at the deposit. For the Wald am Schoberpass deposit at the Paltental-Liesingtal-Fault higher deformation and temperature are reported and talc occurs as impurities along discrete cm to dm shear zones. Deformation structures and temperatures may be linked to subsidence events following Eo-alpine orogeny. The Lassing talc deposit was - until its closure in 1998 - the second largest talc mine in Austria. Its tectonic features give hints of high deformation along one of the major Oligocene to Miocene fault zones of the Eastern Alps.

3.2 Gemerska Poloma

The talc deposit of Gemerska Poloma is situated approx. 60 km west of Košice in the eastern part of Slovakia. The aim of the study is to investigate the origin and characteristics of the fluids that led to the formation of talc as well as the mechanism and timing of the talc formation.

3.2.1 Geology

3.2.1.1 Geological setting

The Carpathians are generally subdivided into Western-, Eastern- and Southern Carpathians.

The Gemerska Poloma talc deposit is part of the Central Western Carpathian Gemer unit. The Western Carpathians can be subdivided into three superunits: Outer Western Carpathians (OWC), Central Western Carpathians (CWC) and in the south the Inner Western Carpathians (IWC). Each unit is separated by oceanic units the Pieniny Klippen belt (separating the OWC and CWC, *Dal Piaz et al.* (1995)) and the Meliata belt (separating the CWC and IWC). The CWC can be further subdivided into three principal crustal-scale superunits from base to top: Tatricum, Veporicum and the Gemericum, which represent the lateral extension of the Austroalpine units of the Eastern Alps (*Dallmeyer et al.* (2008), fig. 3.18). Several cover nappe systems complete the succession: Fatric, Hronic and Silicic. The Gemericum consists of Early Palaeozoic to early Late Carboniferous low-grade metasediments and metavolcanics intruded by small bodies of Permian granitiods and represents the equivalent of the Austroalpine Greywackezone. Its alpine metamorphism reached 350°C with medium pressure (*Krist et al.* (1992)). Within the Early Palaeozoic rocks of the Gemericum three principal complexes can be distinguished: Rakovec, Kltov and Gelnica forming the Volovec group which comprises in the lower part (Betliar formation) detritic phyllites and black laminated pelites and silts as well as green phyllites and flysch psammites to pelites (Smolnk formation) and finally in the upper part (Hnilec Formation) volcanic. The northern complexes (Rakovec and Kltov) contain magnesite deposits.

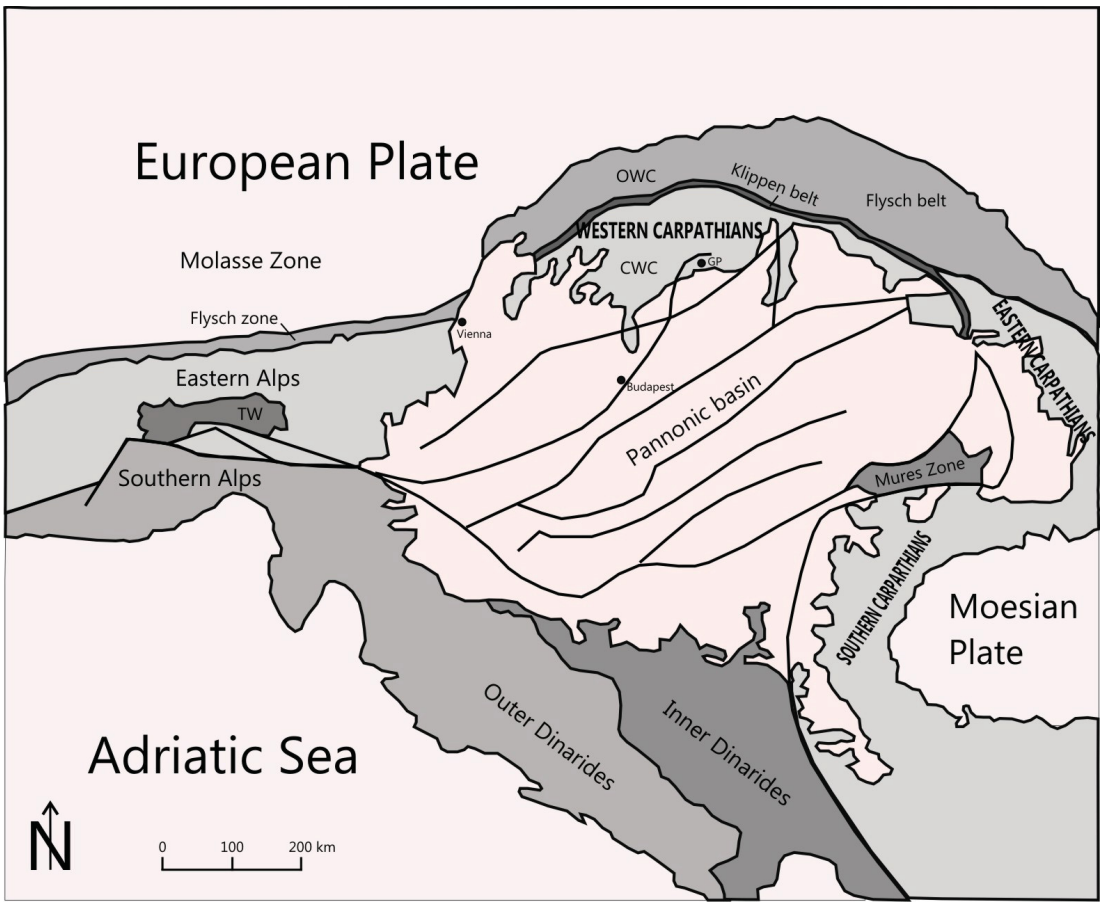

Figure 3.18: *Geological Scetch of the Pannonian Basin and Carpathians with the adjacent Eastern Alps. TW - Tauern Window, GP - Gemerska Poloma Talc deposit. Modified after* Plašienka et al. *(1997)* .

3.2.1.2 Tectonic evolution

The pre-Alpine basement of the Western Carpathians was part of the inner and outer Variscan zones (*Plašienka et al.* (1997)). Different terranes such as the Noric terrane (*Frisch et al.* (1998)) and the so called "Pre-Carpathian terrane" (*Putiš* (1993)) were situated on the northern continental margin of Gondwana and were accreted during Variscan orogeny by closure of Palaeozoic oceanic basins (Prototethys during Late Devonian and Palaeotethys during Early Carboniferous). The Gemericum being related to the Greywacke Zone was separated from the Pre-Carpathian terrane by the Palaeotethys. In the back-arc position of the northward subducting Palaeotethys a deep-water basin formed which developed into the ophiolitic Rakovec complex. After the climax of Variscan orogeny molasse sedimentation started during Permian and subsidence with shelf sedimentation affected the newly formed continent Pangea.

The still ongoing subduction of the Palaeotethys until the Triassic led to the opening of the Meliata-ocean in its back-arc position. Due to the breakaway of the Meliata rift the carbonate ramp was disintegrated into elevating and subsiding domains and became a mature passive continental margin with the Gemericum at its southern most point. During Early Jurassic the CWC together with the Austro-Alpine experienced extensional stress as a result of the opening of the Atlantic ocean. Deep marine basins and elevated highs developed and finaly led to the opening of the Penninic ocean, separating the CWC from the European shelf. Along with these events the Meliata-ocean started its southdirected subduction and locked up during the Upper Jurassic and induced shortening and nappe stacking while overriding the Gemericum. During these events the Gemericum at the southern margin of the Slovakocarpathian domain was overrode by Meliata-derived glaucophanized basalts that yield Ar/Ar phengite ages of 150–160 Ma (*Faryad & Henjes-Kunst* (1997)). The locking of Meliata in Early Cretaceaous goes along with obduction processes. The Veporic core complex (North of the Gemericum) was effected by obductional processes by burial due to its lower plate position with subsequent thermal equilibration and exhumation by east-verging unroofing.
These northdirected tectonic events proceeded for most of the Cretaceaous and ended in the subduction and closure of the Penninic ocean. During these events

parts of the Slovakocarpathian domain were submerged below sealevel and Gosau sediments were deposited (*Wagreich* (1993)). With the closure of the Penninic ocean and the collision of the passive margin north (OWC) and the active margin to the south of the Penninic ocean (Tatricum) the Klippen and Periklippen belt was formed (Late Cretaceous).

The hostrocks of the Gemerska Poloma talc deposit consist of metasedimentary rocks and metavolcanics of the the Smolnk and Hnilec Formation respectively. The steatitionized magnesite body is part of the Smolnk Formation. To the footwall the magnesite body is confined by a tectonized zone. The footwall rock is a Late Palaeozoic granitoid body (Fig.3.19).

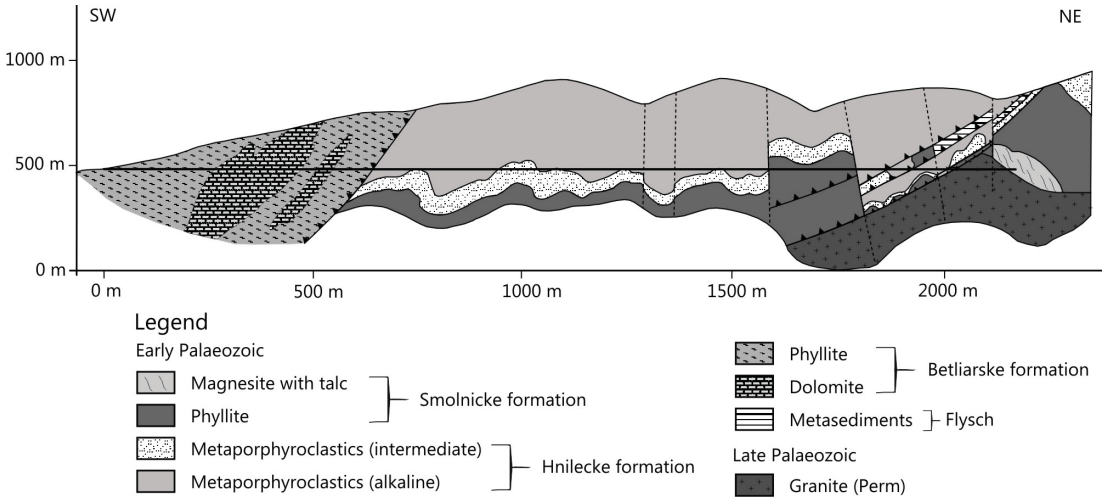

Figure 3.19: *Profile of the Gemerska Poloma talc deposit.*

3.2.2 Results

3.2.2.1 Sample description

At the Gemerska Poloma talc deposit talc appears to be intergranular or as large pure lenses and veins within a magnesite body. It is mostly massive but may also appear flaky and radial fibrously. The color is generally white to lightly green. Less often it may also be grey to black due to chlorite- and graphite impurities.

The contact zone between talc and magnesite is often marked by pyrite (grainsize 0.5 cm).

The magnesite has a whitegrey to greyblack color and is middle to coarsegrained, partly sparry. Generally it has a very compact form. Besides the talc lenses and veins, the magnesite body is penetrated by veins of secondary quartz and dolomite (horse tooth dolomite). For sample description see also fig. 3.20.

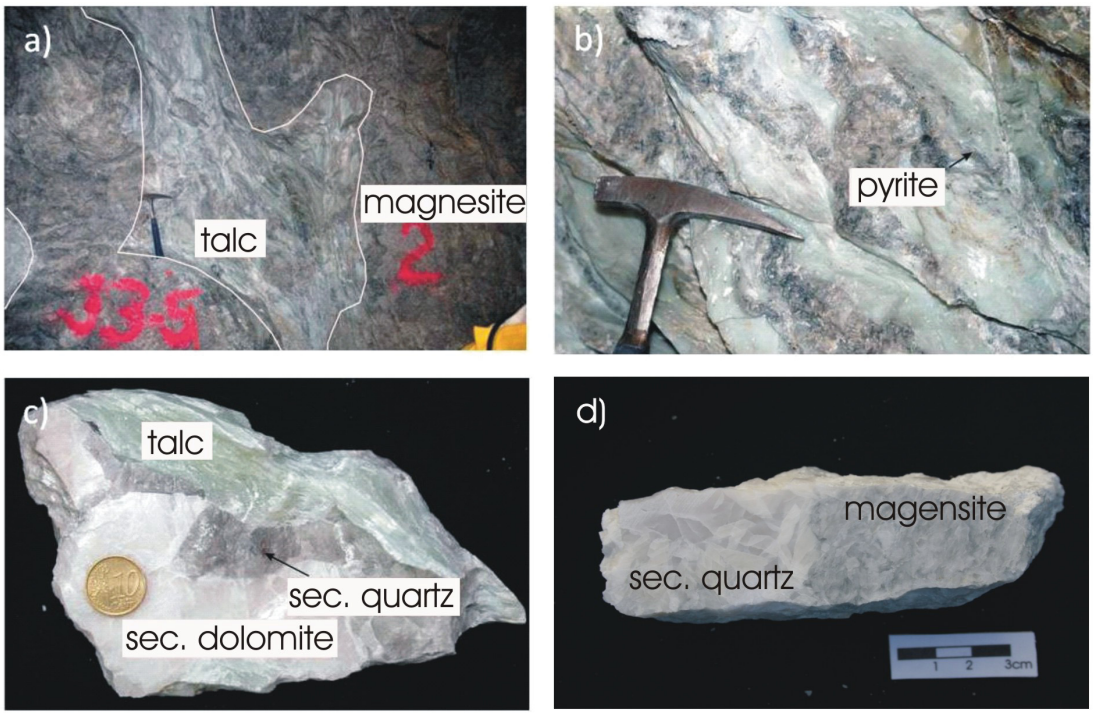

Figure 3.20: *Rocks of the Gemerska Poloma talc deposit a) talc zone within magnesite body, b) pyrite in talc and magnesite, c) talc zone with secondary quartz and dolomite, d) magnesite with secondary quartz vein.*

A closer look on secondary minerals as quartz and dolomite gives another hint on the geological evolution of the deposit. While secondary horse tooth dolomite formed after magnesitisation (fig. 3.21a) simultanously with secondary quartz a younger quartz generation is formed as well. Secondary horse tooth dolomite and quartz grains appear to be large. In addtion quartz grains show signs of bulging such as uneven grain boundaries and undulose extinction (fig. 3.21b) . Also secondary minerals are often broken and fractures are filled with younger small grained quartz crystals with even grain boundaries, triple points and no

sign of undulose extinction ((fig. 3.21c) & fig. 3.21d). The deformation features observed in the thin-sections indicate low-temperature deformation of 300–400°C.

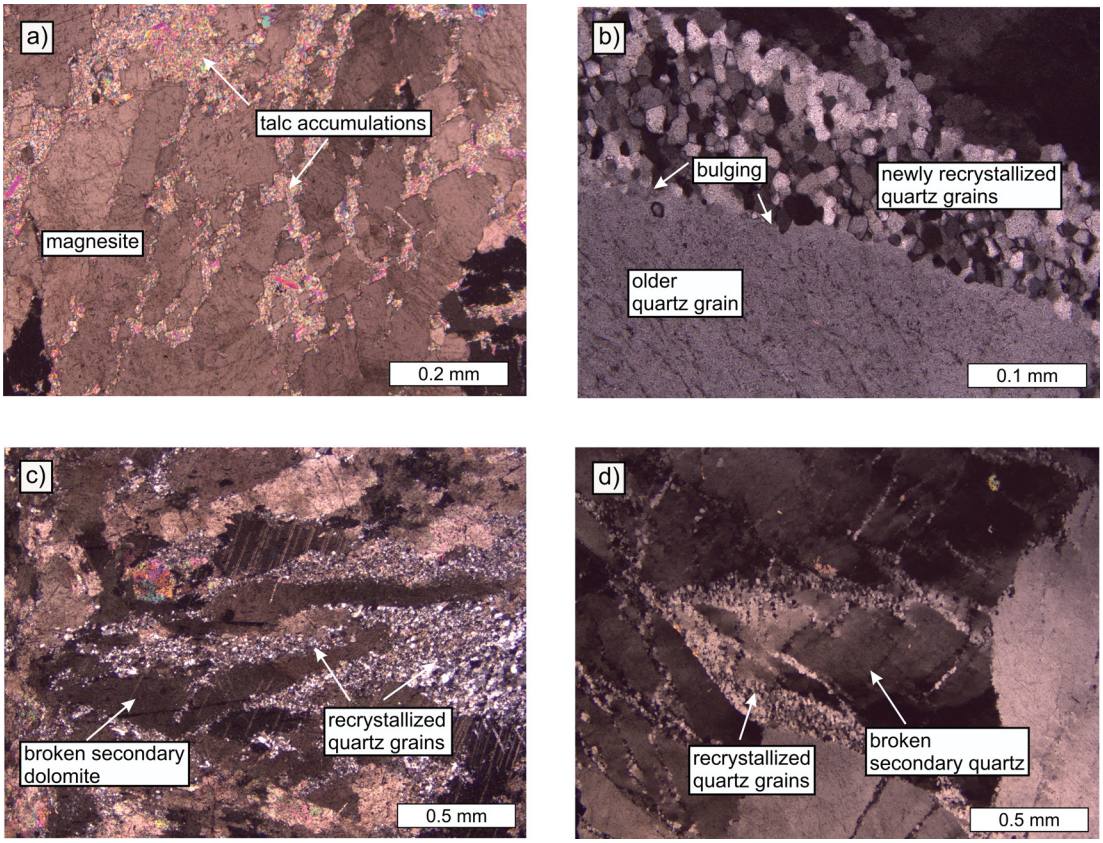

Figure 3.21: *Thinn-sections of carbonates of the Gemerska Poloma talc deposit: a) magnesite hostrock with talc accumulations (GP 8), b) older large grains of secondary quartz are dynamically recrystallized and new small grains of quartz formed (GP 42), c) fractured secondary "horse tooth dolomite" grains with vein fillings of recrystallized quartz (GP 39) d) fractured quartz grains with vein fillings of recrystallized quartz grains (GP 42).*

The altered granitoid body to the footwall of the magnesite body shows attributes of chloritisation. Quartz grains give hints to dynamic recrystallization by lobate grain boundaries and undulose extinction. Interspaces and fractures are filled with chlorite and newly formed quartz grains (fig. 3.22a). Feldspar crystals occur rarely and if present are highly disintegrated (fig. 3.22b).

Samples from the tectonized contact zone between the footwall granitoid body and the magnesite body show elongate interlobate small sized quartz grains within

a matrix of gouge material (fig. 3.22c).

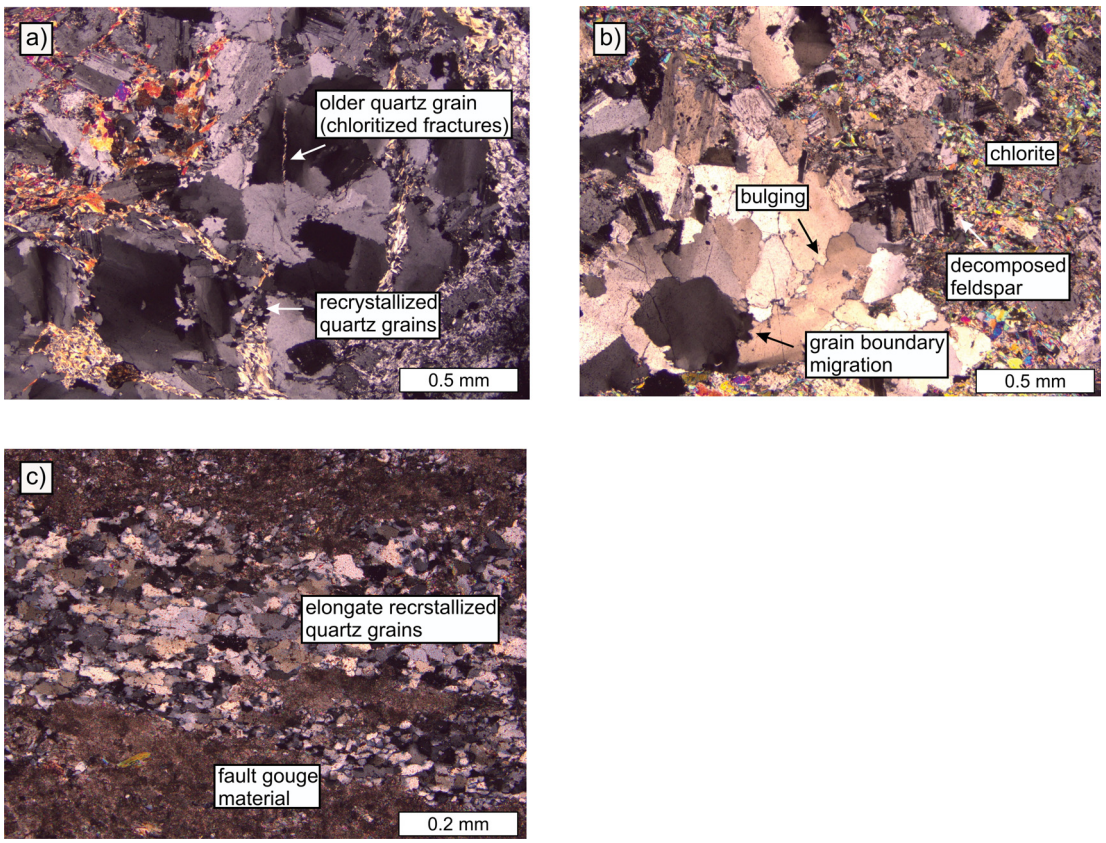

Figure 3.22: *Thinn-sections of granitoid bodies of the Gemerska Poloma talc deposit: a) partly fractured quartz grains filled with with chlorite and recrystallized quartz (GP 7), b) decomposed feldspar in the granitoid body and newly formed chlorite, quartz grains show signs of dynamic recrystallization by bulging and grain boundary migration (GP 7), c) rocks from the tectonized zone show elongate newly recrystallized quartz grains and a matrix of gouge material (GP 45)*

3.2.2.2 Major, minor, trace elements

The content of MgO in the magnesites is 40.44 – 41.64 wt% and CaO contents are slightly elevated (0.46 – 3.65 wt%) while in the secondary dolomite MgO is 19.19 – 20.68 wt% and CaO is 28.28 – 29.90 wt%. Strontium contents in the magnesite are elevated (5 – 24 ppm). As a replacive element for Ca Sr is built into the lattice of secondary dolomite (53 – 77 ppm). SiO_2 shows values be-

tween 2.25 – 9.34 wt% (magnesite) and 0.68 – 5.23 wt% (secondary dolomite). The enrichment of silica in magnesite is due to talc impurities. Aluminum contents are comparable in magnesite (0.04 – 0.09 wt%) and secondary dolomite (0.03 – 0.36 wt%). A difference in element concentration between magnesite and secondary dolomite is detectable for Fe_2O_3 (4.05 – 6.95 wt% and 1.28 – 3.03 wt% respectively). Other minor and trace elements within carbonates are below or at least very close to the detection limit.

3.2.2.3 REE pattern

Rare earth element distributions of magnesite and secondary dolomite were measured. The magnesite samples have a roof-shaped REE-distribution and are slightly enriched in HREE. An exception is sample GP 16 which is enriched in LREE and depleted in HREE. Two of the magnesite samples have a weakly pronounced positive Eu anomaly. Secondary dolomite shows a rising REE pattern with depleted LREE (fig. 3.23a). The precursor dolomite shows a roof-shaped REE-distribution pattern with positive Eu-anomaly and depleted HREE (fig. 3.23b).

3.2.2.4 Stable Isotopes

Stable Isotopes of carbonates (magnesite and secondary dolomite) and secondary quartz were analyzed. Samples of magnesite show a very distinct pattern with values of $\delta^{13}C$ = -5.51 – -1.23 ‰ and $\delta^{18}O$ = 12.78 – 16.54 ‰ (fig. 3.24). The secondary dolomite show far less variation with $\delta^{13}C$ = -6.35 – -3.67 ‰ and $\delta^{18}O$ = 12.26 – 13.44 ‰ .

Oxygene Isotopes of quartz have values of $\delta^{18}O$ = 11.98 – 14.41 ‰ and are in equilibrium with secondary dolomite samples taken in the same spot.

3.2.2.5 Ion-chromatography

Crush leach analysis were performed on carbonate rocks and secondary quartz. Mg ions are present at a very similar level within all carbonate rocks (0.8 – 1.3

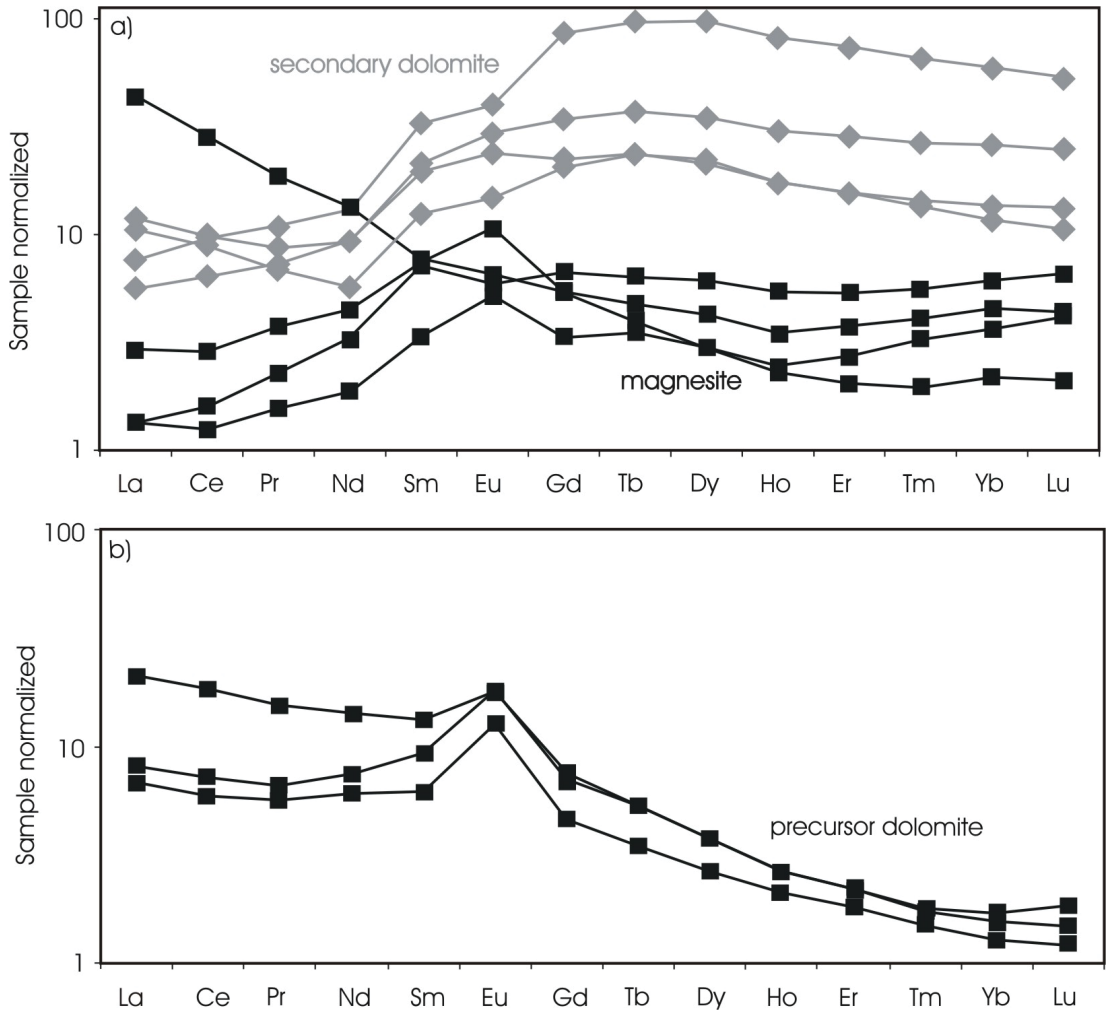

Figure 3.23: *Chondrite normalized REE patterns of a) magnesite and secondary dolomite from the Gemerska Poloma talc deposit. Secondary dolomites from the talc zones have a prominent enrichment in HREE (especially Gd-Dy); magnesites are generally depleted in REE compared to secondary dolomites and are also enriched in HREE, though not as clearly with partly positive Eu anomalies. b) Chondrite normalized REE patterns of precursor dolomite with positive Eu-anomaly and depleted HREE.*

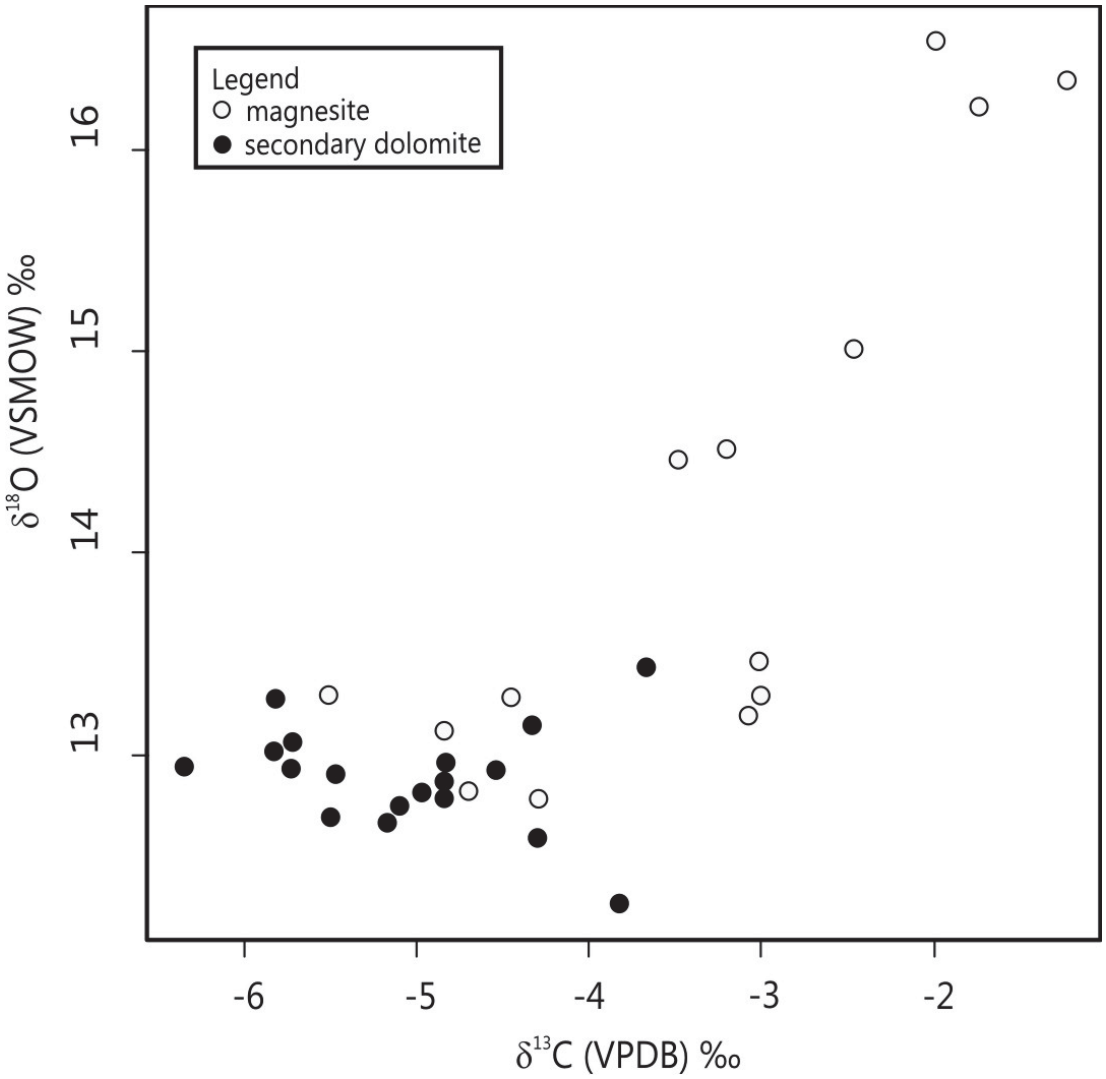

Figure 3.24: *Carbon and oxygene stable isotope data. Secondary dolomites are depleted both in carbon and oxygene isotopes. Magnesites are also generally depleted in carbon and oxygene isotopes.*

mol) but almost absent within silicates (0.0004 – 0.1 mol). The presence of Ca is limited to secondary dolomite. The distribution pattern of the samples relating the ions Na, Cl and Br is very similar. Samples from the deposit show high values of Na, Cl and Br (0.48 – 0.99 mol (Na), 0.62 – 1.23 mol (Cl), 0.005 – 0.01 mol (Br)). Also high values of Li can be observed in carbonate rocks (high in magnesite and secondary dolomite (0.018 – 0.084 mol). But are significantly lower in samples of secondary quartz from the talc zone (0.001 – 0.005 mol). For all carbonate rocks the I content is at a similar level ($2.87*10^{-5}$ – $4.74*10^{-5}$) and substantially lower for quartz samples ($2.99*10^{-6}$ – $2.40*10^{-5}$ mol). The K content varies between 0.03 – 0.08 mol with no significant pattern and F content is < 0.0023 in all samples.

As the absolute amount for ions in fluid inclusions may vary with the amount of fluid inclusions in the mineral phase, the ratio of certain elements is more meaningful. The ratio of certain elements in relation to Br is of special interest. Na, Cl and Br are abundantly occurent in seawater. While Na and Cl form NaCl with ongoing evaporation of seawater, Br behaves rather conservatively and remains in the solution during evaporation. Thus with the continuation of the evaporation process Na and Cl and further also Mg and K are depleted and Br is enriched in the solution. High values of Br then indicate high evaporational processes. The Na/Br ratios (molar) varies between 72.26 – 110.82. For secondary quartz values are higher (111.09 – 257.48). The values of the Cl/Br ratio (molar) is 109.57 – 152.16 (fig. 3.25). For magnesite and secondary dolomite Li/Na values (molar) are highest (0.04 – 0.08) and significant lower (0.002 – 0.005 for secondary quartz, fig. 3.26).

Na-K-Temperatures of magnesite, secondary dolomite and secondary quartz vary between 240 and 270°C. Only one quartz sample (GP 42b) has a significantly lower temperature of 216°C.

Charge balance ($Q^+/Q^- = 1$) for carbonate rocks is imperfect with values 2.4 and 11.4. For quartz samples charge balance is close to being perfect with values between 1.1 and 1.5. The imperfect charge balance within the carbonate samples might be due to volatile phases lost during the crushing process.

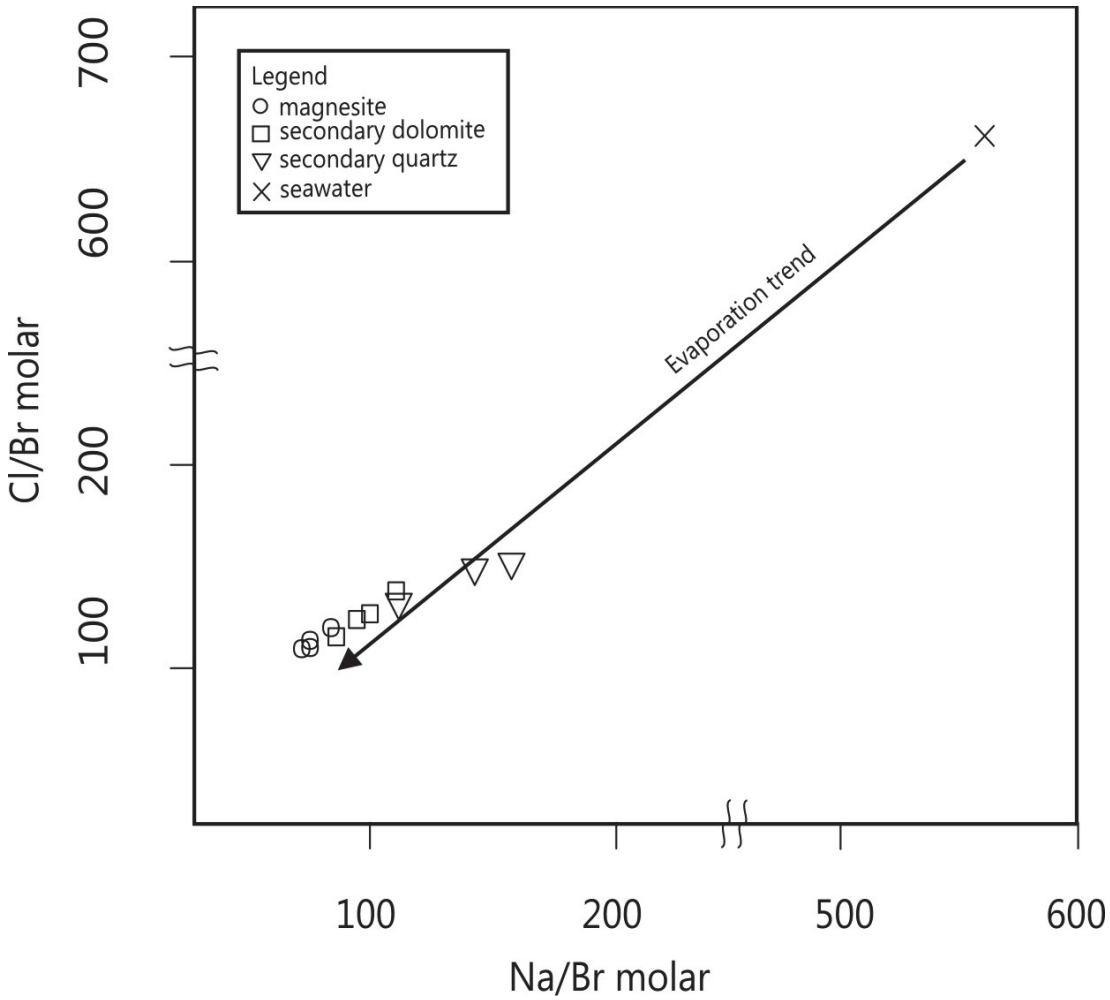

Figure 3.25: *Na/Br to Cl/Br ratios of fluid inclusions from hostrock minerals (magnesite and precursor dolomite) and minerals from the talc zone (secondary quartz and secondary dolomite). All fluid inclusions show ratios far beyond the composition of seawater and follow the evaporation trend.*

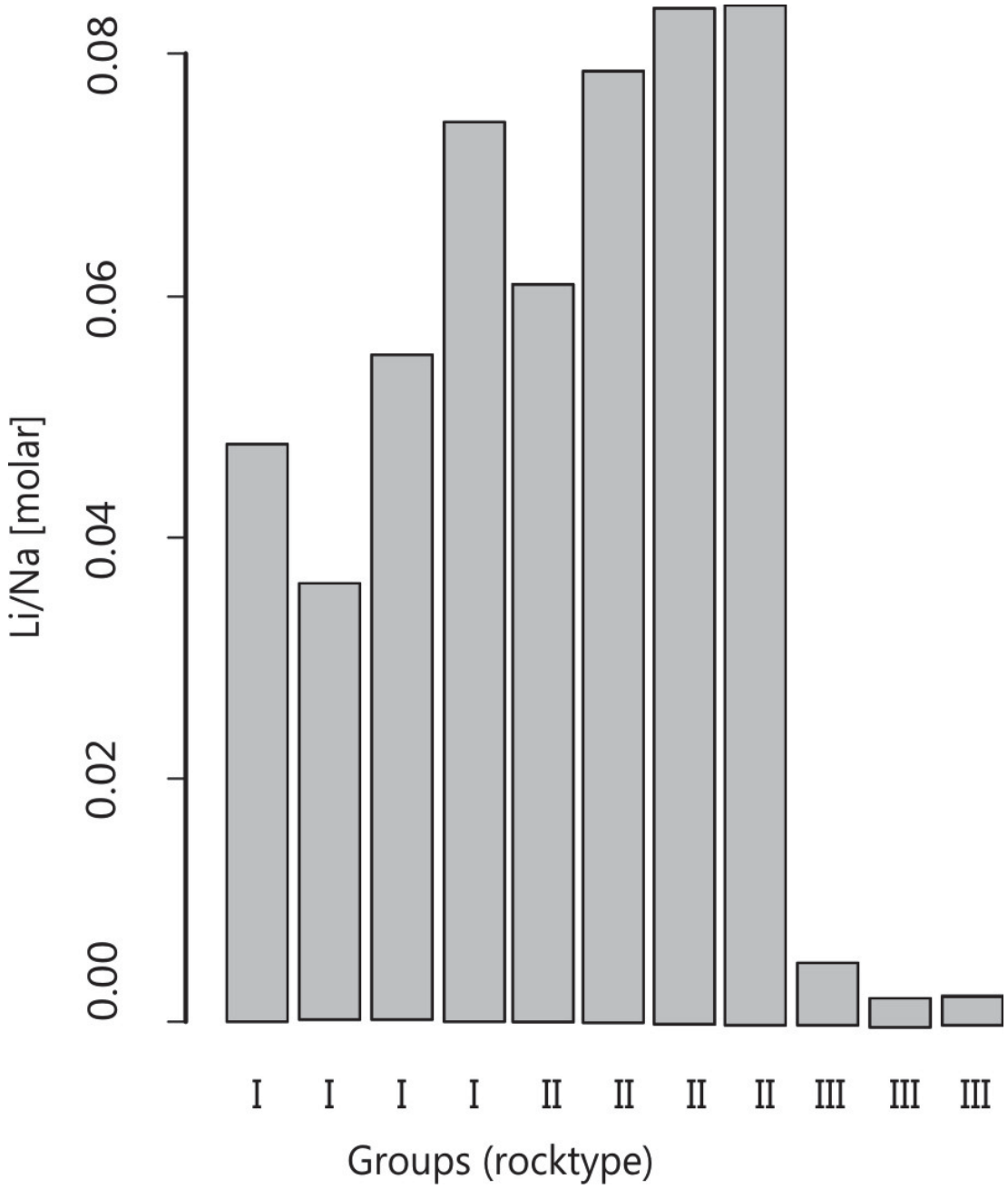

Figure 3.26: *Li/Na ratios of fluid inclusions (group I - magnesite, group II - secondary dolomite, group III - secondary quartz).*

3.2.3 Discussion

The main features of the Gemerska Poloma talc deposit are the steatitized magnesite body in the hanging wall position and the granitoid body in the footwall position. Both are separated by a tectonized zone.
Mineralizations suggest the activity of several geological events. First, the magnesite body is clearly penetrated by large anastomosing shearzones with talc mineralizations. These are accompanied by quartz and horsetooth dolomite mineralizations, which are mostly large grains that show signs of deformation. Quartz features and twinning of dolomite propose deformation temperatures of 300–400°C (*Stipp et al.* (2002)). The quartz and dolomite grains are partly fractured. The interspaces are filled with another generation of quartz grains. In contrast these show no signs of deformation and can be considered to be posttectonic.
The granitoid body in the footwall position is strongly altered. Quartz grains show signs of dynamic recrystallization. They are partly fractured and refilled with chlorite and recrystallized quartz grains. The matrix of the granitoid is widely made of chlorite. Feldspar grains are only left as residual grains and are almost completly decomposed. This trend seems to be stronger for rock samples closer to the tectonized zone.
Material from the tectonized zone shows highly dynamically recrystallized quartz grains with elongate interlobate features and a weak shape preferred orientation (grain boundary migration, i.e. ∼500°C, according to *Stipp et al.* (2002)) and a matrix of fine grained gouge material.
The deformation features of the quartz grains in the carbonates as well as granitoid body and tectonized zone suggest differing concentration of deformation. Quartz grains in the magnesite body and the granitoid body show bulging which indicates low temperature dynamic deformation. Twinning in secondary dolomite indicates a similar temperature range (*Burkhard* (1993), *Ferrill et al.* (2004)). In contrast quartz grains from the tectonized zone with grain boundary migration indicates higher temperature and dynamic deformation. Accordingly a concentration of stress within the tectonized zone can be assumed.
All this indicates that at least part of the talc mineralization is tectonically controlled. Talc as a weak mineral phase accomodates stress. It is formed from Mg deriving from the magnesite body and Si-rich fluids. The talc forming reaction

ceases when Mg is no longer available. The abundance of Si is evolved into quartz nodules within the talc zone. The tectonic features of the quartz nodules are an indicator for the dynamic processes during talc formation.

According to *Kralik et al.* (1989) the C and O isotopte signatures for sparry magnesite (type "Veitsch") are in the range of δ^{13}C = -7 to +4 ‰ (VPDB) and δ^{18}O = 6 to 25 ‰ (VSMOW) respectively. This type of magnesite is assumed to have been recrystallized from precursor rocks during metamorphism or hydrothermal events (*Kralik et al.* (1989), *Pohl* (1990), *Schroll* (2002)). Magnesite forms under diagenetic to metamorphic (generally greenschistfacies) conditions from dolomitic precursor rocks. The stable isotope data measured during this study confirm the metamorphic origin of the fluids that led to the formation of magnesite. The samples of magnesite analysed show a trend towards lighter C and O isotopes, while secondary dolomite shows even lighter C and O values. According to Zheng & Hoefs 1993 this pattern can be attributed to fluid mixing. The magnesite samples were affected by different fluid types with values between δ^{13}C = -8 to -2 and δ^{18}O = 10 to 15. Both can be regarded as endmembers. The first signature is that of slightly depleted marine water, the second is that of metamorphogenic origin. The secondary dolomite is depleted in C and O isotopes – thus its fluid is of metamorphogenic origin, too. It can be assumed that the fluid event that caused the crystallization of the secondary dolomite also affected the magnesite hostrock. In conclusion the stable isotope study suggests the formation of magnesite under low metamorphic conditions and a later overprint of the magnesite body with the precipitation of talc, dolomite and quartz contemporaneously.

The very low Na/Br and Cl/Br ratios are common in all samples from the Gemerska Poloma talc deposit. They plot along the seawater evaporation line and are well below the typical ratio of seawater (Cl/Br = 658 (*Gleeson* (2003))). Generally such fluids are of high salinity such as evaporitic fluids. It is remarkable that all types of minerals that were analyzed show a very similar signature of Na/Br and Cl/Br ratios. Earlier publications confirm these observations (Radvanec & Prochaska 2001, Radvanec et al., 2004). For the magnesite bodies of the Eastern Greywacke Zone *Prochaska* (2000) suggests residual evaporitic bitter brines that percolated through the crust during Permoskythian rifting. A similar formation process for magnesite can be assumed due to the relationship of the Gemericum

and the Eastern Greywacke Zone (*Dallmeyer et al.* (2008)). However the commonly low Na/Br and Cl/Br ratios in all mineral assemblages at the Gemerska Poloma talc deposit suggests that the talc formation was affected by a hydrothermal event postdating magnesite formation. This kind of fluid must have been a highly fractionated one with Br enrichment along its migration through the crust. Na-K temperatures of samples are between 240° and 270°C and are an important indicator for the metamorphic origin of the fluids that first affected the magnesite formation and later led to the precipitation of secondary quartz and dolomite along with the talc formation.
Another important feature of the rock samples are the high Lithium concentrations in carbonate rocks. Typically the Li/Na ratio is below 0.01 but are as high as 0.08 at the Gemerska Poloma talc deposit. This indicates an association of the carbonate forming fluids with the footwall granitoid body. *Hurai et al.* (2011) attributes the phenomenon to an upward directed fluid migration from the Li-rich footwall granitoid body.

The high REE contents of the magnesite body outrule the possibility of a marine origin of the magnesite. According to *Möller* (1989) REE values increase with the induction of hydrothermal fluids during diagenesis. The roof-shaped pattern of REE distribution of the magnesite with a tendency of enriched HREE suggests multiple processes that affected the magnesite body. The roof-shaped pattern gives hints to the existence of Mg-solutions and HREE were enriched during mobilisation processes (*Schroll* (1997)). The pronounced positive Eu-anomaly indicates that the fluid overprinting the magnesite body has a common origin with the footwall granitoid body, since feldspars are the only magmatic rock-forming minerals with excess of Eu (*Möller* (1989), *McLennan* (1989)). Further the Eu-anomaly is a temperature indicator suggesting that the mineralizing fluid had a temperature >200°C (*Bau & Möller* (1992)).
Secondary dolomite is enriched in REE compared to the magnesite hostrock. This may be due to the substitution of REE for Ca^{2+} in dolomite. The roof-shaped REE pattern of the secondary dolomite can be attributed to hydrothermal waters of crustal origin according to *Hecht et al.* (1999), who describes similar observations for vein filling dolomite in the talc deposit of Göpfersgrün.

So far two models are proposed to explain the formation of talc in the Gemerska

Poloma talc deposit. *Malachovský et al.* (1992) was the first one to attribute the talc formation to contact metamorphism and was followed by *Kilík* (1997), *Turanová et al.* (1997) and *Petrasová et al.* (2007). In contrast according to *Radvanec et al.* (2004) explain the transformation of magnesite into talc by regional metamorphism during Alpine orogeny.
Petrasová et al. (2007) calculated p-T conditions from geochemical data that yield temperatures of 430°C at 1 kbar and $X_{CO_2} = 0.8$ and conclude that the main talc-formation was related to metasomatic alteration related to the Permian granite magmatism. Similar assumptions have been made by previous authors. However the existence of a large tectonized zone between the granitoid body and the steatitized magnesite body and the absence of relevant occurences of contact metamorphic mineral phases are important indicators that outrule the thesis of contact metamorphism for the formation of the talc zones.

The results of this study can be interpreted as a two step genetic process. Magnesite was formed at typical sparry magnesite Veitsch type conditions and was later affected by a second event that lead to the precipitation of secondary dolomite, which coincided with the precipitation of talc and secondary quartz. The fluid conditions modeled according to *Zheng & Hoefs* (1993) show clearly the effect of two separate fluid events with one of them coinciding with the precipitation of the secondary dolomite and overprinting the magnesite body. It can be related to the formation of talc as the secondary quartz and dolomite occur as mineralisations withing the talc shearzones. Both secondary mineral phases were affected by deformation of greenschist-facies conditions. K-Na temperatures of fluid inclusion study propose temperatures up to 270°C and are in rough accordance with temperatures estimated from deformation structures in quartzes.

The two models that are proposed are the one according to *Petrasová et al.* (2007) with a contact-metamorphic origin of the fluids and the one from this study where SiO_2-rich fluids evolve during shearzone deformation and induce talc formation within the magnesite body. Both models are illustrated in simplified sketches (fig. 3.27)

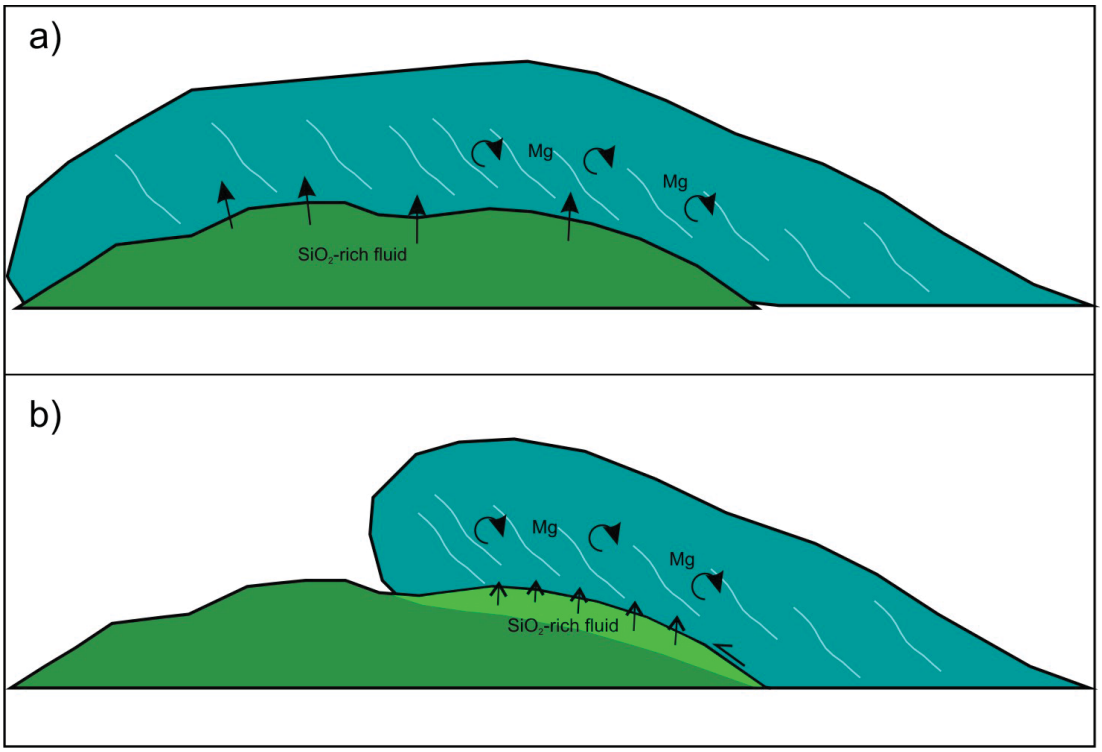

Figure 3.27: *Simplified sketches of the two theories of talc formation at the Gemerska Poloma talc deposit. a) model of contact-metmorphic fluids by* Petrasová et al. *(2007) and b) model of this study by fluids generated during shear zone deformation*

3.2.4 Conclusion

The Gemerska Poloma talc deposit is affected by a large (0.5–30 m) tectonized zone, that separates the steatitized magnesite body in the hangingwall position from a granitoid body in the footwall position. Such fault zones enhance fluid flow drastically (*Caine et al.* (1996)) and may even lead to the formation of ore deposits (*Tagami* (2012)).

The origin of the fluids that led to the precipiation of talc can be traced to the tectonized zone that enhanced fluid flow during fault slip. An important indicator are the high Li/Na ratios in the carbonate samples. According to *Hurai et al.* (2011) such high Li/Na ratios in fluid inclusions may generate from the Li-bearing granitoid body in the footwall position. Also the Eu anomaly in the secondary dolomite and magnesite shows that fluids from the granitoid effected the carbonates as a positve Eu anomaly is attributed to the decomposition of feldspar (*Möller* (1989)). Thus it can be concluded that during fault slip and mylonitization of the granitoid body mineral assemblages decompose and elements are dissolved and transported. With increasing stress and networks of faults developed in the magnesite body and were filled with talc and remnants of quartz and dolomite. Deformation features in the secondary mineral assemblage show that deformation was the driving factor for the talc precipitation. Temperature estimations from fluid inclusion study, stable isotope study and microsturcture study confirm that talc formation was induced during fault slip deformation.

3.3 Sardinia

The talc deposits of Sa Matta and Su Venosu are situated in central-Sardinia, approximatly 20 km southwest of the city of Nuoro.
The aim of the study is to investigate the origin and characteristics of the fluids that lead to the formation of talc and the role that the Nuoro shear zone played. In addition it was intended to date the hydrothermal event by the means of (U-Th)/He dating.

3.3.1 Geology

3.3.1.1 Geological setting

In the past the geological units were grouped into three tectonic zones that reflect the tectonic evolution of the Sardinia-Corsica block (see fig. 3.28). From the north to the south of Sardinia these are: the axial zone, the nappe zone, the external zone. The axial zone in the north of Sardinia and in the west of Corsica represents the remnants of the former oceanic basins. *Cappelli et al.* (1992) propose that these oceanic remnants are part of the South Armorica-Massif Central ocean that branced into northern Sardinia and forms now a south Variscan suture zone – the Posada-Asinara Line. This zone is marked by NE trending strike slip faults. The nappe zone is composed of several nappes with top-to-the-south directed folding towards the unmetamorphosed foreland (external zone) in the southwest of Sardinia (*Conti et al.* (2001)). Deformation and metamorphism decreases from north to south.
Recent interpretation (*Helbing* (2003) and *Helbing et al.* (2006)) suggest that such a division is questionable and that the axial and nappe zones of the Sardinian Variscides belong to the same tectonostratigraphic domain and the Posada- Asinara Line cannot be regarded as a suture zone. Therefore the northern alpine part of Corsica marks the collisional zone of the Sardinia-Corisca block with remnants of alpine nappe stacking while the northeast part of Sardinia is marked by transtensional structures.

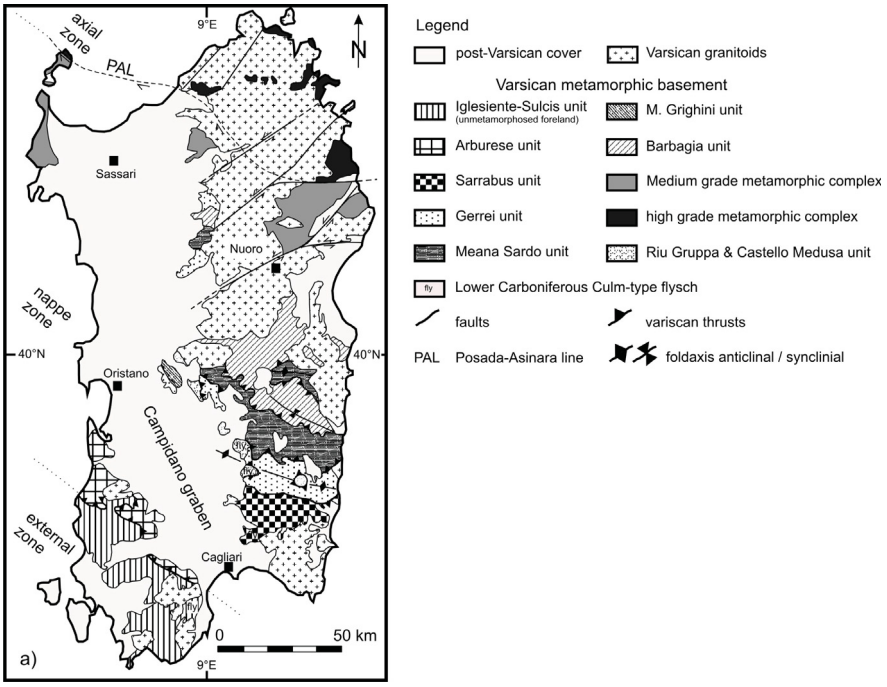

Figure 3.28: *Geological sketch of Sardinia, modified after* Conti et al. *(2001).*

3.3.1.2 Paleozoic history

The Paleozoic geological evolution of Sardinia comprises two phases of mountainbuilding: the early sardic event with folding during Ordovician and the Variscan event starting with the separation of the Paleozoic basement from the Gondwana mainland during Early Ordovician (*Stampfli et al.* (2002)) and the final accretion to northern Laurussia by the closure of two oceanic basins (Rheic ocean and Rheno-Hercynian ocean). The collision of the two continents along with mountainbuilding is further indicated by isoclinal folding and the formation of antiform and synforms within the nappe zone (*Conti et al.* (2001)). Also Culm-type flysch sedimentation (*Barca et al.* (1992)) is incorporated into the nappe pile with the latest deposit covering the nappe front indicating that exhumation and uplift lasted until Late Carboniferous times (*Barca* (1991)). The post-collisional phase of the Varsican orogeny is marked by post tectonic magmatism as the Corsica-Sardinia batholith which forms parts of Corsica and Sardinia.

3.3.1.3 Post-Variscan history

With the break-up of the Pangea supercontinent the geological history of Sardinia took a turn from compressional tectonics to extensional tectonics. The Paleozoic basement is now marked by Permo-Triassic extensional volcanics such as alkaline intrusions as well as sediments and vast carbonate platforms covering Sardinia completely during Jurassic times (*Cocozza & Jacobacci* (1975)). At that time the Sardinia-Cosica block was still part of the Iberian plate and fluvial sedimentation of the molassic Cixerri formation in the southwest of Sardinia derive from Pyrenean uplift and erosion during Late Cretaceous - Paleocene times (*Olivet* (1996)). The northdirected movement of the African plate, resulted in the complete closure of the penninic oceans and the westward movement of the alpine front. It is now that the Apennine subduction zone starts to form south of the Corsica-Sardinia block (*Lacombe & Jolivet* (2005)). The ongoing Apenninic subduction zone led to continental rifting between southern France and the Corsica-Sardinia block and finally to ocean spreading and the opening of the Ligurian-Provençal basin (*Cherchi & Montadert* (1982), *Sérrane* (1999)). This resulted in a $\sim 30°$ counter-clockwise rotation around 21 to 16 Ma (Burdigalian, fig. 3.29 a & b). The Sardinian rift in the west of Sardinia is related to these events (*Vigliotti & Langenheim* (1995), *Casula et al.* (2001)) and cross-cut the structures of the transpressional zone (*Carmignani et al.* (1995)). Another basin (Tyrrhenian basin) was formed east of the Corsica-Sardinia block due to ongoing subduction (*Rosenbaum & Lister* (2004)). These events caused the formation of the NNW-SSE trending Campidano graben in the southwest of Sardinia in Middle-Upper Pliocene (*Casula et al.* (2001))

3.3.1.4 Fault system in NE Sardinia

The Nuoro fault (fig. 3.30) is a major fault in the northeast of Sardinia. Similar faults in this area are the Tavolara fault and the Olbia fault. These faults are left-lateral strike-slip faults and are accompanied by subvertical approx. EW trending dextral strike-slip faults, e.g. the Cedrino fault (to the Nuoro fault) and the Posada fault (to the Tavolara fault). These faults are considered to be antithetic in respect to their main faults (*Carmignani et al.* (1992)). The Nuoro

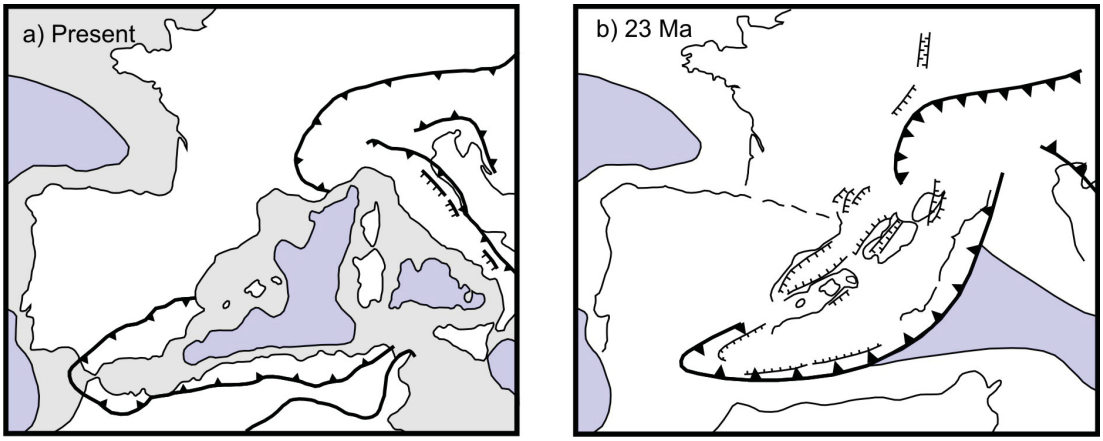

Figure 3.29: *Reconstructions of the western Mediterranean a) Present and b) 23 Ma ago during Lower Miocence. Modified after* Lacombe & Jolivet *(2005)*

and Tavolara faults form a conjugate system with the Cendrino and Posada fault respectively (fig. 3.30a). The activation of these faults are linked to the extensional tectonics of the sardinian rift and the formation of the Tyrrhenian basin. The Nuoro fault strikes ENE to WSE along Mount Albo, a Meso-Cenozoic carbonate massif, and extends for about 60 km from Orani in the southwest to Siniscola in the northeast (*Carmignani et al.* (1992)). It forms a negative flower structure with the Cedrino fault (*Helbing* (2003), fig. 3.30b) that is related to the contemporaneous extensional setting which led to the formation of the Sardic rift (Cherchi & Montadert 1982)

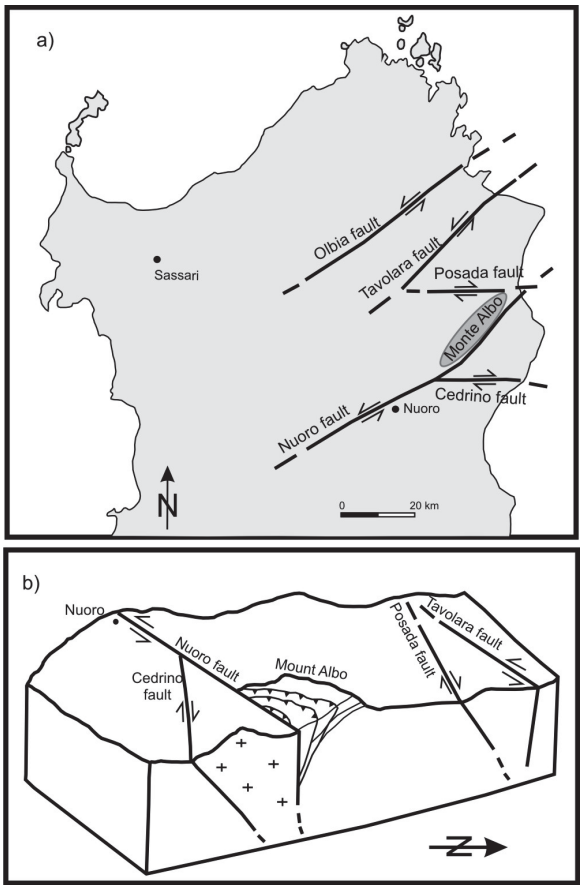

Figure 3.30: *Tertiary fault system of northeast Sardinia. a) The left-lateral Nuoro fault forms a conjugate set with the right-lateral Cendrino fault. b) The Nuoro and Cendrino fault form a negative flower structure. The northeastern fault system was (re-)activated during the extensional events of Lower Miocence. Modified after a)* Carmignani et al. *(1992) and* Helbing *(2003) and b)* Carmignani et al. *(1992)*

3.3.2 Results

3.3.2.1 Sample description

The talc formation of both talc mines are related to NE directed tectonic structures (Arthaud & Matte 1975). It occurs as open-space filling as a precipitate of hydrothermal fluids. Hostrocks at both mines are the granitoids of the Sardinia-Corsica-batholith that intruded into Paleozoic basement rocks (*Del Moro et al.* (1975)). The grantitoids are mostly leucogranites and monzogranites with different degrees of alteration (chloritization and albitization). While some of the chloritised granitoids still show their original texture the completely altered rocks are albitites. The talc mineralization occurs in shearzones with carbonate hostrock bodies (calcitic and dolomitic marble) and is of pale green color that contains nodules of late stage sparry calcite and quartz as well as residuals of hostrock limestone (fig. 3.31).

Two sample profiles were taken in each deposit starting with the hostrock carbonate body and sampling towards the talc shear zone. Additional samples of carbonate from within the shear zones were taken as well as rocks from altered and non-altered granitoid bodies.

Carbonate samples from the Sa Matta and Su Venosu talc deposit show similar features. Relictic older carbonat grains are consumed by younger recrystallized carbonate grains. Within the carbonate body accumulations of chlorite-talc are dispersely distributed (fig. 3.32a). In close vicinity to the talc shear zones chloritization and talc formation seems to increase (fig. 3.32b). The deformations features observed in thin-sections indicate deformation temperatures 300–400°C.

Macroscopically non-altered granitoid bodies show signs of alteration in thin-sections (fig. 3.33a). Quartz grains have uneven grain boundaries and show undulose extinction. Feldspar grains are highly decomposed and beginning chloritization is recognizable (fig. 3.33b). In the strongly altered granitoid body only leftovers of quartz are recognizable and most parts of the thinn-section are composed of chlorite (fig. 3.33c). Feldspar is almost completely disolved and consumed by chlorite (fig. 3.33d)

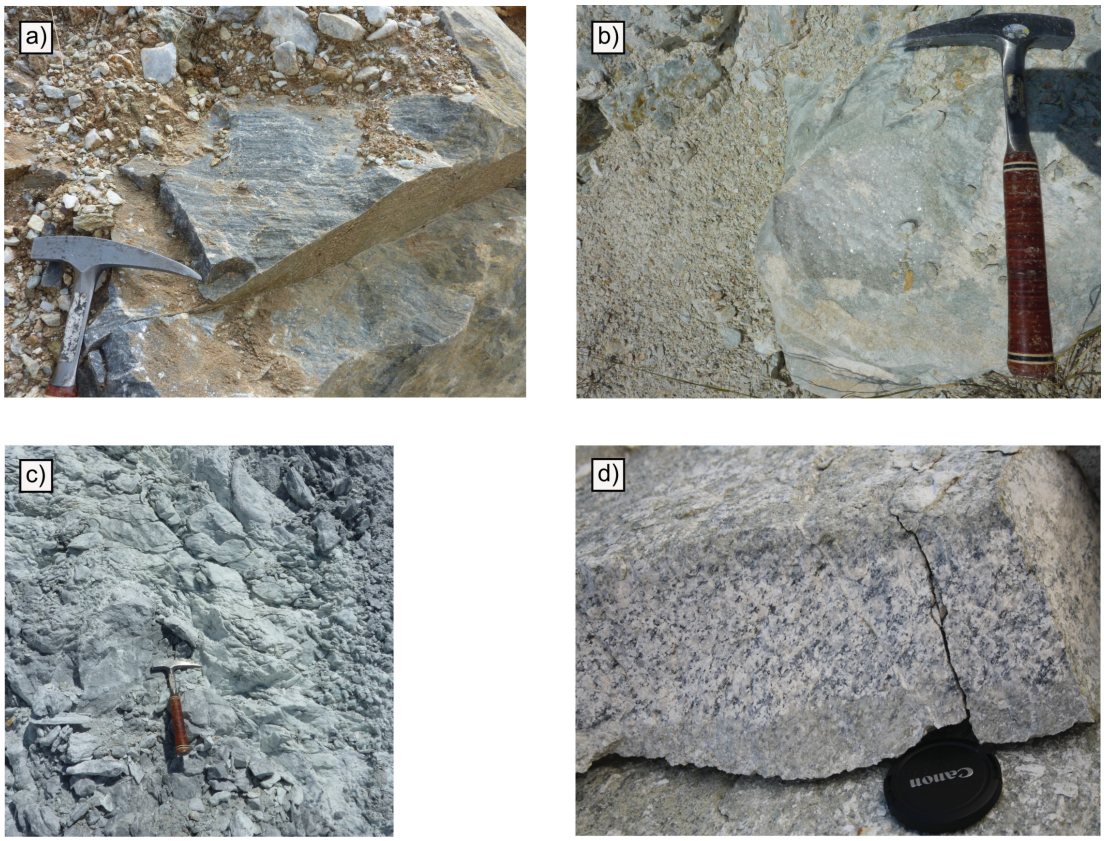

Figure 3.31: *Field observations from the talc deposits Sa Matta and Su Venosu: a)banded marble, b) coarse grainded dolomitic marble, c) talc zone, d) altered and non-altered granitoid body*

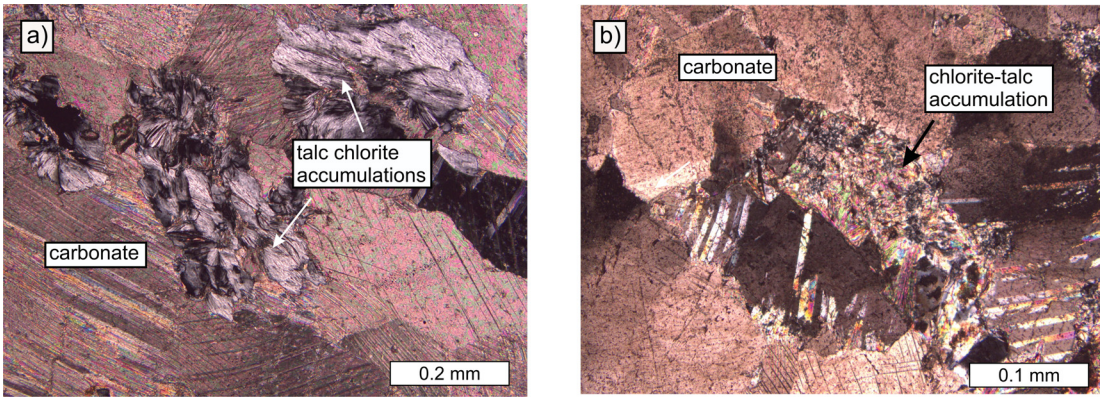

Figure 3.32: *Thinn-section of carbonates of the Sa Matta talc deposit: a) carbonate grains consumed by accumulations of chlorite and talc (SM 35), b) advanced chloritization and talc formation within carbonate body (in closer vicinity to small shear zone)(SM 16)*

3.3.3 Major, minor, trace elements

Hostrock marbles from both deposits are either calcitic or dolomitic. Contents of Fe_2O_3, MnO and NaO are low as well as the content of Sr. Calcitic marbles of both deposits have generally higer Sr-values but lower MnO-values compared to dolomitic marbles. Sr as a substitute for Ca in calcites is expected to be lower in dolomite. Samples from within the talc zone tend to have higher values of MnO but lower values of Fe_2O_3.

3.3.3.1 REE pattern

Marbles from both deposits show similar features (fig. 3.34a & b) . They are slightly depleted in HREE and have a negative Eu anomaly. In addition marbles from Su Venosu have a pronounced negative Ce anomaly. However secondary carbonates from within the talc zone (SM 9 and SV 14) are generally enriched in REE compared to marbles from outside the shearzone and show also a negative Eu anomaly (fig. 3.34c). The higher total amount of REE does not correlate with higher amounts of SiO_2, Al_2O_3, Fe_2O_3 and MnO. Values for the said oxydes are generally low, thus an influence of non-carbonate phases, such as clay minerals, authigenic quartz, Fe-Mn oxides can be ruled out.

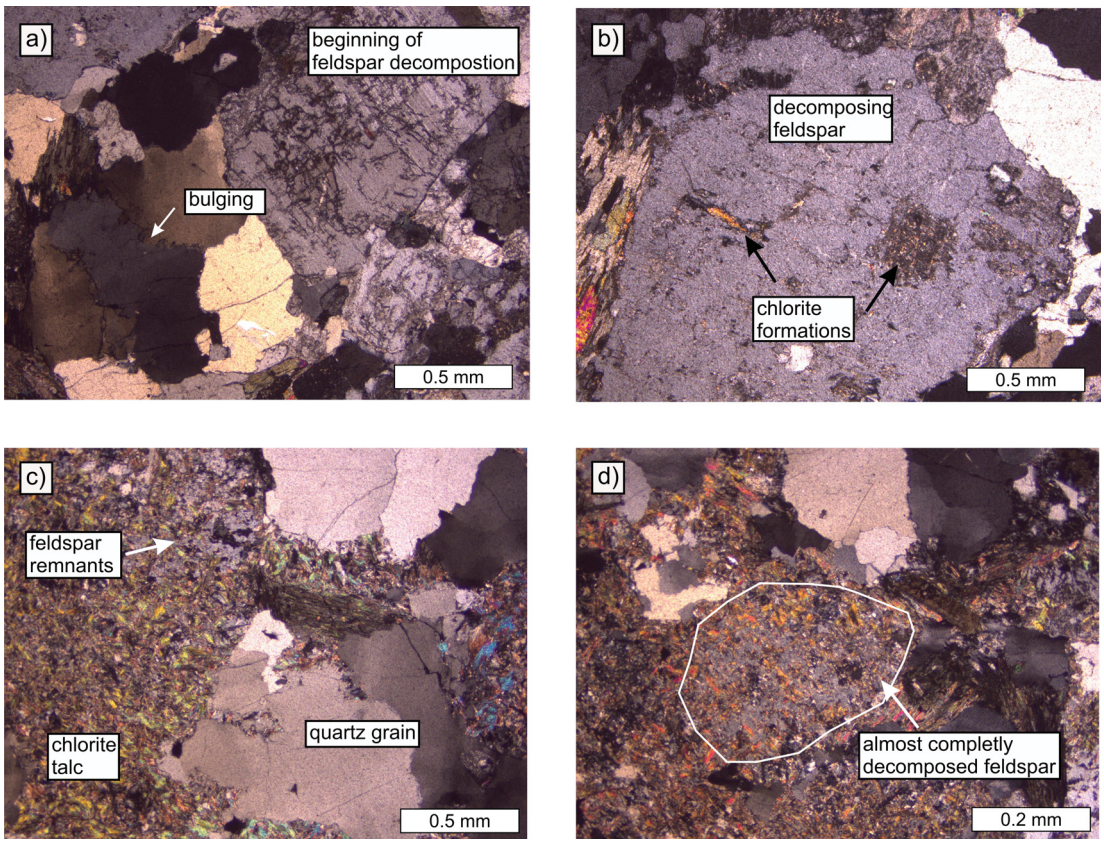

Figure 3.33: *Thinn-section of granitoid bodies of the Sa Matta talc deposit: a)Macroscopically non-altered granite shows first signs alteration by bulging and beginning of feldspar decomposition (SM 20b), b) beginning of chloritization in non-altered granite is dectectable by accumulations of chlorite within feldspar grains (SM 20b), c) advanced chloritization process in macroscopically altered granite; granite is almost completely consumed by chlorite (SM 20a) and d) feldspar is almost completely disolved*

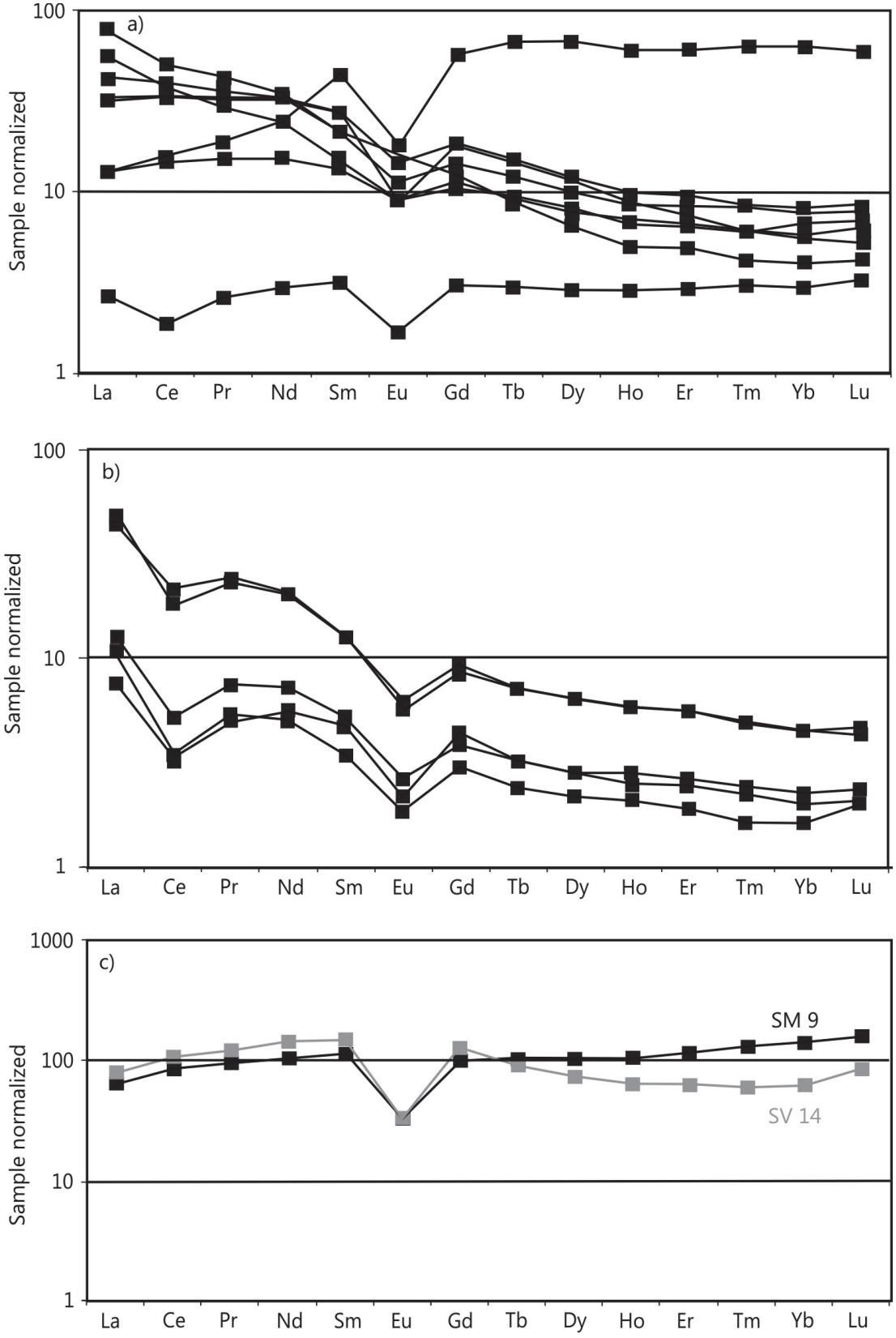

Figure 3.34: *Chondrite normalized REE patterns of marbles from a) the Sa Matta and b) Su Venosu talc deposit and c) secondary calcite from within the talc zones*

3.3.3.2 Stable Isotopes

Carbon isotope values at the Sa Matta and Su Venosu talc deposits range from $\delta^{13}C$ = -1.3 to 2.0 ‰ (VPDB) with the exception of two samples from Su Venosu with $\delta^{13}C$ = -9.5 and -9.4 ‰ (VPDB). Both samples were secondary calcite from a talc zone. Oxygene isotope values range from $\delta^{18}O$ = 6.0 to 20.3 ‰ (VSMOW) (fig. 3.35.).
Oxygene isotope values of quartz have been measured and range from $\delta^{18}O$ = 8.1 to 9.3. ‰ (VSMOW) for secondary quartz from talc zones. Values from granitoid bodies are between $\delta^{18}O$ = 9.3 and 11.4 ‰ (VSMOW). Quartz samples related to albite mineralization at both deposits show values of $\delta^{18}O$ = 3.3 to 4.4 ‰ (VSMOW).

3.3.3.3 Ion-chromatography

At the Sa Matta and Su Venosu bulk fluid inclusion analysis were performed on marbles and secondary quartz and secondary calcite from within the talc zones. In addition samples from outside the deposits were taken and analyzed.
All samples have very low Na/Br (< 203) and Cl/Br (< 390) ratios compared to modern sea water with most samples even well below Na/Br (< 100) and Cl/Br (< 150) (fig. 3.36.)
Temperatures calculated using the ratios of Na and K in fluid inclusions give very differing temperatures (+300°C) Secondary calcite from the talc zone has high Na-K-temperatures of 420° to 460°C and secondary quartz shows Na-K-temperatures of 230° to 290°C.
Charge balance ($Q^+/Q^- = 1$) for carbonates vary greatly but are close to 1 for quartz samples from the talc zone.

3.3.4 (U-Th)/He

Measurements of (U-Th)/He were performed on 14 single crystals from five samples (AHe) and 9 single crystals from four samples (ZHe) of altered and non-altered granitoid rocks. AHe ages range from Upper Eocene to Lower Oligocene

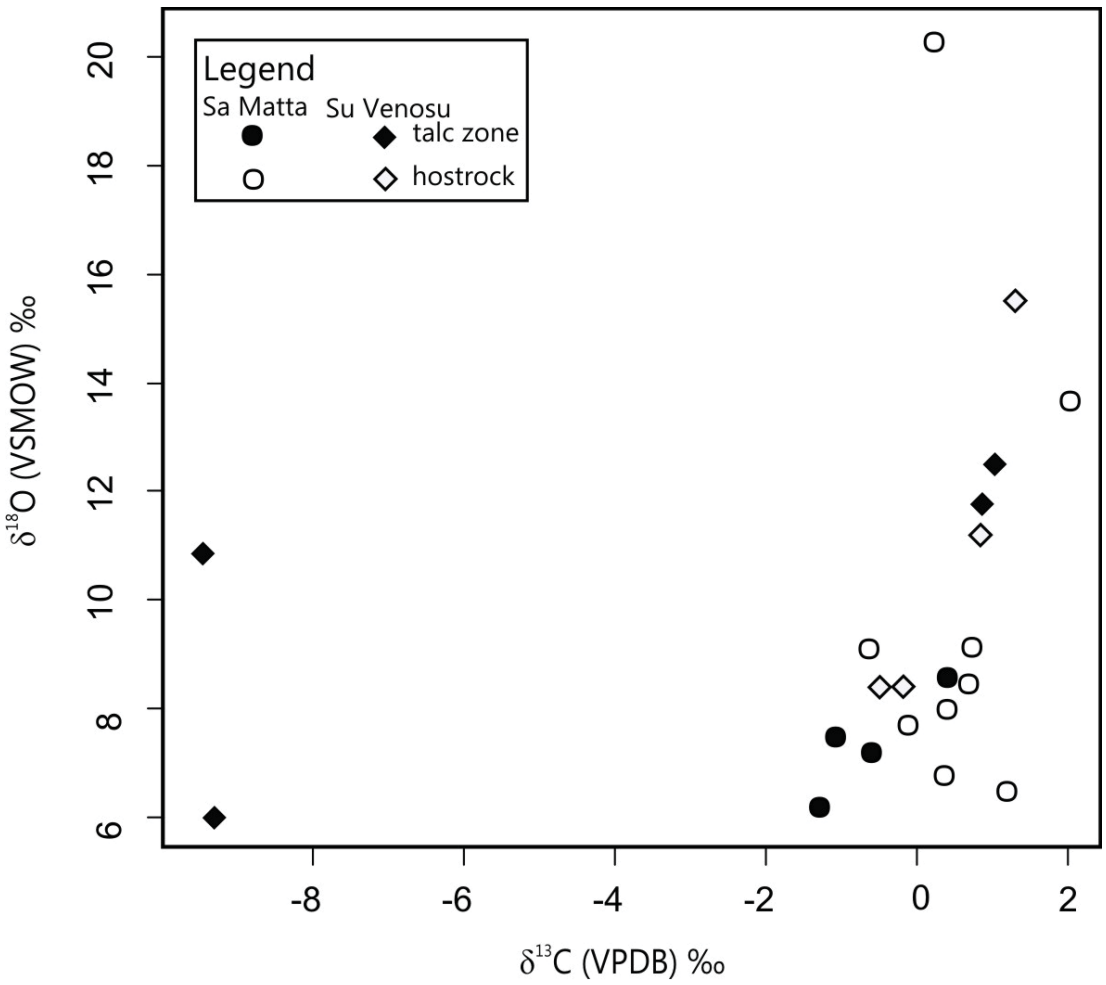

Figure 3.35: *Stable isotope data from the Sa Matta and Su Venosu talc deposits*

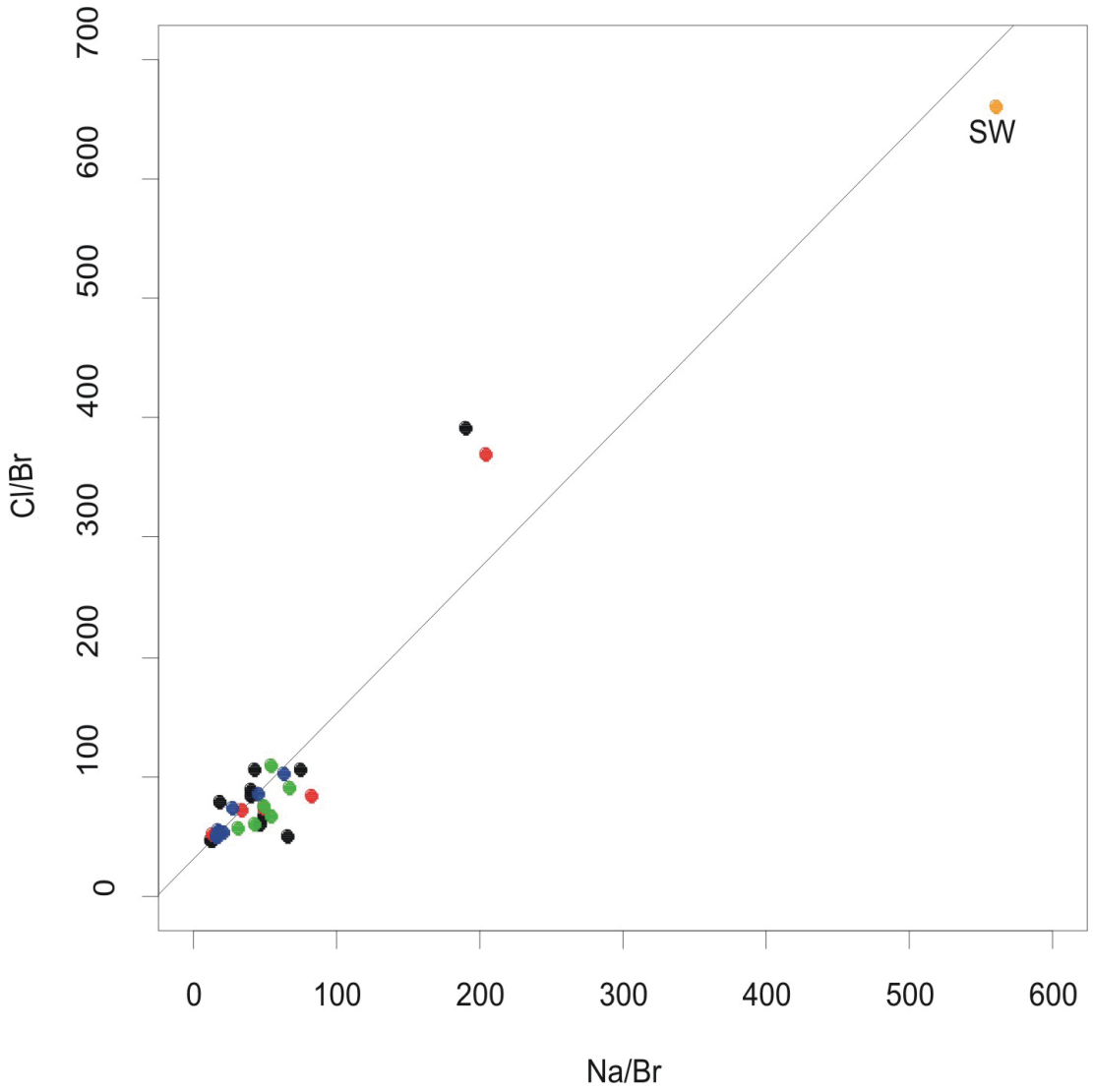

Figure 3.36: *Chondrite normalized REE patterns of marbles from a) the Sa Matta and b) Su Venosu talc deposit and c) secondary calcite from within the talc zones*

(36.1 to 23.7 Ma) but can generally be considered as Oligocene. ZHe ages are of Upper Cretaceaous ages and range from Campanium to Maastrichtium (75.6 to 66.8 Ma, see fig. 3.37). Age differences do not differ with rock type. Altered and non-altered granitoid rocks yield the same ages.

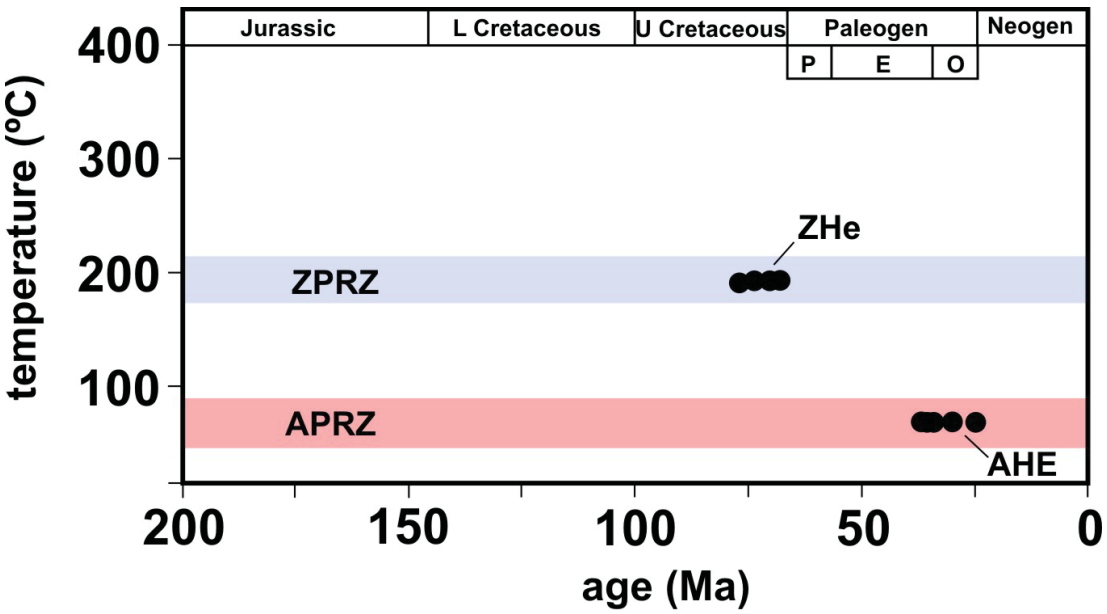

Figure 3.37: *AHe and ZHe ages from granitoid rocks from the talc deposits Sa Matta and Su Venosu, Sardinia)*

3.3.5 Discussion

According to *Arthaud & Matte* (1975) the talc formation of the Sa Matta and Su Venosu talc mines are related to NE trending tectonic structures. *Grillo & Prochaska* (2007) assume that the talc-chlorite mineralizations are pre-Alpine and question whether the Mg-carbonate rocks of the deposit are the source for Mg to form talc during a hydrothermal event or whether the dolomites themselves are a product of a hydrothermal event.

Talc at both deposits occurs most abundantly within m-wide shearzones that are part of carbonate hostrocks. The talc shearzones also contain relicts of carbonate hostrocks as well as newly formed mineral phases such as quartz and carbonate. The carbonate hostrock bodies also contain dispersely distributed talc mineralizations which seems to increase with decreasing distance to the talc shearzones.

The low Sr content in dolomitic marbles is an indicator for diagenetic or metamorphic overprint of the formerly marine origin of the hostrocks. During dolomitization Sr is enriched in the poresolution and Mn and Fe are incorporated into

the crystal lattice and would lead to higher values in the dolomitic marbles.

The carbonates form Su Venosu and a single carbonate samples form Sa Matta show a negative Ce anomaly. This anomaly in the carbonates is inherited from marine waters that formed the carbonates (*Bau & Möller* (1992) and *Elderfield et al.* (1990). Ce^{3+} in seawater is oxidized to the less mobile Ce^{4+} which results in the depletion of Ce of the seawater and a negative Ce anomaly. In both deposits HREE are generally depleted indicating fluid remobilisation (*Schroll* (1997)). In addition all carbonate samples have a very pronounced Eu anomaly. According to *Lüders et al.* (1993) this can only occur in carbonates that interacted with granites. Samples of secondary minerals from the talc zone are generally higher in their REE distribution. No typical negative Ce anomaly occurs. Equally to other carbonate samples from the Sardinian talc mines, these samples also have a pronounced negative Eu anomaly. The high values of REE and the negative Eu anomaly are high indicators that the mineralizing fluids interacted with the granites.

Carbonate samples are depleted in their δ^{18}O values compared to seawater. However $\delta^{13}C$ values are still in the range of seawater. Marbles have a tendency to act as a barrier that impedes fluid flow. Thus there is no homogenization with metamorphic fluids and the rocks keep their original sedimentary isotopic signature (*Valley et al.* (1990)). Still fluid-rock interaction with a fluid of metamorphic origin can be assumed as the δ^{18}O are below the typical values for seawater. Quartz samples from the talc zone have equally low δ^{18}O values indicating a metamorphic origin of the mineralizing fluid. Quartz samples related to albite mineralization at both deposits have higher δ^{18}O values reflecting the influence of meteoric water.

Na/Br and Cl/Br ratios from the talc deposits and its surroundings are well below the ratio of seawater (typically Cl/Br = 658m *Gleeson* (2003)) and plot along the seawater evaporation line. During evaporation Br is not incorporated into the crystal lattice and remains in the solution where it continous to be enriched while Cl and Na form NaCl. Also other ions as Mg and K are further incorporated into the crystal lattice, while the value of Br increases in the solution (see also *Prochaska* (1997)). Thus a high Br concentration leads to low Cl/Br and Na/Br ratios. So far the mineralizing fluid is highly evaporated one.
Na-K-temperatures are generally high. Given that hostrock marbles and grani-

toid bodies from the deposit contain different generations of fluid inclusion also temperatures might differ. However secondary quartz and secondary calcite from the talc deposit might show temperatures from the talc forming event. These temperatures also differ with the type of mineral. Secondary calcite has high Na-K-temperatures of 420° to 460°C and secondary quartz shows Na-K-temperatures of 230° to 290°C.

An analysis of (U-Th)/He on apatite and zircon of altered and non-altered granitoid rocks from the deposits was performed in order to determine the time of fluid flow that can be linked to the mineralization of talc. Fluid flow (*Caine et al.* (1996)) and temperature are generally enhanced along fault zones and ore deposits may form in and around them (*Tagami* (2012) and references therein) regardless of depth and mode of fault motion (*Cox* (2010)). It is assumed that fault slip produces ruptures in the fault zone that enhances fluid flow to form mineral veins. In the past the effect of elevated temperature along fault zones has been usefull to determine the time of fluid flow and thus the age of the fault zone (*Yamada et al.* (2007), *Wölfler et al.* (2010), *Emmel et al.* (2012)).
In order to do so, two pairs (SM20a & SM20b and SM31 & SM33) of altered and non-altered granitoid body yielded material good enough to perform the task. Additional samples of altered and non-altered rocks were considered as well. The idea was to show an age difference between the altered and non-altered rock to determine the age of the chloritization (i.e. the fluid event).
However the AHe and ZHe ages of altered and non-altered rocks do not differ. Both rock types yield AHe ages that range from 36.1 to 23.7 Ma and ZHe from 75.6 to 66.8 Ma. It can be assumed that the fluid that caused chloritization was of higher temperature than the temperature ranges of the Partial Rention Zone (APRZ and ZPRZ for Apatite and Zircons respectively).
The data does proclaim that the crystals have been below 200°C for zircons for at least 75.6 Ma and below 80°C for apatites for at least 36.1 Ma. Thus it can be argued that the fluid event (that must have been of higher temperature as is also known from fluid inclusion study) that caused chloritization is older than 75.6 Ma.

By the means of thermonchronological methods that yield higher closing temperatures (e.g. Fission track up to 300°C (zircons) or Ar/Ar up to 450°C (muscovite)),

that age determination of the chloritising fluid event might have been possible.

Additionaly with the analyzed data during this study it is possible to reconstruct and discuss the thermal history of the area.

In order to reconstruct the thermal history of the area, a cooling path was constructed (fig. 3.38). Since fission track and (U-Th)/He from Sardinia is scarce data from the Variscan part of Corsica has been added. According to *Danišík et al.* (2007) and references therein, apatite fission track ages (ApFT) for the majority of the Variscan basement are in the range of 34.6 to 16.4 Ma and 105.3 to 46.4 Ma for the southernmost part of Corsica. Zircon fission track ages (ZrFT) from the Variscan basement of Corsica range from 159.8 to 144.6 Ma (fig. 3.38). The data indicates that rocks from the deposit were reheated around 75 Ma.

Most recently some AFT and AHe data from Sardinia has been published by *Malusá et al.* (2014). They yield AFT from the Varsican basement from central Sardinia and the eastern coast that range from 201 to 169 Ma and AHe ages from 204 to 133 Ma (fig. 3.39). Without complete knowledge of the sampling location it is assumed that they were not taken in very close vicinity to the talc deposits of Sa Matta and Su Venosu. The question that is imposed is why these ages are so much older than the ones from the talc mine. It is possible that the hydrothermal event that led to the talc mineralization overprinted the granitoid body and has been cooling down for 75.6 Ma. This cooling event would not have affected rocks from outside the deposit, which have a different cooling history. So with very careful interpretation dating of the talc and chlorite forming event has been succesful in the means that it is now known that rocks from the talc deposits were overprinted by a hydrothermal event at least 75.6 Ma ago while at the same time rocks outside the deposit were cooled down already.

3.3.6 Conclusion

It can be concluded that the formation of the talc deposits Sa Matta and Su Venosu is a multiple step process. The carbonate hostrocks show clearly overprinting by a diagenetic or metamorphic fluid. It is also obvious that the fluid that penetrated the carbonates and led to the formation of talc interacted with

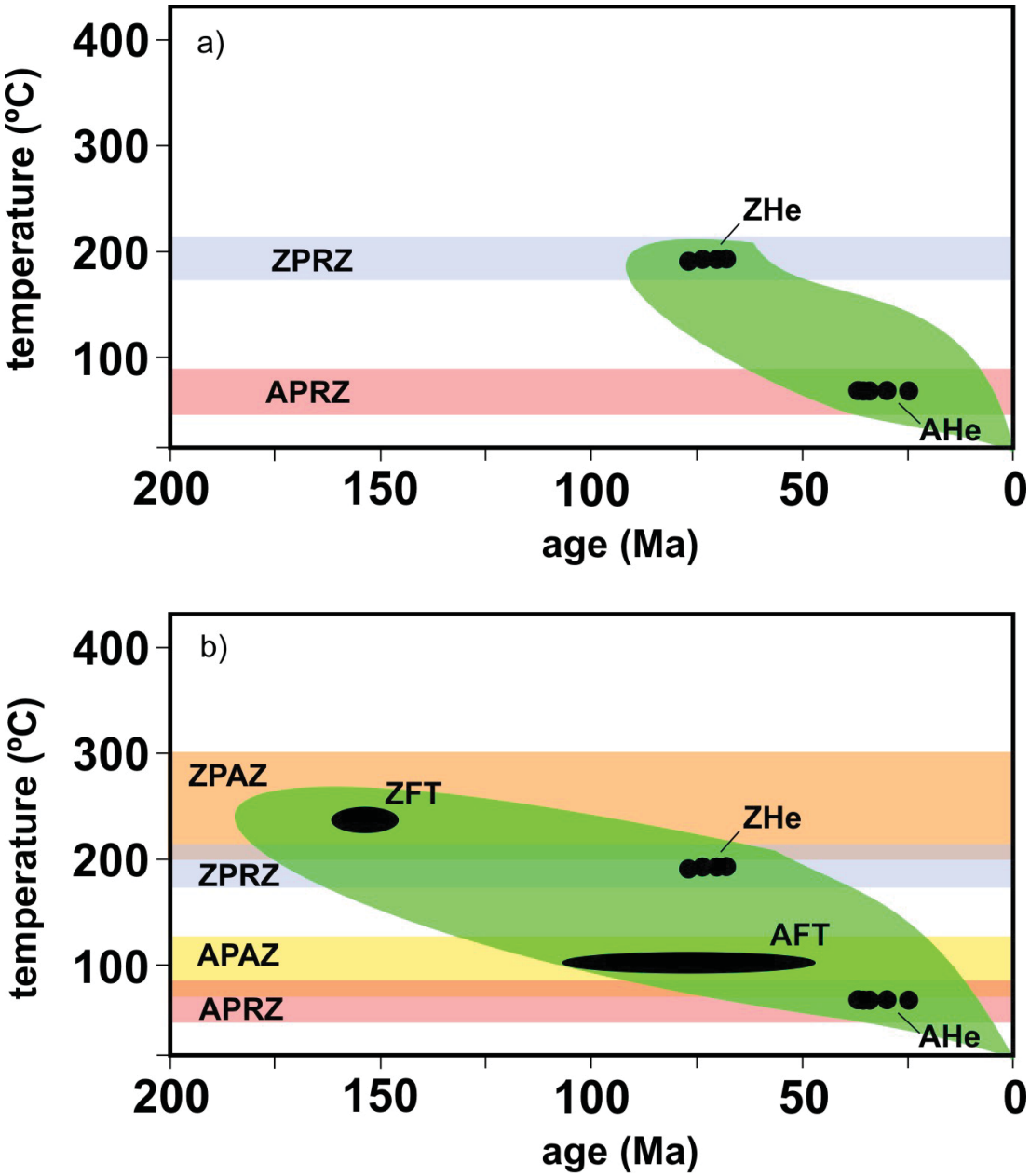

Figure 3.38: *a) Estimated cooling path Sardinia from this study, b) Estimated cooling path with additional data from Corsica from* Danišík et al. *(2007)*

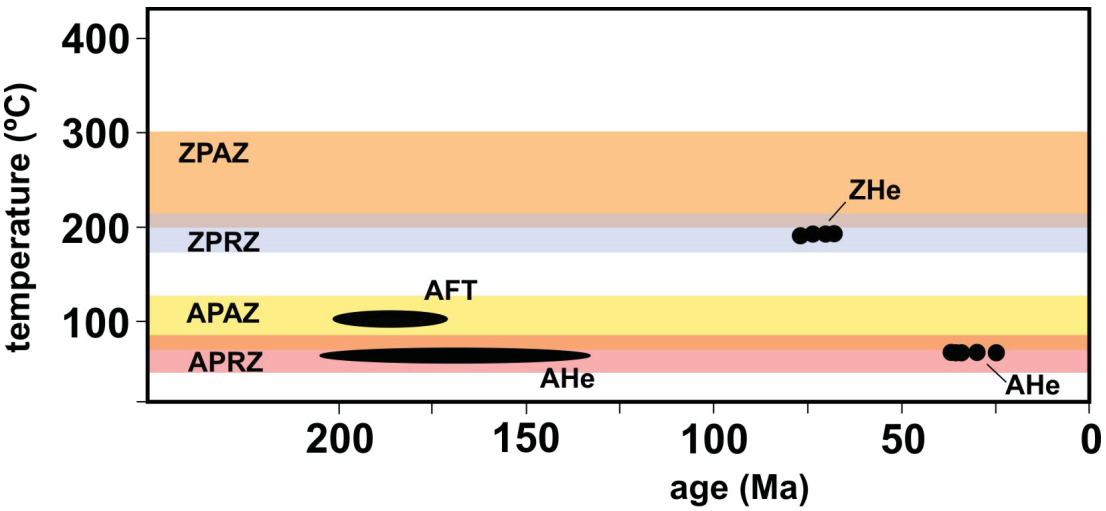

Figure 3.39: *AHe and ZHe ages from this study and AHe and AFT ages according to* Malusá et al. *(2014) (black oval)*

the granitoid bodies. The secondary minerals quartz and calcite that are part of the talc shearzones show fluid-rock interaction with a fluid of metamorphic origin. Stable isotope measurement of the albite bodies show that they were rather affected by superficial fluids. The mineralizing fluids of the carbonate and secondary minerals from the talc shear zone are a highly evaporated one and are of high temperature. The He ages of the talc-chlorite forming event can be dated to at least 75 Ma years. Especially very recent fission track and (U-Th)/He data from Sardinia show the occurence of a special hydrothermal event that led to the talc-chlorite formation. The data confirms the assumption made by *Grillo & Prochaska* (2007) that the talc-chlorite forming event is pre-Alpine.

Chapter 4

General Conclusion

The study has shown the importance of fault zones for the formation of talc. They act as fluid pathways and as zones of enhanced deformation that allow enrichment of weak mineral phases like talc.

The investigation of the deposits Veitsch, Wald am Schoberpass and Lassing of the Eastern Greywacke Zone in the Eastern Alps are an example for changing conditions with distance to the fault zones. The Eastern Greywacke Zone is penetrated by a fault system evolving from Oligocene to Miocene escape tectonics in the Eastern Alps. The Veitsch deposit is furtherst away from the Mur-Mürz-fault and it is characterized by low temperature deformation features and talc mineralization does not occure. In contrast the Lassing talc deposit is situated at the junction of two fault zones: the SEMP being one of the major Oligocene-Miocene faults in the Eastern Alps and the Paltental-Liesingtal-fault. It is characterized by high deformation features and rich occurrences of talc. In addition the Wald am Schoberpass deposit is situated at the Paltental-Liesingtal-fault. This fault is also related to the Oligocene-Miocene fault system, however structures and temperatures at the Wald am Schoberpass deposit are more characteristic for the subsidence movements following Eo-alpine orogeny. The small scale talc mineralizations cannot be considered Alpine assuming that deformation along the Paltental-Liesingtal-fault was not strong enough to yield an enrichment of talc as it is the case in Lassing. It can therefore be assumed that the first formation of talc can be attributed to Eo-alpine subsidence movements however the

enrichment of talc is due to tectonical activity during the Oligocene and Miocene extensional events.

The Gemerska Poloma talc deposit is another example of a fault zone that acted as fluid pathway and enhanced fluid flow during deformation. The fault that separates the granitoid body in the footwall from the magnesite body in the hanging wall transfered stress into the magnesite body where talc was formed and accomodated stress. With ongoing deformation and fluid flow talc was enriched. Temperature ranges and deformation features within the talc zones of the magnesite body are a strong indicator for the tectonic nature of the talc formation. Fluids involved are in relation with the granitoid body as is indicated by geochemical analyis and fluid inclusion study. The mineralizing fluid with its high Br content can be attributed to fuid-rock interaction while migrating through the crust.

For the talc deposits Sa Matta and Su Venosu interpretations are not as straight forward as for the deposits of the Eastern Greywacke Zone and Gemerska Poloma. Even though *Arthaud & Matte* (1975) relate the talc mineralization of the two Sardinian deposits to NE directed tectonic structures, *Grillo & Prochaska* (2007) already assume that the talc-chlorite mineralizations are rather pre-Alpine in contrast to the Alpine Nuoro fault that strikes NE and is part of the Northeastern Sardinian extensional tectonic fault system. The ages constrained during this study support the hypothesis of the pre-Alpine age of the talc-chlorite mineralization. It is obvious that the carbonate hostrocks and secondary minerals from within the talc zones of the deposits were overprinted and formed by metamorphic fluids and that the fluids interacted with the granitoid bodies.

In conclusion the study on shear zone related talc mineralization has provided insights on the role of fault zones as fluid pathways and the enrichment of talc due to increasing deformation. Geochemical analysis as well as stable isotope analysis and fluid inclusion study has shown that fluids that lead to the formation of talc for this type of deposit are of elevated temperature. The fluid inclusion study has also shown that the fluids related to the talc mineralization were all highly evaporated. As the fluids are also of metamorphic origin evaporating processes as they are typical in marine basins seem not to be the most suitable thesis of the formation of the fluids. It is rather assumed that fluids fractionated

during deformation processes and thus enrich Br continously leading to such a high “evaporation trend”. Further investigations on shear zone related deposits should provide more insights to the formation processes of these fluids. The (U-Th)/He dating has given meaningful ideas on the age of the Sardinian talc deposits. Dating methods of higher closing temperatures may give direct insight on the age of the talc-chlorite mineralization. The method may also be applied to the Gemerksa Poloma talc deposit to actually place the timing of the tectonized zone.

Further study of the subject is possible and will yield fruitfull result.

Bibliography

Aharon, P. (1988): A stable-isotope study of magnesites from the Rum Jungle uranium field, Australia: implications for the origin of strata-bound massive magnesites. *Chem Geol*, vol. 69, 127–145.

Anders, E., Grevesse, N. (1989): Abundances of the elements: Meteoritic and solar. *Geochimica et Cosmochimica Acta*, vol. 53, 197–214.

Arthaud, F., Matte, P. (1975): Les decrochements tardi-hercyniens du sud-ouest de l'Europe: Geometrie et essai de reconstitution des conditions de la deformation. *Tectonoph*, vol. 25, 139–171.

Barca, S. (1991): Resedimentation and Hercynian flysch in Culm facies within the Sarrabus Syncline, SE Sardinia, Italy. In: *Comptes Rendus Academie-des-Sciences, Serie II*, vol. 313 of *IIa* (Academie des Sciences), pp. 1051–1057.

Barca, S., Carmignani, L., Eltrudis, A., Franceschelli, M. (1992): Relationships between foredeep deposits and Hercynian nappe building in south-eastern Sardinia, Italy. In: L. Carmignani, F. Sassi (Eds.), *Contributions to the Geology of Italy with special regard to the Paleozoic basement, IGCP No 276, Newsletter 5, special issue*, pp. 23–44.

Bau, M. (1991): Rare-Earth element mobility during hydrothermal and metamorphic fluid-rock interaction and the significance of the oxidation state of europium. *Chem Geol*, vol. 93, 219–230.

Bau, M., Möller, P. (1992): Rare Earth Element Fractionation in Metamorphogenic Hydrothermal Calcite, Magnesite and Siderite. *Mineralogy and Petrology*, vol. 45, 231–246.

Baumgartner, L., Valley, J. (2001): Stable Isotope transport and contact metamorphic fluid flow. In: *Stable Isotope Geochemistry. Rev. Miner. Geochem.*, vol. 43, pp. 415–467.

Blanckenburg, F., Davies, J. (1995): Slab breakoff: A model for syncollisional magmatism and tectonics in the Alps. *Tectonics*, vol. 14, 120–131.

Bottrell, S., Yardley, B., Buckley, F. (1988): A modified crush-leach method for the analysis of fluid inclusion electrolytes. *Bulletin de Mineralogie*, vol. 111, 297–290.

Boulvais, P., de Parseval, P., D'Hulst, A., Paris, P. (2006): Carbonate alteration associated with talc-chlorite mineralization in the eastern Pyrenees, with emphasis on the St. Barthelemy Massif. *Mineralogy and Petrology*, vol. 88, 499–526.

Brosch, F., Kurz, W. (2008): Fault damage zone dominated by high-angle fractures within layer-parallel brittle shear zones: examples from the eastern Alps. In: C. Wibberley, W. Kurz, J. Imber, R. Holdsworth, C. Collettini (Eds.), *The internal Structure of Fault Zones: Implications for Mechanical and Fluid-Flow Properties*, vol. 299 (The Geological Society of London), pp. 75–95.

Burkhard, M. (1993): Calcite twins, their geometry, appearance and significance as stress-strain markers and identicators of tectonic regime: a review. *Journal of Structural Geology*, vol. 15, 351–368.

Caine, J., Evans, J., Forster, C. (1996): Fault zone architecture and permeability structure. *Geology*, vol. 24, 1025–1029.

Can, I. (2002): A new improved Na/K geothermometer by artificial neural networks. *Geothermics*, vol. 31, 751–760.

Cappelli, B., Carmignani, L., Castorina, F., Di Paola, A., Oggiano, G., Petrini, R. (1992): A Hercynian Suture zone in Sardinia: geological and geochemical evidence. *Geodinamica Acta*, vol. 5, 101–118.

Carmignani, L., Carosi, R., Disperati, L., Funedda, A., Musumeci, G., Pasci, S., Pertusati, P. (1992): Tertiary Transpressional Tectonics in NE Sardinia, Italy. *IGCP No. 276*, vol. 5, 83–96.

Carmignani, L., Decandia, F., Disperati, L., Fantozzi, P., Lazzarotto, A., Liotta, D., Oggiano, G. (1995): Relationships between the Tertiary structural evolution of the Sardinia-Corsica-Provençal Domain and the Northern Apennines. *Terra Nova*, vol. 7, 128–137.

Casula, G., Cherchi, A., Montadert, L., Murru, M., Sarria, E. (2001): The Cenozoic graben system of Sardinia (Italy): geodynamic evolution from new seismic field data. *Marine and Petroleum Geology*, vol. 18, 863–888.

Cherchi, A., Montadert, L. (1982): Oligo-Miocene rift of Sardinia and the early history of the western Mediterranean basin. *Nature*, vol. 298, 736–739.

Cocozza, T., Jacobacci, A. (1975): Geologial Outline of Sardinia. In: C. Squyres (Ed.), *Geology of Italy* (Earth Science Society Libyan Arab Rep.), pp. 49–81.

Collettini, C., Viti, C., Smith, S., Holdsworth, R. (2009): Development of interconnected talc networks and weakening of continental low-angle normal faults. *Geology*, vol. 37, 567–570.

Conti, P., Carmignani, L., Funedda, A. (2001): Change of nappe transport direction during the Variscan collisional evolution of central-southern Sardinia (Italy). *Tectonoph*, vol. 332, 255–273.

Cox, S. (2010): The application of failure mode diagrams for exploring the roles of fluid pressure and stress states in controlling styles of fracture-controlled permeability enhancement in faults and shear zones. *Geofluids*, vol. 10, 217–233.

Dal Piaz, G., Martin, S., Villa, I., Gosso, G., Marschalko, R. (1995): Late Jurassic blueschist-facies pebbles from the Western Carpathian orogenic wedge and paleostructural implications for Western Tethys evolution. *Tectonics*, vol. 14, 874–885.

D'Alessio, M., Blythe, A., Bürgmann, R. (2003): No frictional heat along the San Gabriel fault, California: Evidence from fission-track thermochonology. *Geology*, vol. 31, 541–544.

Dallmeyer, R.D., Neubauer, F., Fritz, H. (2008): The Meliata suture in the Carpathians: regional significance and implications for the evolution of high-pressure wedges withing collisional orogens. In: S. Siegesmund, B. Fügenschuh, N. Froitzheim (Eds.), *Tectonic Aspects of the Alpine-Dinaride-Carpathians System*, vol. 298 (Geological Society of London, Special Publications), pp. 101–115.

Danišík, M., Kuhlemann, J., Dunkl, I., Székely, B. (2007): Burial and exhumation of Corsica (France) in the light of fission track data. *Tectonics*, vol. 26, 1–24.

Deer, W., Howie, R., Zussman, J. (1992): *An Introduction to the Rock Forming Minerals* (Pearson Education Limited).

Del Moro, A., Di Simplicio, P., Ghezzo, C., Guasparri, G., Rita, F., Sabatini, G. (1975): Radiometric data and intrusive sequence in the Sardinian Batholith. *Neues Jahrbuch für Mineralogie, Abhandlungen*, vol. 126(1), 28–44.

Elderfield, H., Upstill-Goddard, R., Sholkovitz, E. (1990): The rare earth elements in rivers, estuaries, and coastal seas and their significance to the composition of ocean waters. *Geochimica et Cosmochimica Acta*, vol. 54, 971–991.

Emmel, B., Lisker, F., Hewawasam, T. (2012): Thermochronological dating of brittle structures in basement rocks: A case study from the onshore passive margin of SW Sri Lanka. *Journal of Geophysical Research*, vol. 117, 1–3.

Evans, B., Guggenheim, W. (1991): Talc, pyrophyllite, and related minerals. In: S. Bailey (Ed.), *Hydrous Phyllosilicates (exclusive of micas). Reviews in Mineralogy*, vol. 19 (Mineralogical Society of America), pp. 225–294.

Farley, K. (2002): (U-Th)/He dating: Techniques, calibrations, and applications. *Mineral. Soc. Am. Rev. Mineral. Geochem.*, vol. 47, 819–844.

Farley, K., Wolf, R., SIlver, L. (1996): The effects of long alpha-stopping distances on (U-Th)/He ages. *Geochimica et Cosmochimica Acta*, vol. 60(21), 4223–4229.

Faryad, S., Henjes-Kunst, F. (1997): Petrological and K–Ar and $^{40}Ar/^{39}Ar$ age constraints for the tectonithermal evolution of the high-pressure Meliata unit, Western Carparthians (Slovakia) . *Tectonoph*, vol. 280, 141–156.

Faupl, P. (1991): Subduction and continent collision in the Jurassic and Cretaceous history of the Eastern Alps. *Terra Abstr*, vol. 3/1, 259.

Faure, G., Mensing, T. (2005): *Isotopes – Principles and Applications* (Wiley).

Felser, K. (1977): Die stratigraphische Stellung der Magnesitvorkommen in der östlichen Grauwackenzone (Steiermark, Österreich). *BHM*, vol. 122(2a), 17–23.

Ferrill, D., Morris, A., Evans, M., Burkhard, M., Groshong Jr., R., Onasch, C. (2004): Calcite twin morphology: a low-temperature deformation geothermometer. *Journal of Structural Geology Acta*, vol. 26, 1521–1529.

Fiori, M., Grillo, S. (2002): Chlorite-talc mineralizations in central Sardinia, Italy. *Mineralia Slovaca*, vol. 33, 557–560.

Franz, E., Ponce, J., Wetzenstein, W. (1979): Geochemie und Petrographie der Magnesitlagerstätten des Alto Chapare/Bolivien. *Radex-Rdsch*, 1105–1119.

Frisch, W. (1976): Ein Modell zur alpidischen Evolution und Orogenese des Tauern Fensters. *Geologische Rundschau*, vol. 65, 375–393.

Frisch, W., Dunkel, I., Kuhlemann, J. (2000): Post-collisional orogen-parallel large-scale extension in the Eastern Alps. *Tectonophysics*, vol. 327, 239–265.

Frisch, W., Kuhlemann, J., Dunkel, I., Brügel, A. (1998): Palinspastic reconstruction and topographic evolution of the Eastern Alps during late Tertiary tectonic extrusion. *Tectonophysics*, vol. 297, 1–15.

Genser, J., Neubauer, F. (1989): Low angle normal faults at the eastern margin of the Tauern Window (Eastern Alps). *Mitt. Österr. Geol. Ges.*, vol. 81, 233–243.

Gleeson, S. (2003): Bulk analysis of electrolytes in fluid inclusions. In: I. Samson, A. Anderson, D. Marshall (Eds.), *Fluid inclusions: analysis and interpretation*, vol. 32 (Mineralogical Association of Canada), pp. 233–246.

Grillo, S., Prochaska, W. (2007): Fluid Chemistry and Stable Isotope Evidence of Shearzone related Talc and Chlorite Mineralizations in Central Sardinia-Italy. In: *Conference Abstracts SGA-Meeting.*

Hafellner, M. (1995): Chemische Untersuchungen lagerstättenbildender Fluide ausgewählter Lagerstätten in den Ostalpen. Master's thesis, Montanuniversität Leoben.

Handler, R., Dallmeyer, R.D., Neubauer, F., Frank, W., Hermann, S. (1992): Chronology of metamorphic events in the Kaintaleck complex, Eastern Alps: Cadomian versus Caledonian/Acadian evolution of the Austro-Alpine basement. *Terra Abstr*, vol. 4, 29.

Handler, R., Dallmeyer, R.D., Neubauer, F., Hermann, S. (1999): $^{40}Ar/^{39}Ar$ mineral ages from the Kaintaleck nappe, Austroalpine basement, Eastern Alps. *Geol Carpathica*, vol. 50, 229–239.

Handler, R., Dallmeyer, R., Neubauer, F. (1997): $^{40}Ar/^{39}Ar$ ages of detrital white mica from Upper Austroalpine units in the Easten Alps, Austria: Evidence for Cadomian and contrasting Variscan sources. *Geol Rundsch*, vol. 86, 69–80.

Handy, M. (1990): The Solid-State Flow of Polymineralic Rocks. *Journal of Geophysical Research*, vol. 95, 8647–8661.

Hecht, L., Freiberger, R., Gilg, H., Grundmann, G., Kostitsyn, Y. (1999): Rare earth element and isotope (C, O, Sr) characteristics of hydrothermal carbonates: genetic implications for dolomite-hosted talc mineralization at Göpfersgrün (Fichtelgebirge, Germany). *Chem Geol*, vol. 155, 115 130.

Helbing, H. (2003): No suture in the Sardinian Variscides: A structural, petrological and geochronological analysis. Ph.D. thesis, Universität Tübingen.

Helbing, H., Frisch, W., Bons, P. (2006): South Variscan terrane accretion: Sardinian constraints on the intra-Alpine Variscides. *Journal of Structrual Geology*, vol. 28, 1277–1291.

Hoefs, J. (2009): *Stable Isotope Geochemistry* (Springer).

Hurai, V., Huraiová, M., Koděra, P., Prochaska, W., Vozárová, A., Dianiška, I. (2011): Fluid inclusion and stable C-O isotope constraints on the origin of metasomatic magnesite deposits of the Western Carparthians, Slovakia. *Russian Geology and Geophysics*, vol. 52, 1474–1490.

Jordan, P. (1987): The deformational behaviour of bimineralic limestone–halite aggregates. *Tectonoph*, vol. 135, 185–197.

Kasemann, S., Meixner, A., Rocholl, A., Vennemann, T., Schmitt, A., Wiedenbeck, M. (2001): Boron and oxygen isotope composition of certified reference materials NIST SRM 610/612, and reference materials JB-2G and JR-2G. *Geostand. Newsl.*, vol. 25, 405–416.

Kilík, J. (1997): Geological characteristics from talc deposit Gemerska Poloma – Dlhá Dolina. *Acta Montanistica Slovaca*, vol. 2, 71–80.

Koch, M. (1893): Mitteilung über einen Fundpunkt von Unter-carbon-Fauna in der Grauwackenzone der Nordalpen. *Z. Dtsch. Geol. Ges.*, vol. 45, 198–294.

Kralik, M., Aharon, P., Schroll, E., Zachmann, D. (1989): Carbon and oxygen isotope systematics of magnesites. In: P. Möller (Ed.), *Magnesite — Geology, Mineralogy, Geochemistry, Formation of Mg-Carbonates*, vol. 28, Gebrüder Borntraeger (Mon. Ser. Min. Deposits), pp. 197–223.

Krist, E., Korikovskij, S., Putiš, M., Janák, M., Faryad, S. (1992): Geology and Petrology of metamorphic rocks of the Western Carpathian crystalline complexes. Ph.D. thesis, Comenius University Bratislava.

Kuhlemann, J., Frisch, W., Dunkel, I., Szekely, B. (2001): Quantifying tectonic versus erosive denudation by the sediment budget; the Miocene core complexes of the Alps. *Tectonophysics*, vol. 330, 1–23.

Kurz, W., Fritz, H. (2003): Tectonometamorphic Evolution of the Austroalpine Nappe Complex in the Central Eastern Alps – Consequences for the Eo-Alpine Evolution of the Eastern Alps. *International Geology Review*, vol. 45, 1100–1127.

Kurz, W., Wölfler, A., Rabitsch, R., Genser, J. (2011): Polyphase movement on the Lavanttal Fault Zone (Eastern Alps): reconciling the evidence from different geochronological indicators. *Swiss Journal of Geosciences*, vol. 104, 323–343.

Lacombe, O., Jolivet, L. (2005): Structural and kineamtic relationships between Corsica and the Pyrenees-Provence domain at the time of the Pyrenean orogeny. *Tectonics*, vol. 24, 1–20.

Laubscher, H. (1987): *Der Bau der Alpen* (Spektrum der Wissenschaft), 5. ed.

Linzer, H.G., Decker, K., Peresson, H., Dell'Mour, R., Frisch, W. (2002): Balancing lateral orogenic float of the Eastern Alps. *Tectonoph*, vol. 354, 211–237.

Lüders, V., Möller, P., Dulski, P. (1993): REE Fractionation in carbonates and fluorites. In: P. Möller, V. Lüders (Eds.), *Formation of hydrothermal vein deposits*, Monogr. Ser. Miner. Dep. (Bornträger), pp. 133–150.

Malachovský, P., Turanová, L., Dianiška, I. (1992): Final report of mineral exploration from Gemerska Poloma. Tech. rep., Slovak Geological Survey, Spišská Nová (Archive).

Malusá, M., Danišík, M., Kuhlemann, J. (2014): Thermochronological response to rifting and subduction in the Corsica-Sardinia block. *Geophysical Research Abstracts*, vol. 16, 1.

McCaffrey, M., Lazar, B., Holland, H. (1987): The evaporation path of seawater and coprecipitation of Br- and K+ with halite. *Journal of Sediment Geol*, vol. 57, 928–937.

McLennan, S. (1989): Rare earth elements in sedimentary rocks: Influence of provenance and sedimentary processes. *Reviews in Mineralogy*, vol. 21, 169–200.

Moine, B., Fortuné, J., Moreau, P., Viguier, F. (1989): Comperative mineralogy, geochemistry, and conditions of formation of two metasomatic talc and chlorite deposits: Trimouns (Pyrenees, France) and Rabenwald Eastern Alps, Austria. *Econ Geol*, vol. 84, 1398–1416.

Möller, P. (1989): Minor and trace elements in magnesite. In: P. Möller (Ed.), *Magnesite — Geology, Mineralogy, Geochemistry, Formation of Mg-Carbonates*, vol. 28, Gebrüder Borntraeger (Mon. Ser. Min. Deposits), pp. 173–195.

Moore, D., Rymer, M. (2007): Talc-bearing serpentinite and the creeping section of the San Andreas fault. *Nature*, vol. 448, 795–797.

Nabelek, P., Labotka, T., O'Neil, J., Papike, J. (1984): Contrasting fluid/rock interaction between the Notch Peak granitic intrusion and argillites and limestones in western Utah: evidence from stable isotopes and phase assemblages. *Contrib Mineral Petrol*, vol. 86, 25–43.

Neubauer, F. (2001): Structural control on the formation of talc deposits: Lassing, Austria. In: A. Piestrynski (Ed.), *Mineral Deposits at the Beginning of the 21st Century* (Swets & Zeitlinger Publishers Lisse), pp. 1011–1014.

Neubauer, F., Frisch, W., Hansen, B.T. (2002): Early Palaeozoic tectonothermal events in basement complexes of the eastern Greywacke Zone (Eastern Alps): evidence from U-Pb zircon dating. *Internation Journal of Earth Science*, vol. 91, 775–786.

Neubauer, F., Handler, R., Hermann, S., Paulus, G. (1993): Tectonostratigraphy and structure of the east Graywacke Zone, Eastern Alps. *Mitteilungen der Österreichischen Geologischen Gesellschaft*, vol. 87, 61–74.

Neubauer, F., Handler, R., Hermann, S., Paulus, G. (1994): Revised Lithostratigraphy and Structure of the Eastern Graywacke Zone (Eastern Alps). *Mitteilungen der Österreichischen Geologischen Gesellschaft*, vol. 86, 61–74.

Olivet, J. (1996): La cinématique de la plaque Ibérique. In: *Bulletin des Centres de Recherches Exploration-Production Elf-Aquitaine*, vol. 20, pp. 131–195.

Petrasová, K., Faryad, S., Jeřábek, P., Žáčová, E. (2007): Origin and metamorphic evolution of magnesite-talc and adjacent rocks near Gemerská Poloma, Slovak Republic. *Jounral of Geosciences*, vol. 52, 125–132.

Plašienka, D., Grecula, M., Putiš, M., Kováč, M., Hovorka, D. (1997): Evolution and Structure of the Western Carpathians: an overview. In: P. Grecula, D. Hovorka, M. Putiš (Eds.), *Geological evolution of the Western Carpathians* (Mineralia Slovaca – Monograph, Bratislava), pp. 1–24.

Pohl, W. (1990): Genesis of magnesite deposits – model and trends. *Geologische Rundschau*, vol. 79/2, 291–299.

Polgári, M., Prochaska, W., Beran, A. (2010): Alpine carbonate mining sites: Aspects of carbonate mineralizations related to the manganese mine of Úrkút, Hungary, the magnesite deposit of Veitsch and the siderite mine Steirischer Erzberg, Austria. *Acta Mineralogica-Petrographica*, vol. 4, 1–16.

Prochaska, W. (1989): Geochemistry and genesis of Austrian talc deposits. *Applied Geochemistry*, vol. 4, 511–525.

Prochaska, W. (1997): Die Bedeutung der chemischen Zusammensetzung von Einschlussfluiden und laugbaren Salzen für die Genese von hydrothermalen und sedimentären Karbonatgesteinen in den Ostalpen. *Mitteilungen der Österreichischen Geologischen Gesellschaft*, vol. 90, 175–183.

Prochaska, W. (2000): Magnesite and talc deposits in Austria. *Mineralia Slovaca*, vol. 32, 543–548.

Putiš, M. (1993): South Tatric - Veporic basement geology: Variscan nappe structures; Alpine thick-skinned and extensional tectonics in the Western Carparthians (eastern Low Tatra Mountains, northwestern Slovak Ore Mountains). *Mitteilungen der Österreichischen Geologischen Gesellschaft*, vol. 86, 83–99.

Radvanec, M., Koděra, P., Prochaska, W. (2004): Mg replacement of the Gemerská Poloma talk-magnesite deposit, Western Carpathians, Slovakia. *Acta Petrologica Sinica*, vol. 20, 773–790.

Rantitsch, G., Grogger, W., Teichert, C., Ebner, F., Hofer, C., Maurer, E.M., Schaffer, B., Toth, M. (2004): Conversion of carbonaceous material to graphite within the Greywacke Zone of the Eastern Alps. *Internation Journal of Earth Science*, vol. 93, 959–973.

Rantitsch, G., Sachsenhofer, R., Hasenhüttl, C., Russegger, B., Rainer, T. (2005): Thermal evolution of an extensional detachment as constrained by organic metamorphic data and thermal modeling: Graz Palaeozoic Nappe Complex (Eastern Alps). *Tectonoph*, vol. 411, 57–72.

Ratschbacher, L. (1987): Stratigraphy, tectonics and paleogeography of the Veitsch nappe/Graywackezone, Eastern Alps, Austria: a rearrangement. *Mineralia Slovaca*, vol. 5, 407–414.

Ratschbacher, L., Frisch, W. (1993): Palinspastic Reconstruction of the Pre-Triassic Basement Units in the Alps: The Eastern Alps. In: J.v. Raumer, F. Neubauer (Eds.), *Pre-Mesozoic Geology in the Alps* (Springer), pp. 41–51.

Redlich, K. (1909): Die Typen der Magnesitslagerstätten. *Z. f. prakt. Geol.*, vol. 17, 300–310.

Reiners, P., Zhou, Z., Ehlers, T., Xu, C., Brandon, M., Donelick, R., Nicolescu, S. (2003): Post-orogenic evolution of the Dabie Shan, Eastern China, from (U-Th)/He and fission track thermochonology. *American Journal of Science*, vol. 303, 489–518.

Rosenbaum, G., Lister, G. (2004): Neogene and Quaternary rollback evolution of the Tyrrhenian Sea, the Apennines and the Sicilian Maghrebides. *Tectonics*, vol. 23, 1–17.

Schmid, S., Fügenschuh, B., Kissling, E., Schuster, R. (2004): Tectonic map and overall architecture of the Alpine orogen. *Eclogae geol. Helv.*, vol. 97, 93–117.

Schoenlaub, H. (1981): Die Grauwackenzone in den Eisenerzer Alpen. *Jahrbuch der Geologischen Bundesanstalt*, vol. 124, 361–423.

Schroll, E. (1997): Geochemische und geochronologische Daten und Erläuterungen. In: L. Weber (Ed.), *Handbuch der Lagerstätten der Erze, Industrieminerale und Energierohstoffe Österreichs*, vol. 19 (Geologische Bundesanstalt), pp. 395–538.

Schroll, E. (2002): Genesis of magnesite deposits in the view of isotope geochemistry. *Boletim Paranaense de Geociências*, vol. 50, 59–68.

Schulz, B., Bombach, K., Pawlig, S., Brätz, H. (2004): Neoproterozoic to Early-Paleozoic magmatic evolution in the Gondwana-derived Austroalpine basement to the south of the Tauern Window (Eastern Alps). *Int J Earth Sci (Geol Rundsch)*, vol. 93, 824–843.

Schuster, R., Frank, W. (1999): Metamorphic evolution of the Austroalpine units east of the Tauern Window: indications for Jurassic strike slip tectonics. *Mitt. Ges. Geol. Bergbaustud. Österr.*, vol. 42, 37–58.

Schuster, R., Scharbert, S., Abart, R. (1999): Permo-Triassic crustal extension during opening of the Neotethyan Ocean in the Austroalpine - Southalpine realm. *Tbinger Geowissenschaftliche Arbeiten - Serie A*, vol. 52, 5–6.

Selverstone, J. (1988): Evidence for east-west crustal extension in the Eastern Alps: Implications for unroofing of the Tauern Window. *Tectonics*, vol. 7, 87–105.

Sérrane, M. (1999): The Gulf of Lion continental margin (NW Mediterranean) revistited by IBS: an overview. In: B. Durand, L. Jolivet, F. Horváth, M. Séranne (Eds.), *The Mediterranean basins: Tertiary extension within the Alpine Orogen*, vol. 156 (Geological Society of London, Special Publications), pp. 15–36.

Shepherd, T. (1985): *A practical guide to fluid inclusion studies* (Blackie, London).

Siebel, W., Hann, H., Danišík, M., Shang, C., Berthold, C., Rohrmüller, J., Wemmer, K., Evans, N. (2010): Age constraints on faulting and fault reactivation: a multi-chronological approach. *Int J Earth Sci*, vol. 99, 1187–1197.

Spandler, C., Hermann, J., Faure, K., Mavrogenes, J., Arculus, R. (2008): The improtance of talc and chlorite hybrid rocks for volatile recycling through subduction zone; evidence from the high-pressure subduction melange of New Caledonia. *Contrib Mineral Petrol*, vol. 155, 181–198.

Spiegel, C., Kuhlemann, J., Dunkel, I., Frisch, W., von Eynatten, H., Kadosa, B. (2000): Erosion history of the Central Alps: evidence from zircon fission track data of the foreland basin sediments. *Terra Nova*, vol. 12, 163–170.

Spiegel, C., Siebel, W., Kuhlemann, J., Frisch, W. (2004): Toward a comprehensive provenance analysis: A multi-method approach and its implication for the evolution of the Central Alps. *Geological Society of America, Special Paper*, vol. 378, 37–50.

Spötl, C., Vennemann, T. (2003): Continous-flow isotope ratio mass spectrometric analyis of carbonate minerals. *Rapid Communications in Mass Spectrometry*, vol. 17, 1004–1006.

Stampfli, G., Raumer, J., Borel, G. (2002): Paleozoic evolution of pre-Variscan terranes: From Gondwana to the Variscan collision. *Geological Society of America*, vol. 364, 1–18.

Stipp, M., Stünitz, H., Heilbronner, R., Schmid, S. (2002): The eastern Tonale fault zone: a "natural laboratory" for crystal plastic deformation of quartz over a temperature range from 250 to 700°C. *Journal of Structural Geology*, vol. 24, 1861–1884.

Tagami, T. (2012): Thermochronological investigations of fault zones. *Tectonoph*, vol. 538-540, 67–85.

Tollmann, A. (1977): *Geologie von Österreich - Die Zentralalpen* (Deuticke).

Tornos, F., Spiro, B. (2000): The Geology and Isotope Geochemistry of the Talc Deposits of Puebla de Lillo (Cantabrian Zone, Northern Spain). *Econ Geol*, vol. 95, 1277–1296.

Turanová, L., Turan, J., Kilík, J. (1997): Mineralization of a magnesite-talc deposit Gemerska Poloma (Spišsko-Gemerské Rudohorie Mts). *Acta Geol Univ Com*, vol. 52, 5–13.

Valley, J., Bohlen, S., Essene, E., Lamb, W. (1990): Metamorphism in the Adirondacks. *J Petrol*, vol. 31, 555–596.

Vigliotti, L., Langenheim, V. (1995): When did Sardinia stop rotating? New palaeomagnetic results. *Terra Nova*, vol. 7, 424–435.

Wagreich, M. (1993): Subcrustal tectonic erosion in orogenic belts – a model for the Late Cretaceous subsidence of the Northern Calcareous Alps (Austria). *Geology*, vol. 21, 941–944.

Wagreich, M. (1995): Subduction tectonic erosion and Late Cretaceous subsidence along the northern Austroalpine margin (Eastern Alps, Austria). *Tectonoph*, vol. 242, 63–78.

Willingshofer, E., Neubauer, F., Cloetingh, S. (1999a): The Significance of Gosau-Type Basins for the Late Cretaceous Tectonic History of the Alpine-Carpathian Belt. *Phys. Chem. Earth*, vol. 24, 687–695.

Willingshofer, E., van Wees, J., Cloetingh, S. (1999b): Thermomechanical consequences of Cretaceous continent-continent collision in the eastern Alps (Austria): Insights from two dimensional modeling. *Tectonics*, vol. 18, 809–826.

Wolf, R., Farley, K., Kass, D. (1998): Modeling of the temperature sensitivity of the apatite (U-Th)/He thermochronometer. *Chem Geol*, vol. 148, 105–114.

Wolf, R., Farley, K., Silver, L. (1996): Helium diffusion and low-temperature thermochronometry of apatite. *Geochimica et Cosmochimica Acta*, vol. 60(21), 4231–4240.

Wölfler, A., Kurz, W., Danišík, Rabitsch, R. (2010): Dating of fault zone activity by apatite fission track and apatite (U-Th)/He thermochronometry: a case study from the Lavanttal fault system (Eastern Alps). *Terra Nova*, vol. 00, 1–9.

Yamada, R., Matsuda, T., Omura, K. (2007): Apatite and zircon fission-track dating from the Hirabayashi-NIED borehole, Nojima Fault, Japan: Evidence for anomalous heating in fracture zones. *Tectonoph*, vol. 443, 153–160.

Zheng, Y.F., Hoefs, J. (1993): Carbon and oxygen isotopic covariations in hydrothermal calcites. *Mineralium Deposita*, vol. 28, 79–89.

Ziegler, J. (1977): *Helium: stopping porwers and ranges in all element matter* (Pergamon, New York).

List of Figures

Appendix A

Geochemical Analysis

Sample	VE 2a	VE 7	VE 9	VE 14a	VE 14c	VE 2b	VE 5c	VE 5b	VE 5d	VE 5a	SU 1	SU 2	WS 7	WS 8
Rocktype	dol	dol	dol	dol	mgs	dol	dol	dol	dol	mgs	cc marble	cc marble	dol marble	dol marble
remarks	vein	hostrock	hostrock	hostrock	hostrock	vein	vein	vein	vein	hostrock	Triebensteinkalk	Triebensteinkalk	Triebensteinkalk	Triebensteinkalk
deposit	Veitsch	Veitsch	Veitsch	Veitsch	Veitsch	Veitsch	Veitsch	Veitsch	Veitsch	Veitsch	outside	outside	outside	outside
wt%														
SiO_2	1.73	1.47	0.73	1.4	2.5	2.15	0.13	0.18	0.76	0.28	2.32	1.44	4.58	2.15
Al_2O_3	1.15	0.26	0.41	0.77	0.79	0.24	0.03	0.07	0.05	0.16	0.53	0.16	0.07	0.13
Fe_2O_3(T)	3	0.98	1.27	1.35	4.82	1.64	1.63	2.75	2.47	3.55	0.4	0.17	0.12	0.4
MnO	0.156	0.124	0.16	0.102	0.243	0.124	0.132	0.186	0.168	0.223	0.014	0.036	0.019	0.033
MgO	28.34	21.42	21.57	21.79	36.77	20.28	20.88	19.5	20.14	43.22	0.66	0.53	20.22	20.8
CaO	20.34	30.2	30.33	29.3	8.17	29.24	30.47	30.03	29.96	2.24	52.52	54.41	28.98	29.83
Na_2O	0.03	0.06	0.07	0.06	0.04	0.08	0.02	0.03	0.04	0.02	0.07	0.07	0.03	0.03
K_2O	< 0.01	< 0.01	0.01	0.01	< 0.01	0.02	< 0.01	< 0.01	< 0.01	< 0.01	0.1	0.03	< 0.01	< 0.01
TiO_2	0.096	0.006	0.01	0.016	0.027	0.002	< 0.001	0.002	< 0.001	0.004	0.022	0.004	0.003	0.01
P_2O_5	0.02	0.04	0.05	0.04	0.07	0.04	< 0.01	0.03	0.02	0.05	0.03	0.02	0.06	0.11
LOI	45.77	46.27	46.38	45.79	47.17	45.71	46.94	46.41	46.21	50.35	42.93	44.1	44.43	46
Total	100.6	100.8	101	100.6	100.6	99.53	100.2	99.19	99.83	100.1	99.61	101	98.52	99.5
ppm														
Sc	2	< 1	1	1	1	1	1	2	2	< 1	1	< 1	< 1	< 1
Be	< 1	< 1	< 1	< 1	< 1	< 1	< 1	< 1	< 1	< 1	< 1	< 1	< 1	< 1
V	23	17	18	15	16	15	12	10	12	8	11	8	11	15
Cr	< 20	< 20	< 20	< 20	< 20	< 20	< 20	< 20	< 20	< 20	< 20	< 20	< 20	< 20
Co	8	< 1	< 1	1	5	< 1	< 1	< 1	< 1	2	6	8	< 1	< 1
Ni	30	< 20	< 20	< 20	< 20	< 20	< 20	< 20	< 20	< 20	< 20	< 20	< 20	< 20
Cu	< 10	< 10	< 10	< 10	20	< 10	< 10	< 10	< 10	30	10	10	< 10	< 10
Zn	< 30	< 30	< 30	< 30	< 30	< 30	< 30	50	< 30	< 30	< 30	< 30	< 30	< 30
Ga	2	< 1	< 1	1	1	< 1	< 1	< 1	< 1	< 1	< 1	< 1	< 1	< 1
Ge	< 0.5	< 0.5	< 0.5	< 0.5	< 0.5	< 0.5	< 0.5	< 0.5	< 0.5	< 0.5	< 0.5	< 0.5	< 0.5	< 0.5
As	43	< 5	8	16	22	< 5	< 5	< 5	< 5	12	< 5	< 5	< 5	< 5
Rb	< 1	< 1	< 1	< 1	< 1	< 1	< 1	< 1	< 1	< 1	4	< 1	< 1	< 1
Sr	246	51	32	77	63	334	308	233	260	27	336	720	116	119
Y	5.9	1.2	2	5	7.7	14	7.5	27.4	20.7	3.4	9.5	2.5	< 0.5	0.6
Zr	22	2	3	3	6	< 1	3	< 1	4	2	6	2	< 1	2
Nb	1.9	< 0.2	< 0.2	< 0.2	< 0.2	< 0.2	< 0.2	< 0.2	< 0.2	< 0.2	0.4	< 0.2	< 0.2	< 0.2
Mo	< 2	< 2	< 2	< 2	< 2	< 2	< 2	< 2	< 2	< 2	< 2	< 2	< 2	< 2
Ag	< 0.5	< 0.5	< 0.5	< 0.5	< 0.5	< 0.5	< 0.5	< 0.5	< 0.5	< 0.5	< 0.5	< 0.5	< 0.5	< 0.5
In	< 0.1	< 0.1	< 0.1	< 0.1	< 0.1	< 0.1	< 0.1	< 0.1	< 0.1	< 0.1	< 0.1	< 0.1	< 0.1	< 0.1
Sn	< 1	< 1	< 1	< 1	< 1	< 1	< 1	< 1	< 1	< 1	< 1	< 1	< 1	< 1
Sb	2.7	< 0.2	0.9	< 0.2	2.7	< 0.2	< 0.2	0.6	0.2	6.6	< 0.2	0.7	< 0.2	< 0.2
Cs	< 0.1	< 0.1	< 0.1	< 0.1	< 0.1	< 0.1	< 0.1	< 0.1	< 0.1	< 0.1	0.1	< 0.1	< 0.1	< 0.1
Ba	< 3	< 3	3	< 3	5	< 3	< 3	< 3	< 3	< 3	19	7	< 3	< 3
Hf	0.5	< 0.1	< 0.1	< 0.1	0.1	< 0.1	< 0.1	< 0.1	0.2	< 0.1	0.1	< 0.1	< 0.1	< 0.1
Ta	0.11	< 0.01	< 0.01	< 0.01	< 0.01	< 0.01	< 0.01	< 0.01	< 0.01	< 0.01	0.02	< 0.01	< 0.01	< 0.01
W	< 0.5	< 0.5	< 0.5	< 0.5	< 0.5	2.3	1.1	< 0.5	< 0.5	< 0.5	< 0.5	6.4	< 0.5	< 0.5
Tl	< 0.05	< 0.05	< 0.05	< 0.05	< 0.05	< 0.05	< 0.05	< 0.05	< 0.05	< 0.05	< 0.05	< 0.05	< 0.05	< 0.05
Pb	5	< 5	< 5	< 5	< 5	< 5	< 5	< 5	< 5	< 5	< 5	< 5	< 5	< 5
Bi	1.4	< 0.1	0.9	0.5	1.5	< 0.1	< 0.1	< 0.1	< 0.1	0.2	0.3	< 0.1	< 0.1	< 0.1
Th	1.79	0.18	0.23	0.44	0.43	< 0.05	< 0.05	< 0.05	0.06	0.13	0.6	0.14	< 0.05	0.13
U	2.42	0.75	1.38	1.12	1.33	0.11	0.19	0.18	0.23	1.04	0.94	8.41	0.51	2.62
La	7.28	1.35	1.41	0.97	1.32	6.67	13.2	7.97	8.14	0.67	5.16	1.33	0.48	0.56
Ce	11.7	2.46	2.56	2.45	3.84	15.6	24.2	20.3	18.1	2.06	7.1	1.73	0.8	1.21
Pr	1.37	0.3	0.33	0.43	0.54	2.18	2.61	2.76	2.41	0.4	1.08	0.22	0.1	0.15
Nd	5.71	1.32	1.52	2.43	2.86	9.3	9.86	12.5	10.2	2.23	4.65	0.9	0.4	0.66
Sm	1.61	0.28	0.37	1.48	1.92	2.58	1.86	3.61	2.8	1.01	1.05	0.17	0.08	0.14
Eu	1.39	0.13	0.141	0.531	0.756	1.14	0.895	0.696	0.712	0.5	0.228	0.043	0.021	0.083
Gd	1.5	0.3	0.36	1.7	2.49	2.52	1.7	3.67	2.78	1.05	1.16	0.24	0.07	0.14
Tb	0.21	0.04	0.06	0.23	0.36	0.39	0.22	0.66	0.51	0.13	0.18	0.04	0.01	0.02
Dy	1.07	0.19	0.34	1.13	1.75	2.27	1.3	4.58	3.28	0.59	1.17	0.26	0.07	0.12
Ho	0.2	0.04	0.07	0.18	0.27	0.42	0.23	0.92	0.65	0.1	0.26	0.06	0.01	0.02
Er	0.56	0.11	0.21	0.44	0.64	1.19	0.68	2.84	1.98	0.25	0.72	0.18	0.04	0.05
Tm	0.084	0.016	0.031	0.051	0.083	0.154	0.102	0.427	0.297	0.033	0.103	0.028	< 0.005	0.008
Yb	0.56	0.1	0.19	0.3	0.44	0.96	0.67	2.65	1.86	0.2	0.65	0.19	0.04	0.05
Lu	0.079	0.015	0.034	0.044	0.068	0.127	0.099	0.419	0.277	0.031	0.105	0.032	0.006	0.008

Sample	WS 12	WS 9c a	WS 9c b	WS 10b a	WS 1	WS 2	WS 3	WS 4	WS 9b d	WS 9b h	WS 9b g	WS 11	WS 20	WS 21	WS 23 h	WS 23 d
Rocktype	mgs	mgs	mgs	mgs	dol	mgs	mgs	mgs	mgs	mgs	mgs	mgs	mgs	mgs	mgs	mgs
remarks	with talc	with talc	with talc	with talc	vein	no talc	with talc	no talc	no talc	no talc	with talc	with talc	with talc	with talc	no talc	no talc
deposit	Wald a S	Wald a S	Wald a S	Wald a S	Wald a S	Wald a S	Wald a S	Wald a S	Wald a S	Wald a S	Wald a S	Wald a S	Wald a S	Wald a S	Wald a S	Wald a S
wt%																
SiO_2	4.94	1.86	1.65	1.76	0.24	4.98	2.82	1.47	1.06	1.17	1.78	5.93	14.05	2.89	1.77	1.09
Al_2O_3	0.36	0.25	0.21	0.33	0.1	0.38	0.08	0.09	0.09	0.09	0.11	0.12	1.08	0.02	0.03	0.1
Fe_2O_3(T)	1.22	1.22	1.29	1.25	0.54	1.48	1.65	1.57	1.26	1.31	1.29	1.21	2.1	1.65	1.85	2.2
MnO	0.081	0.077	0.08	0.085	0.037	0.076	0.096	0.091	0.079	0.08	0.08	0.074	0.079	0.104	0.091	0.099
MgO	45.53	42.85	44.64	45.97	21.28	45.71	45.59	46.52	46.35	46.9	45.87	45.83	38.58	45.91	46.07	45.42
CaO	0.69	5.02	2.63	0.7	30.03	0.5	0.59	0.67	1.11	0.44	1.35	0.62	4.76	0.56	0.63	1.03
Na_2O	0.05	0.03	0.05	0.06	0.04	0.02	0.03	0.03	0.05	0.04	0.03	0.02	0.03	0.03	0.04	0.07
K_2O	0.02	< 0.01	0.01	0.02	< 0.01	< 0.01	< 0.01	< 0.01	< 0.01	< 0.01	< 0.01	< 0.01	< 0.01	< 0.01	< 0.01	0.02
TiO_2	0.032	0.009	0.005	0.024	< 0.001	0.031	0.004	0.006	0.002	0.002	0.004	0.013	0.118	0.002	0.002	0.002
P_2O_5	< 0.01	< 0.01	0.03	0.04	0.02	0.02	0.04	< 0.01	0.03	0.02	0.02	0.01	0.03	0.01	0.02	0.02
LOI	47.89	49.58	50.14	50.11	47.05	47.65	49.37	50.49	50.86	50.88	50.17	47.1	39.72	49.57	50.34	50.7
Total	100.8	100.9	100.7	100.4	99.34	100.8	100.3	100.9	100.9	100.9	100.7	100.9	100.5	100.7	100.8	100.8
ppm																
Sc	< 1	< 1	< 1	3	6	1	< 1	< 1	< 1	< 1	< 1	< 1	6	< 1	2	1
Be	< 1	< 1	< 1	< 1	< 1	< 1	< 1	< 1	< 1	< 1	< 1	< 1	< 1	< 1	< 1	< 1
V	30	15	18	16	14	20	20	24	19	17	13	17	76	18	20	22
Cr	< 20	< 20	< 20	< 20	< 20	< 20	< 20	< 20	< 20	< 20	< 20	< 20	< 20	< 20	< 20	< 20
Co	< 1	< 1	< 1	< 1	< 1	< 1	< 1	< 1	< 1	< 1	< 1	< 1	< 1	< 1	1	1
Ni	< 20	< 20	< 20	< 20	< 20	< 20	< 20	< 20	< 20	< 20	< 20	< 20	< 20	< 20	< 20	< 20
Cu	< 10	< 10	< 10	< 10	< 10	< 10	< 10	< 10	< 10	< 10	< 10	< 10	< 10	< 10	< 10	< 10
Zn	< 30	< 30	< 30	< 30	< 30	< 30	< 30	< 30	< 30	< 30	< 30	< 30	< 30	< 30	< 30	< 30
Ga	< 1	< 1	< 1	< 1	< 1	< 1	< 1	< 1	< 1	< 1	< 1	< 1	2	< 1	< 1	< 1
Ge	< 0.5	< 0.5	< 0.5	< 0.5	< 0.5	< 0.5	< 0.5	< 0.5	< 0.5	< 0.5	< 0.5	< 0.5	1.3	< 0.5	< 0.5	< 0.5
As	< 5	< 5	< 5	< 5	< 5	< 5	< 5	< 5	< 5	< 5	< 5	< 5	< 5	< 5	< 5	< 5
Rb	< 1	< 1	< 1	< 1	< 1	< 1	< 1	< 1	< 1	< 1	< 1	< 1	< 1	< 1	< 1	< 1
Sr	4	29	19	4	65	< 2	2	3	4	3	5	4	46	3	5	6
Y	1	2.8	2.2	2.2	11.4	3.3	1.6	1.1	2.2	2	2	1	6.2	6.4	4.6	3.4
Zr	3	2	1	2	< 1	5	< 1	1	< 1	< 1	1	2	9	< 1	< 1	< 1
Nb	< 0.2	< 0.2	< 0.2	< 0.2	< 0.2	< 0.2	< 0.2	< 0.2	< 0.2	< 0.2	< 0.2	< 0.2	< 0.2	< 0.2	< 0.2	< 0.2
Mo	< 2	< 2	< 2	< 2	< 2	< 2	< 2	< 2	< 2	< 2	< 2	< 2	< 2	< 2	< 2	< 2
Ag	< 0.5	< 0.5	< 0.5	< 0.5	< 0.5	< 0.5	< 0.5	< 0.5	< 0.5	< 0.5	< 0.5	< 0.5	< 0.5	< 0.5	< 0.5	< 0.5
In	< 0.1	< 0.1	< 0.1	< 0.1	< 0.1	< 0.1	< 0.1	< 0.1	< 0.1	< 0.1	< 0.1	< 0.1	< 0.1	< 0.1	< 0.1	< 0.1
Sn	< 1	< 1	< 1	< 1	< 1	< 1	< 1	< 1	< 1	< 1	< 1	< 1	< 1	< 1	< 1	< 1
Sb	< 0.2	< 0.2	< 0.2	< 0.2	0.2	< 0.2	< 0.2	< 0.2	< 0.2	< 0.2	< 0.2	< 0.2	0.6	< 0.2	< 0.2	< 0.2
Cs	< 0.1	< 0.1	< 0.1	< 0.1	< 0.1	< 0.1	< 0.1	< 0.1	< 0.1	< 0.1	< 0.1	< 0.1	< 0.1	< 0.1	< 0.1	< 0.1
Ba	< 3	< 3	< 3	< 3	< 3	< 3	< 3	< 3	< 3	< 3	< 3	< 3	< 3	< 3	< 3	< 3
Hf	< 0.1	< 0.1	< 0.1	< 0.1	< 0.1	0.1	< 0.1	< 0.1	< 0.1	< 0.1	< 0.1	< 0.1	0.2	< 0.1	< 0.1	< 0.1
Ta	< 0.01	< 0.01	< 0.01	< 0.01	< 0.01	< 0.01	< 0.01	< 0.01	< 0.01	< 0.01	< 0.01	< 0.01	0.01	< 0.01	< 0.01	< 0.01
W	< 0.5	< 0.5	< 0.5	< 0.5	< 0.5	< 0.5	< 0.5	< 0.5	< 0.5	< 0.5	< 0.5	< 0.5	< 0.5	< 0.5	< 0.5	< 0.5
Tl	< 0.05	< 0.05	< 0.05	< 0.05	< 0.05	< 0.05	< 0.05	< 0.05	< 0.05	< 0.05	< 0.05	< 0.05	< 0.05	< 0.05	< 0.05	< 0.05
Pb	< 5	< 5	< 5	< 5	< 5	< 5	< 5	< 5	< 5	< 5	< 5	< 5	< 5	< 5	< 5	< 5
Bi	< 0.1	< 0.1	< 0.1	< 0.1	< 0.1	< 0.1	< 0.1	< 0.1	< 0.1	< 0.1	< 0.1	< 0.1	< 0.1	0.2	< 0.1	< 0.1
Th	0.17	0.14	0.09	0.05	< 0.05	0.17	< 0.05	< 0.05	< 0.05	0.06	0.08	0.06	0.31	< 0.05	< 0.05	< 0.05
U	0.26	0.28	0.22	0.21	0.03	0.2	0.07	0.09	0.19	0.28	0.22	0.18	0.17	0.02	0.03	0.01
La	0.56	0.45	0.36	0.34	1.22	0.37	0.57	0.45	0.19	0.15	0.17	0.16	0.32	0.22	0.69	0.55
Ce	1.49	1.66	1.27	1.08	9.21	1.36	2.15	2	0.56	0.41	0.48	0.61	0.93	0.73	2.75	2.21
Pr	0.26	0.35	0.26	0.22	2.28	0.28	0.4	0.39	0.12	0.08	0.1	0.13	0.19	0.18	0.54	0.47
Nd	1.66	2.44	1.89	1.5	15.9	1.65	2.23	2.08	0.8	0.62	0.77	0.91	1.53	1.42	3.36	2.81
Sm	1.03	1.38	1.06	0.81	8.45	0.74	0.88	0.65	0.63	0.45	0.52	0.46	1.21	1.41	1.37	1.42
Eu	0.342	0.391	0.295	0.213	3.69	0.327	0.442	0.406	0.126	0.103	0.12	0.157	0.401	0.514	0.515	0.57
Gd	0.77	1.34	1.1	0.76	7.58	0.82	0.9	0.52	0.64	0.59	0.67	0.37	1.58	2.02	1.35	1.4
Tb	0.06	0.14	0.11	0.08	0.79	0.11	0.08	0.05	0.09	0.08	0.09	0.04	0.24	0.28	0.18	0.17
Dy	0.26	0.64	0.53	0.41	3.41	0.62	0.33	0.24	0.45	0.41	0.43	0.21	1.37	1.44	0.9	0.79
Ho	0.04	0.1	0.09	0.08	0.46	0.11	0.05	0.04	0.08	0.07	0.07	0.04	0.25	0.23	0.16	0.13
Er	0.12	0.26	0.21	0.23	1.05	0.3	0.12	0.1	0.19	0.18	0.17	0.09	0.75	0.6	0.46	0.34
Tm	0.016	0.031	0.025	0.036	0.095	0.043	0.019	0.015	0.024	0.021	0.021	0.012	0.115	0.075	0.064	0.046
Yb	0.11	0.16	0.14	0.23	0.53	0.26	0.14	0.09	0.13	0.12	0.11	0.07	0.7	0.4	0.38	0.28
Lu	0.018	0.022	0.019	0.035	0.056	0.038	0.02	0.014	0.017	0.017	0.016	0.012	0.102	0.054	0.059	0.038

Sample	LA 2	LA 4	LA 1a	LA 8	LA 12	LA 9a	LA 9b	LA PR 31	LA PR 33	LA PR 48	LA PR 65	LA PR 85	LA PR 121
Rocktype	ccM	ccM	dolM	ccM	ccM	ccM	ccM	dolM	mgs	dolM	dolM	dolM	dolM
remarks	hostrock	hostrock	hostrock	hostrock	hostrock	hostrock	hostrock	hostrock	hostrock	hostrock	hostrock	hostrock	hostrock
deposit	Lassing	Lassing	Lassing	Lassing	Lassing	Lassing	Lassing	Lassing	Lassing	Lassing	Lassing	Lassing	Lassing
wt%													
SiO_2	6.64	3.94	1.38	3.73	1.61	4.48	5.24	7.54	3.3	10.94	6.86	18.27	1.7
Al_2O_3	0.41	0.25	0.3	0.22	0.15	0.2	0.91	0.18	0.38	0.3	0.12	0.28	0.16
Fe_2O_3(T)	0.43	0.26	0.82	0.18	0.11	0.17	0.51	0.78	1.15	0.69	0.36	0.37	0.4
MnO	0.078	0.02	0.071	0.01	0.014	0.034	0.041	0.067	0.063	0.057	0.023	0.018	0.026
MgO	1.91	2.05	18.73	0.68	2.1	5.19	4.08	21.2	42.77	22.39	21.47	13.73	20.95
CaO	49.18	50.99	33.1	53.51	51.36	49.1	49.22	27.3	3.47	24.67	27.69	28.67	29.69
Na_2O	0.16	0.07	0.03	0.06	0.05	0.04	0.04	0.06	0.04	0.06	0.04	0.04	0.06
K_2O	0.08	0.04	0.05	0.06	0.05	0.01	0.01	0.01	< 0.01	0.02	< 0.01	< 0.01	0.02
TiO_2	0.009	0.009	0.008	0.015	0.006	0.012	0.083	0.006	0.019	0.018	0.004	0.016	0.006
P_2O_5	< 0.01	0.01	0.03	0.02	0.01	0.01	0.06	0.01	0.03	< 0.01	0.02	0.03	0.01
LOI	40.98	42.57	45.93	42.23	43.42	41.63	40.28	42.95	49.56	40.65	43.68	38.32	46.69
Total	99.88	100.2	100.4	100.7	98.88	100.9	100.5	100.1	100.8	99.8	100.3	99.76	99.72
ppm													
Sc	< 1	< 1	< 1	< 1	< 1	< 1	2	< 1	< 1	1	< 1	< 1	< 1
Be	< 1	< 1	< 1	< 1	< 1	< 1	< 1	< 1	< 1	< 1	< 1	< 1	< 1
V	8	6	13	8	14	9	20	6	16	8	10	7	< 5
Cr	< 20	< 20	< 20	< 20	< 20	< 20	< 20	< 20	< 20	< 20	< 20	< 20	< 20
Co	< 1	< 1	< 1	< 1	< 1	< 1	< 1	3	< 1	2	2	3	2
Ni	< 20	< 20	< 20	< 20	< 20	< 20	< 20	< 20	< 20	< 20	< 20	< 20	< 20
Cu	< 10	< 10	< 10	< 10	10	< 10	< 10	< 10	< 10	< 10	< 10	< 10	< 10
Zn	< 30	< 30	< 30	< 30	< 30	< 30	< 30	< 30	< 30	< 30	< 30	< 30	< 30
Ga	< 1	< 1	< 1	< 1	< 1	< 1	2	< 1	< 1	< 1	< 1	< 1	< 1
Ge	< 0.5	< 0.5	< 0.5	< 0.5	< 0.5	< 0.5	< 0.5	< 0.5	< 0.5	1	< 0.5	< 0.5	< 0.5
As	< 5	< 5	< 5	< 5	< 5	< 5	< 5	< 5	< 5	< 5	< 5	< 5	< 5
Rb	< 1	< 1	< 1	< 1	< 1	< 1	< 1	< 1	< 1	< 1	< 1	< 1	< 1
Sr	206	207	170	193	186	301	281	74	51	208	106	92	90
Y	3.2	1.6	1.7	1.2	< 0.5	1.2	6.2	< 0.5	1	3.4	0.7	0.7	< 0.5
Zr	22	11	2	5	1	2	31	1	4	2	1	2	2
Nb	< 0.2	< 0.2	0.5	< 0.2	< 0.2	0.3	2.7	< 0.2	0.4	0.2	< 0.2	< 0.2	< 0.2
Mo	< 2	< 2	< 2	< 2	< 2	< 2	< 2	< 2	< 2	< 2	< 2	< 2	< 2
Ag	< 0.5	< 0.5	< 0.5	< 0.5	< 0.5	< 0.5	< 0.5	< 0.5	< 0.5	< 0.5	< 0.5	< 0.5	< 0.5
In	< 0.1	< 0.1	< 0.1	< 0.1	< 0.1	< 0.1	< 0.1	< 0.1	< 0.1	< 0.1	< 0.1	< 0.1	< 0.1
Sn	< 1	< 1	< 1	< 1	< 1	< 1	< 1	< 1	< 1	< 1	1	< 1	2
Sb	< 0.2	< 0.2	< 0.2	< 0.2	< 0.2	< 0.2	< 0.2	0.7	0.7	0.6	0.9	< 0.2	< 0.2
Cs	< 0.1	< 0.1	< 0.1	< 0.1	< 0.1	< 0.1	< 0.1	< 0.1	< 0.1	0.1	< 0.1	< 0.1	< 0.1
Ba	7	7	15	6	6	6	5	4	< 3	3	43	< 3	< 3
Hf	0.8	0.3	< 0.1	0.1	< 0.1	< 0.1	0.8	< 0.1	0.1	< 0.1	< 0.1	< 0.1	< 0.1
Ta	< 0.01	< 0.01	< 0.01	< 0.01	< 0.01	0.02	0.17	< 0.01	0.05	0.03	0.03	0.02	0.04
W	17.5	< 0.5	< 0.5	< 0.5	< 0.5	< 0.5	< 0.5	< 0.5	< 0.5	< 0.5	< 0.5	< 0.5	< 0.5
Tl	< 0.05	< 0.05	< 0.05	< 0.05	< 0.05	0.07	< 0.05	< 0.05	< 0.05	< 0.05	< 0.05	< 0.05	< 0.05
Pb	< 5	< 5	< 5	< 5	< 5	< 5	< 5	< 5	< 5	< 5	< 5	< 5	< 5
Bi	< 0.1	< 0.1	0.2	< 0.1	< 0.1	< 0.1	< 0.1	< 0.1	< 0.1	< 0.1	< 0.1	< 0.1	< 0.1
Th	0.56	0.29	0.17	0.05	0.11	0.13	0.31	0.07	0.41	0.06	0.09	0.13	0.07
U	0.44	0.24	0.37	0.76	0.43	0.21	0.54	0.31	0.41	0.25	2.31	0.32	0.2
La	1.86	0.88	1.62	0.85	0.61	2.17	3.14	0.81	0.55	2.05	0.76	0.67	0.47
Ce	3.33	1.8	2.71	1.66	3.04	3.91	7.27	1.46	1.48	6.08	1.68	1.19	0.85
Pr	0.39	0.2	0.37	0.22	0.09	0.42	0.97	0.16	0.23	0.98	0.22	0.14	0.09
Nd	1.77	0.88	1.66	0.94	0.37	1.79	4.51	0.57	1.17	4.6	0.85	0.67	0.38
Sm	0.46	0.21	0.34	0.26	0.08	0.39	1.16	0.1	0.3	1.2	0.17	0.14	0.07
Eu	0.211	0.101	0.098	0.067	0.023	0.1	0.261	0.088	0.123	0.437	0.058	0.027	0.037
Gd	0.58	0.27	0.35	0.23	0.08	0.32	1.26	0.08	0.24	1.04	0.16	0.14	0.06
Tb	0.09	0.05	0.06	0.04	0.01	0.05	0.21	0.01	0.03	0.13	0.02	0.02	< 0.01
Dy	0.53	0.3	0.3	0.23	0.08	0.25	1.23	0.07	0.17	0.7	0.12	0.13	0.05
Ho	0.11	0.06	0.06	0.04	0.01	0.04	0.23	0.02	0.03	0.13	0.03	0.03	< 0.01
Er	0.33	0.18	0.16	0.12	0.03	0.12	0.69	0.05	0.1	0.34	0.08	0.08	0.03
Tm	0.05	0.028	0.023	0.017	0.006	0.015	0.096	0.008	0.015	0.045	0.01	0.013	< 0.005
Yb	0.31	0.18	0.15	0.11	0.04	0.08	0.62	0.05	0.09	0.24	0.06	0.08	0.03
Lu	0.055	0.025	0.025	0.018	0.006	0.012	0.098	0.007	0.015	0.036	0.01	0.014	0.005

Sample	GP 16	GP 6	GP 10G	GP 12	GP 43	GP 54	GP 52	GP 17	GP 9	GP 42a	GP 39	GP 30	GP 31a	GP 33	GP 48	GP 34	GP 32
Rocktype	mgs	mgs	mgs	mgs	dol	dol	dol	sec. dol	sec. dol	sec. dol	sec. dol	granite	granite	granite	granite	granite	granite
remarks	hostrock	hostrock	hostrock	hostrock	hostrock	hostrock	hostrock	talc zone	talc zone	talc zone	talc zone	hostrock	hostrock	hostrock	hostrock	hostrock	hostrock
wt%																	
SiO_2	2.25	9.34	3.95	8.04	0.18	0.28	0.17	0.68	1.56	3.18	5.23	75.24	74.84	75.99	69.43	75.57	74.76
Al_2O_3	0.09	0.07	0.04	0.09	0.1	0.08	0.09	0.03	0.16	0.36	0.2	14.82	13.68	12.56	14.9	13.48	13.33
Fe_2O_3(T)	5.66	6.12	6.95	4.05	5.21	2.3	5.17	3.03	1.28	2.64	2.53	1.15	1.21	1.22	0.92	1.48	1.17
MnO	0.288	0.274	0.301	0.205	0.313	0.158	0.306	0.195	0.113	0.16	0.176	0.046	0.017	0.039	0.01	0.052	0.017
MgO	42.64	40.6	41.95	40.44	26.87	20.26	24.34	19.19	20.68	19.22	19.39	0.55	0.42	0.94	4.87	0.08	0.18
CaO	0.74	1.12	0.46	3.65	18.73	29.53	23.7	29.7	29.9	28.71	28.28	0.64	0.39	1.31	0.68	0.34	0.44
Na_2O	0.05	0.04	0.05	0.05	0.03	0.05	0.04	0.04	0.09	0.17	0.11	3.19	4.34	1.62	0.19	3.49	3.52
K_2O	0.01	< 0.01	< 0.01	0.01	0.02	0.02	0.01	< 0.01	0.03	0.07	0.04	3.51	2.07	3.59	4.87	4.83	4.65
TiO_2	0.012	0.003	0.002	0.004	0.006	0.005	0.003	0.001	< 0.001	0.006	0.001	0.028	0.073	0.072	0.027	0.061	0.062
P_2O_5	0.05	0.08	0.01	0.05	0.02	0.01	< 0.01	0.04	< 0.01	0.02	< 0.01	0.41	0.24	0.24	0.49	0.26	0.25
LOI	48.5	42.68	46.92	44.11	47.15	46.06	46.69	46.11	46.23	44.84	44.07	0.85	1.11	2.55	3.35	0.9	0.78
Total	100.3	100.3	100.6	100.7	98.63	98.76	100.5	99.03	100.1	99.38	100	100.4	98.39	100.1	99.72	100.5	99.15
ppm																	
Sc	1	3	< 1	2	< 1	< 1	< 1	8	2	10	2	7	4	3	6	4	3
Be	< 1	< 1	< 1	< 1	< 1	< 1	< 1	< 1	< 1	< 1	< 1	3	3	7	5	8	3
V	< 5	< 5	5	< 5	< 5	< 5	< 5	12	5	7	8	< 5	6	8	6	6	7
Cr	< 20	< 20	< 20	< 20	< 20	< 20	< 20	< 20	< 20	< 20	< 20	< 20	< 20	< 20	< 20	< 20	< 20
Co	2	1	3	2	< 1	3	< 1	< 1	< 1	< 1	< 1	< 1	< 1	< 1	< 1	< 1	< 1
Ni	< 20	< 20	< 20	< 20	< 20	< 20	< 20	< 20	< 20	< 20	< 20	< 20	< 20	< 20	< 20	< 20	< 20
Cu	< 10	< 10	< 10	< 10	< 10	< 10	< 10	< 10	< 10	< 10	< 10	< 10	< 10	< 10	< 10	< 10	< 10
Zn	< 30	< 30	< 30	< 30	< 30	< 30	< 30	< 30	< 30	< 30	< 30	50	40	< 30	< 30	50	30
Ga	< 1	< 1	< 1	< 1	< 1	< 1	< 1	< 1	< 1	< 1	< 1	37	28	23	41	25	24
Ge	< 0.5	1.3	< 0.5	1.1	< 0.5	< 0.5	< 0.5	< 0.5	< 0.5	< 0.5	< 0.5	3.8	3.1	2.8	3.6	3.3	2.5
As	< 5	< 5	< 5	< 5	< 5	19	< 5	< 5	< 5	< 5	< 5	< 5	23	< 5	< 5	11	20
Rb	< 1	< 1	< 1	< 1	< 1	< 1	< 1	< 1	< 1	2	< 1	> 1000	469	542	> 1000	781	562
Sr	17	9	5	24	176	120	220	53	68	77	60	20	12	15	10	14	14
Y	5.6	4.2	7.7	4.2	4.4	4.4	5.4	122	25	48.7	24.9	4.2	12.8	13.6	4.1	13.6	15.6
Zr	4	2	< 1	1	1	1	< 1	< 1	< 1	2	< 1	26	57	54	34	45	48
Nb	7.1	< 0.2	< 0.2	< 0.2	< 0.2	< 0.2	< 0.2	< 0.2	< 0.2	< 0.2	< 0.2	45.3	16.3	15.5	61	14.3	14.3
Mo	< 2	< 2	< 2	< 2	< 2	< 2	< 2	< 2	< 2	< 2	< 2	< 2	< 2	< 2	< 2	< 2	< 2
Ag	< 0.5	< 0.5	< 0.5	< 0.5	< 0.5	< 0.5	< 0.5	< 0.5	< 0.5	< 0.5	< 0.5	< 0.5	0.5	< 0.5	< 0.5	< 0.5	< 0.5
In	< 0.1	< 0.1	0.1	< 0.1	< 0.1	< 0.1	< 0.1	0.1	< 0.1	0.2	0.1	0.1	< 0.1	< 0.1	< 0.1	< 0.1	< 0.1
Sn	< 1	< 1	< 1	2	< 1	< 1	< 1	< 1	< 1	< 1	< 1	110	59	48	94	43	68
Sb	< 0.2	0.5	< 0.2	0.3	< 0.2	< 0.2	< 0.2	< 0.2	0.4	1.1	0.2	2.7	0.6	0.9	1.2	1.2	1.1
Cs	1.6	1.1	1.2	1.8	0.2	0.5	0.1	1.4	1.3	1.8	1.4	30.7	23.7	29.1	111	55.4	17.9
Ba	35	< 3	< 3	< 3	5	4	4	< 3	< 3	6	3	33	37	54	107	28	73
Hf	< 0.1	< 0.1	< 0.1	< 0.1	< 0.1	< 0.1	< 0.1	0.2	< 0.1	0.1	< 0.1	1.7	2.5	2.3	2.7	2	2
Ta	0.05	< 0.01	< 0.01	< 0.01	< 0.01	< 0.01	< 0.01	< 0.01	< 0.01	< 0.01	< 0.01	13	5.66	6.08	22.8	6.73	6.68
W	2.8	< 0.5	< 0.5	< 0.5	< 0.5	< 0.5	< 0.5	< 0.5	< 0.5	< 0.5	0.6	21.2	10	18.4	23.1	16.3	5.5
Tl	< 0.05	< 0.05	< 0.05	< 0.05	< 0.05	< 0.05	< 0.05	< 0.05	< 0.05	< 0.05	< 0.05	4.05	1.48	1.59	4.17	4.05	2.44
Pb	6	< 5	< 5	< 5	< 5	< 5	< 5	< 5	< 5	5	< 5	6	< 5	< 5	< 5	12	11
Bi	0.4	0.9	< 0.1	0.1	0.3	0.2	0.3	< 0.1	0.1	0.1	0.2	90.2	2	3.3	1.2	17.1	4.7
Th	0.65	0.25	0.08	0.16	0.24	0.23	0.11	< 0.05	< 0.05	0.2	< 0.05	8.12	10.5	9.13	11.1	7.75	10.2
U	0.61	1.06	0.35	0.96	0.21	0.13	0.09	0.17	0.01	0.1	0.07	21.7	21.7	22.2	21.5	17.7	19.2
La	10.6	0.33	0.33	0.71	1.67	5.13	1.98	1.88	1.38	2.92	2.58	0.73	5.36	5.37	0.67	4.46	6.67
Ce	18.2	0.79	1.03	1.84	3.78	11.8	4.57	6.1	4.04	6.38	5.76	2.43	12.6	12.7	2.3	10.6	14.9
Pr	1.81	0.15	0.22	0.36	0.55	1.5	0.64	1.05	0.71	0.85	0.66	0.36	1.5	1.49	0.35	1.27	1.74
Nd	6.29	0.88	1.54	2.14	2.85	6.75	3.47	6.23	4.44	4.39	2.68	1.39	5.64	5.6	1.6	4.94	6.3
Sm	1.19	0.52	1.1	1.09	0.95	2.05	1.42	5.09	3.01	3.26	1.94	0.78	1.71	1.8	0.82	1.68	1.94
Eu	0.383	0.296	0.35	0.624	0.732	1.03	1.05	2.33	1.4	1.68	0.877	0.044	0.061	0.085	0.277	0.047	0.064
Gd	1.11	0.69	1.37	1.1	0.94	1.56	1.43	17.4	4.52	7.06	4.19	0.64	1.59	1.68	0.75	1.64	1.78
Tb	0.18	0.13	0.24	0.15	0.13	0.2	0.2	3.7	0.87	1.4	0.9	0.14	0.39	0.4	0.14	0.39	0.43
Dy	1.09	0.76	1.55	0.76	0.68	0.94	0.96	24.7	5.43	8.9	5.65	0.88	2.58	2.64	0.82	2.65	2.93
Ho	0.2	0.14	0.31	0.13	0.12	0.15	0.15	4.63	0.99	1.73	0.99	0.12	0.46	0.49	0.13	0.47	0.53
Er	0.62	0.45	0.88	0.34	0.3	0.36	0.37	12.4	2.61	4.77	2.58	0.33	1.36	1.42	0.34	1.36	1.57
Tm	0.105	0.083	0.143	0.05	0.038	0.044	0.046	1.69	0.364	0.692	0.352	0.065	0.237	0.237	0.062	0.233	0.262
Yb	0.75	0.6	1.02	0.36	0.21	0.26	0.28	9.91	2.25	4.33	1.95	0.48	1.54	1.62	0.41	1.61	1.81
Lu	0.11	0.106	0.165	0.053	0.031	0.038	0.046	1.37	0.339	0.642	0.269	0.064	0.225	0.226	0.063	0.222	0.252

Sample	SM 9	SM 10	SM 11	SM 12	SM 17	SM 19	SM 22	SM 23	SM 52	SM 20b	SM 20a	SM 41	SM 51	SM 50
Rocktype	cc	dolM	dolM	ccM	ccM	dolM	dolM	ccM	dolM	granite	granite	granite	granite	granite
remarks	talc zone	hostrock	hostrock	hostrock	hostrock	hostrock	talc zone	talc zone	hostrock	chloritised	non-chl.	chloritised	chloritised	chloritised
deposit	Sa Matta	Sa Matta	Sa Matta	Sa Matta	Sa Matta	Sa Matta	Sa Matta	Sa Matta	Sa Matta	Sa Matta	Sa Matta	Sa Matta	Sa Matta	Sa Matta
wt%														
SiO_2	0.76	1.38	3.46	2.59	12.3	7.42	2.79	0.73	4.8	72.83	71.95	74.32	75.43	46.83
Al_2O_3	0.09	0.58	0.71	0.84	5.03	2.86	0.53	0.08	1.92	14.03	13.36	13.79	12.75	13.92
Fe_2O_3(T)	0.14	0.7	0.85	0.47	1.97	1.14	0.71	0.09	2.19	2.28	0.86	2.19	0.87	3.81
MnO	0.059	0.073	0.083	0.016	0.077	0.042	0.053	0.104	0.113	0.029	0.01	0.024	0.016	0.028
MgO	0.86	21.61	19.16	1.19	1.28	22.8	21.73	0.95	21.27	0.47	0.54	0.42	0.29	22.4
CaO	54.58	29.32	32.09	52.93	44.24	25.02	28.37	54.18	26.29	2.04	3.5	1.9	0.53	1.26
Na_2O	0.04	0.04	0.06	0.03	0.21	0.03	0.05	0.03	0.06	3.17	0.46	2.87	4.15	0.07
K_2O	0.02	0.01	0.02	0.03	1.33	0.01	0.02	0.01	0.02	3.61	5.37	4.04	3.43	0.04
TiO_2	< 0.001	0.033	0.035	0.039	0.263	0.128	0.029	0.001	0.096	0.241	0.2	0.193	0.075	0.187
P_2O_5	0.01	0.03	0.03	0.05	0.08	0.08	0.03	0.01	0.07	0.06	0.06	0.04	0.14	0.71
LOI	43.61	46.01	44.11	42.03	33.23	40.16	45.11	43.59	42.24	1.14	4.21	0.59	0.78	10.84
Total	100.2	99.79	100.6	100.2	100	99.7	99.42	99.78	99.08	99.89	100.5	100.4	98.47	100.1
ppm														
Sc	28	2	3	2	5	4	2	4	3	4	3	3	2	4
Be	< 1	< 1	< 1	< 1	1	< 1	< 1	< 1	< 1	< 1	< 1	1	2	7
V	< 5	6	9	9	37	26	7	5	21	21	17	20	8	16
Cr	< 20	< 20	< 20	< 20	20	< 20	< 20	< 20	< 20	< 20	< 20	< 20	< 20	< 20
Co	< 1	< 1	< 1	< 1	4	< 1	< 1	< 1	< 1	2	< 1	2	< 1	3
Ni	< 20	< 20	< 20	< 20	20	20	< 20	< 20	< 20	< 20	< 20	< 20	< 20	< 20
Cu	< 10	< 10	< 10	< 10	30	< 10	< 10	< 10	< 10	< 10	< 10	< 10	< 10	< 10
Zn	< 30	< 30	< 30	< 30	30	< 30	< 30	< 30	< 30	< 30	< 30	40	< 30	< 30
Ga	< 1	1	1	1	6	4	1	< 1	3	15	15	16	15	19
Ge	< 0.5	< 0.5	< 0.5	< 0.5	< 0.5	< 0.5	< 0.5	< 0.5	0.8	1.3	1.2	1.6	1.6	1.5
As	< 5	< 5	< 5	< 5	< 5	< 5	< 5	< 5	< 5	< 5	< 5	< 5	< 5	< 5
Rb	< 1	< 1	< 1	< 1	43	< 1	< 1	< 1	< 1	69	116	86	112	< 1
Sr	98	25	41	171	207	11	17	176	32	172	33	128	64	3
Y	194	7.8	15.8	5.4	14.6	11.2	12.4	105	14.8	10	8.9	7.4	4	13.9
Zr	6	5	6	39	50	25	5	< 1	21	150	139	135	39	62
Nb	< 0.2	0.6	0.7	0.9	7.2	3.5	0.6	< 0.2	3.4	5.9	4.8	6.8	5.6	28.2
Mo	< 2	< 2	< 2	< 2	< 2	< 2	< 2	< 2	< 2	< 2	< 2	< 2	< 2	< 2
Ag	< 0.5	< 0.5	< 0.5	< 0.5	< 0.5	< 0.5	< 0.5	< 0.5	< 0.5	1.7	1.1	1.2	< 0.5	0.6
In	< 0.1	< 0.1	< 0.1	< 0.1	< 0.1	< 0.1	< 0.1	< 0.1	< 0.1	< 0.1	< 0.1	< 0.1	< 0.1	< 0.1
Sn	< 1	< 1	< 1	< 1	1	1	< 1	< 1	< 1	3	3	2	4	6
Sb	< 0.2	< 0.2	< 0.2	< 0.2	< 0.2	< 0.2	< 0.2	< 0.2	< 0.2	< 0.2	< 0.2	< 0.2	< 0.2	< 0.2
Cs	< 0.1	< 0.1	< 0.1	< 0.1	2.5	0.2	< 0.1	< 0.1	< 0.1	2.2	1.2	3.1	2.4	1.2
Ba	< 3	< 3	5	8	112	< 3	< 3	< 3	< 3	974	655	999	185	< 3
Hf	0.4	0.1	0.2	0.9	1.3	0.7	0.1	0.1	0.5	4	3.7	3.6	1.2	2.2
Ta	< 0.01	0.04	0.04	0.06	0.55	0.24	0.02	< 0.01	0.16	0.52	0.4	0.57	0.9	11.1
W	< 0.5	< 0.5	0.6	< 0.5	< 0.5	2.7	< 0.5	< 0.5	< 0.5	< 0.5	< 0.5	< 0.5	< 0.5	< 0.5
Tl	< 0.05	< 0.05	< 0.05	< 0.05	0.12	< 0.05	< 0.05	< 0.05	< 0.05	0.38	0.32	0.42	0.59	< 0.05
Pb	< 5	< 5	< 5	< 5	13	< 5	< 5	< 5	< 5	23	7	20	17	< 5
Bi	< 0.1	< 0.1	< 0.1	< 0.1	0.5	< 0.1	< 0.1	< 0.1	< 0.1	1.1	< 0.1	1.5	0.3	< 0.1
Th	< 0.05	0.7	0.64	0.96	5.76	3.49	0.73	< 0.05	2.01	16	13.8	22.2	3.87	25.1
U	0.04	0.1	0.19	0.2	0.76	0.38	0.11	0.1	0.16	2.42	1.86	2.78	1.05	2.09
La	16	10.2	7.69	0.64	19.8	3.1	7.93	3.05	13.7	49.7	46.2	54.1	7.69	4.33
Ce	55.3	25.4	21.2	1.19	31.7	9.32	21.3	10	23	88.1	82.3	95.1	14.7	14
Pr	9.21	3.51	3.16	0.25	4.08	1.46	3.14	1.8	2.81	9.45	8.67	9.94	1.75	2.24
Nd	49.9	15	15.7	1.38	16.2	7.2	15.2	11.1	11.6	33.1	30.8	35.2	6.82	10.9
Sm	17.6	3.24	4.07	0.48	3.37	2.07	4.17	6.74	2.33	4.75	4.59	5.15	1.65	3.7
Eu	2	0.939	0.825	0.096	0.647	0.536	0.511	1.01	0.524	0.953	0.926	0.925	0.346	0.437
Gd	20.5	2.5	3.75	0.62	2.94	2.12	3.59	11.4	2.3	3.13	2.57	3.13	1.36	3.64
Tb	3.91	0.32	0.56	0.11	0.45	0.34	0.52	2.5	0.34	0.38	0.34	0.36	0.18	0.58
Dy	26.6	1.64	3.03	0.72	2.54	2.03	2.81	16.9	1.92	2.08	1.83	1.74	0.87	2.94
Ho	5.99	0.28	0.54	0.16	0.48	0.38	0.48	3.39	0.4	0.38	0.35	0.27	0.14	0.45
Er	19.4	0.8	1.54	0.48	1.39	1.07	1.2	9.92	1.11	1.15	1.08	0.71	0.41	1.19
Tm	3.36	0.105	0.212	0.077	0.204	0.155	0.151	1.62	0.155	0.17	0.168	0.098	0.062	0.17
Yb	23.3	0.66	1.35	0.48	1.24	1.1	0.89	10.4	0.94	1.11	1.14	0.63	0.44	1.11
Lu	4.01	0.106	0.211	0.082	0.195	0.171	0.132	1.47	0.16	0.197	0.194	0.115	0.075	0.188

Sample	SV 1	SV 2	SV 3	SV 4	SV 5	SV 14	SV 9	SV 11
Rocktype	ccM	ccM	ccM	ccM	ccM	cc	granite	granite
remarks	hostrock	hostrock	gostrock	hostrock	hostrock	talc zone	non-chl	chloritised
deposit	Su Venosu	Su Venosu	Su Venosu	Su Venosu	Su Venosu	Su Venosu	Su Venosu	Su Venosu
wt%								
SiO_2	1.25	1.04	1.71	0.38	0.28	0.22	63.65	62.83
Al_2O_3	0.56	0.46	0.09	0.17	0.1	< 0.01	13.01	17.21
Fe_2O_3(T)	0.35	0.27	0.05	0.09	0.06	0.13	5.17	5.6
MnO	0.015	0.016	0.012	0.013	0.016	0.079	0.049	0.107
MgO	1.29	1.08	0.44	0.58	0.43	0.24	6.68	1.6
CaO	53.2	53.82	55.1	54.68	55.97	54.97	1.5	3.76
Na_2O	0.05	0.01	0.04	0.02	0.02	0.01	3.73	3.84
K_2O	0.04	0.02	0.02	0.03	0.01	< 0.01	0.09	2.84
TiO_2	0.025	0.024	0.002	0.008	0.003	< 0.001	0.471	0.654
P_2O_5	0.04	0.03	< 0.01	0.02	0.01	0.01	0.18	0.25
LOI	43.01	43.24	43.22	43.68	43.77	43.97	4.13	1.08
Total	99.83	100	100.7	99.67	100.7	99.63	98.65	99.76
ppm								
Sc	1	1	< 1	< 1	< 1	32	13	12
Be	< 1	< 1	< 1	< 1	< 1	< 1	13	3
V	19	21	< 5	7	7	< 5	70	80
Cr	< 20	< 20	< 20	< 20	< 20	< 20	< 20	< 20
Co	< 1	< 1	< 1	< 1	< 1	< 1	7	8
Ni	< 20	20	< 20	< 20	< 20	< 20	< 20	< 20
Cu	< 10	< 10	< 10	< 10	< 10	< 10	< 10	< 10
Zn	< 30	< 30	< 30	< 30	< 30	< 30	< 30	90
Ga	< 1	< 1	< 1	< 1	< 1	< 1	25	24
Ge	< 0.5	< 0.5	< 0.5	< 0.5	< 0.5	< 0.5	1.6	1.7
As	< 5	< 5	< 5	< 5	< 5	< 5	< 5	< 5
Rb	< 1	< 1	< 1	< 1	< 1	< 1	3	133
Sr	182	258	133	139	135	164	62	226
Y	11.5	11.3	4.5	5.5	5.8	142	117	24.8
Zr	5	5	< 1	1	< 1	< 1	167	180
Nb	0.6	0.6	< 0.2	< 0.2	< 0.2	< 0.2	8.8	11.1
Mo	< 2	< 2	< 2	< 2	< 2	< 2	< 2	< 2
Ag	< 0.5	< 0.5	< 0.5	< 0.5	< 0.5	< 0.5	1.6	1
In	< 0.1	< 0.1	< 0.1	< 0.1	< 0.1	< 0.1	< 0.1	< 0.1
Sn	< 1	< 1	< 1	< 1	< 1	< 1	3	6
Sb	< 0.2	< 0.2	< 0.2	< 0.2	< 0.2	< 0.2	< 0.2	0.6
Cs	< 0.1	< 0.1	< 0.1	< 0.1	< 0.1	< 0.1	0.7	6.6
Ba	4	6	5	5	5	< 3	13	518
Hf	0.1	0.1	< 0.1	< 0.1	< 0.1	0.2	4.6	5
Ta	0.03	0.02	< 0.01	< 0.01	< 0.01	< 0.01	0.73	1.13
W	< 0.5	< 0.5	< 0.5	< 0.5	< 0.5	< 0.5	< 0.5	0.8
Tl	< 0.05	< 0.05	< 0.05	< 0.05	< 0.05	< 0.05	0.24	0.8
Pb	< 5	< 5	< 5	< 5	< 5	< 5	< 5	20
Bi	< 0.1	< 0.1	< 0.1	< 0.1	< 0.1	< 0.1	0.1	1.2
Th	1.01	0.97	0.11	0.31	0.18	< 0.05	13.2	20.7
U	4.11	3.37	0.18	0.52	0.44	0.01	8.65	5.58
La	11.9	10.9	2.67	3.1	1.86	19.7	60.1	66.2
Ce	11.6	13.7	2.19	3.33	2.03	67.5	108	126
Pr	2.22	2.33	0.52	0.71	0.49	11.7	12.8	14.3
Nd	9.49	9.62	2.42	3.42	2.63	68.3	53.1	53
Sm	1.93	1.94	0.53	0.8	0.73	23	15.3	9.53
Eu	0.36	0.328	0.108	0.153	0.127	1.94	4.19	1.27
Gd	1.91	1.78	0.62	0.79	0.9	25.9	19.8	6.54
Tb	0.27	0.27	0.09	0.12	0.12	3.5	3.34	0.89
Dy	1.66	1.62	0.56	0.73	0.71	19	20.7	4.75
Ho	0.32	0.33	0.12	0.14	0.16	3.67	3.91	0.86
Er	0.91	0.93	0.32	0.41	0.44	10.5	9.72	2.31
Tm	0.122	0.126	0.042	0.058	0.062	1.54	1.08	0.335
Yb	0.75	0.74	0.27	0.33	0.37	10.3	5.68	2.37
Lu	0.108	0.117	0.051	0.051	0.059	2.15	0.801	0.406

Appendix B

Stable Isotopes

Sample	Deposit	Mineral	$\delta^{18}O_{VSMOW}$	$\delta^{13}C_{VPDB}$	remarks
VE 1 a	Veitsch	dol	13.64	-1.68	vein
VE 1 b	Veitsch	mgs	15.82	-4.72	red
VE 1 c	Veitsch	dol	14.14	-2.38	vein
VE 1 d	Veitsch	mgs	15.82	-4.52	red
VE 1 e	Veitsch	mgs	15.53	-3.93	red
VE 2a a	Veitsch	mgs	19.98	-5.42	red
VE 2a b	Veitsch	dol	16.97	-5.83	vein
VE 2b a	Veitsch	mgs	15.55	-2.84	red
VE 2b b	Veitsch	mgs	20.16	-2.81	red
VE 2b c	Veitsch	dol	14.56	-2.26	vein
VE 2b d	Veitsch	dol	13.67	-2.21	vein
VE 2b e	Veitsch	dol	13.72	-3.09	vein
VE 4 a	Veitsch	dol	13.72	-1.93	vein
VE 4 b	Veitsch	mgs	17.97	-4.99	red
VE 5 a	Veitsch	mgs	13.30	-2.29	red
VE 5 b	Veitsch	dol	13.04	-2.02	vein
VE 5 c	Veitsch	dol	15.19	-3.11	vein
VE 5 d	Veitsch	dol	15.12	-3.32	vein
VE 6 a	Veitsch	mgs	16.92	-2.93	red
VE 6 b	Veitsch	dol	13.63	-2.12	vein
VE 6 c	Veitsch	dol	13.55	-1.84	vein
VE 6 e	Veitsch	dol	15.98	-2.12	vein
VE 6 f	Veitsch	dol	13.87	-2.01	vein
VE 6 g	Veitsch	mgs	15.81	-3.12	red
VE 7 a	Veitsch	dol	14.19	-5.30	grey, marble
VE 8 a	Veitsch	dol	13.46	-6.33	grey, marble
VE 8 b	Veitsch	dol	13.59	-6.80	grey, marble
VE 9 a	Veitsch	dol	14.41	-7.00	grey, marble
VE 10 a	Veitsch	dol	27.21	-3.59	coral
VE 10 b	Veitsch	dol	27.44	-3.37	coral
VE 14 a	Veitsch	dol	25.46	-5.29	grey, marble
VE 14 b	Veitsch	dol	28.22	-2.61	grey, marble
VE 14 c	Veitsch	mgs	26.74	-4.04	red
VE 14c	Veitsch	mgs	14.72	-4.40	red
VE 14a	Veitsch	dol	14.13	-5.55	grey, marble
VE 14b	Veitsch	dol	15.58	-4.89	grey, marble
VE 1 f	Veitsch	qtz	14.95		vein
VE 4 c	Veitsch	qtz	15.22		vein
VE 5 e	Veitsch	qtz	15.42		vein
VE 7 b	Veitsch	qtz	14.70		vein
VE 9 b	Veitsch	qtz	15.21		vein

Sample	Deposit	Mineral	$\delta^{18}O_{VSMOW}$	$\delta^{13}C_{VPDB}$	remarks
LA 2 a	Lassing	cc	26.64	4.20	marble
LA 3 a	Lassing	cc	19.60	1.48	marble
LA 4 a	Lassing	cc	16.67	0.41	marble
LA 8 a	Lassing	cc	20.42	0.92	marble
LA 9 a	Lassing	cc	14.13	-1.11	marble
LA 10 a	Lassing	cc	14.10	-0.88	marble
LA 11 a	Lassing	cc	15.40	0.68	vein
LA 12 a	Lassing	cc	19.79	-0.02	marble
LA PR 48	Lassing inside	dol	13.53	-1.12	marble
LA PR 33	Lassing inside	mgs	15.40	-0.32	
LA PR 65	Lassing inside	dol	13.66	-1.24	marble
LA PR 101	Lassing inside	dol	15.92	0.72	marble
LA PR 85	Lassing inside	dol	15.88	0.71	marble
LA PR 31	Lassing inside	dol	15.72	1.57	marble
LA 1 b	Lassing inside	qtz	16.20		vein
LA 4 b	Lassing inside	qtz	17.84		vein
LA 5	Lassing inside	qtz	16.56		vein
LA 6	Lassing inside	qtz	16.84		vein
WS 1 a	Wald	dol	11.64	-2.98	vein
WS 3 a	Wald	mgs	12.86	-2.08	containing talc
WS 12 a	Wald	mgs	20.47	-12.88	containing talc
WS 2 a	Wald	mgs	12.18	-2.38	no talc
WS 4 a	Wald	mgs	12.44	-2.26	no talc
WS 9b a	Wald	mgs	12.89		close to shearzone
WS 9b b	Wald	mgs	12.87	-3.42	close to shearzone
WS 9c a	Wald	mgs	15.30	-2.95	close to shearzone
WS 9c b	Wald	mgs	15.03	-3.92	close to shearzone
WS 11 a	Wald	mgs	13.48	-3.08	containing talc
WS 20 a	Wald	mgs	12.92	-3.09	containing talc
WS 21 a	Wald	mgs	12.51	-3.11	containing talc
WS 10b a	Wald	mgs	12.22	-3.37	close to shearzone
WS 10b b	Wald	mgs	12.24	-3.38	close to shearzone
WS 23 a	Wald	mgs	12.78	-1.73	no talc
WS 23 b	Wald	mgs	12.82	-2.05	no talc
SU 1	hostrock	cc marble	27.25	1.73	hostrock
SU 2	hostrock	cc marble	28.47	2.05	hostrock
WS 7 a	hostrock	dol marble	20.46	-0.17	hostrock
WS 8 a	hostrock	dol marble	17.34	-1.13	hostrock

Sample	Deposit	Mineral	$\delta^{18}O_{VSMOW}$	$\delta^{13}C_{VPDB}$	remarks
GP 9 a	Gemerska Poloma	sec. dol	12.87	-4.84	talc zone
GP 9 b	Gemerska Poloma	sec. dol	12.81	-4.97	talc zone
GP 9 c	Gemerska Poloma	sec. dol	12.95	-4.83	talc zone
GP 9 d	Gemerska Poloma	sec. dol	12.78	-4.84	talc zone
GP 14 a	Gemerska Poloma	mgs	14.46	-3.48	hostrock
GP 16 b	Gemerska Poloma	mgs	16.34	-1.23	hostrock
GP 16 c	Gemerska Poloma	mgs	16.21	-1.74	hostrock
GP 16 d	Gemerska Poloma	mgs	16.54	-1.99	hostrock
GP 18 a	Gemerska Poloma	sec. dol	12.94	-6.35	talc zone
GP 39 a	Gemerska Poloma	sec. dol	12.66	-5.17	talc zone
GP 39 b	Gemerska Poloma	sec. dol	12.69	-5.50	talc zone
GP 39 c	Gemerska Poloma	sec. dol	12.75	-5.10	talc zone
GP 40 a	Gemerska Poloma	sec. dol	13.44	-3.67	talc zone
GP 40 b	Gemerska Poloma	sec. dol	12.26	-3.82	talc zone
GP 40 c	Gemerska Poloma	mgs	14.52	-3.20	hostrock
GP 40 d	Gemerska Poloma	mgs	13.28	-4.45	hostrock
GP 41 a	Gemerska Poloma	mgs	13.19	-3.07	hostrock
GP 41 b	Gemerska Poloma	mgs	13.30	-3.00	hostrock
GP 41 c	Gemerska Poloma	mgs	13.46	-3.01	hostrock
GP 46 a	Gemerska Poloma	sec. dol	13.15	-4.33	talc zone
GP 46 b	Gemerska Poloma	sec. dol	12.59	-4.30	talc zone
GP 46 c	Gemerska Poloma	sec. dol	12.92	-4.54	talc zone
GP 17 a	Gemerska Poloma	sec. dol	13.06	-5.72	talc zone
GP 55I a	Gemerska Poloma	sec. dol	12.90	-5.47	talc zone
GP 55II a	Gemerska Poloma	sec. dol	12.93	-5.73	talc zone
GP 55III a	Gemerska Poloma	mgs	15.01	-2.46	hostrock
GP 42 a	Gemerska Poloma	sec. dol	13.01	-5.83	talc zone
GP1mgs	Gemerska Poloma	mgs	13.30	-5.51	hostrock
GP12mgs	Gemerska Poloma	mgs	12.78	-4.29	hostrock
GP11dol	Gemerska Poloma	sec. dol	13.28	-5.82	talc zone
GP9dol	Gemerska Poloma	sec. dol	13.12	-4.84	talc zone
GP10mgs	Gemerska Poloma	mgs	12.82	-4.70	hostrock
GP-31b	Gemerska Poloma	qtz	13.798		chlor. granite
GP-42 b	Gemerska Poloma	qtz	13.392		talc zone
GP-55	Gemerska Poloma	qtz	13.436		talc zone
GP-23	Gemerska Poloma	qtz	14.413		talc zone
GP-26	Gemerska Poloma	qtz	13.068		talc zone
GP-55	Gemerska Poloma	qtz	13.508		talc zone
GP-15	Gemerska Poloma	qtz	13.85		talc zone
GP-9	Gemerska Poloma	qtz	13.812		talc zone
GP-31 a	Gemerska Poloma	qtz	12.1		chlor. granite
GP-33 a	Gemerska Poloma	qtz	11.983		chlor. granite
GP-7 a	Gemerska Poloma	qtz	12.954		chlor. granite
GP-31 a	Gemerska Poloma	qtz	12.326		chlor. granite
GP-32 a	Gemerska Poloma	qtz	12.536		non-chlor. granite
GP-39	Gemerska Poloma	qtz	12.2285		talc zone

Sample	Deposit	Mineral	$\delta^{18}O_{VSMOW}$	$\delta^{13}C_{VPDB}$	remarks
SM9	Sa Matta	cc	7.46	-0.55	talc zone
SM10	Sa Matta	dol	8.22	0.30	marble, hostrock
SM11	Sa Matta	dol	7.88	-0.22	marble, hostrock
SM12	Sa Matta	cc	14.12	2.01	marble, hostrock
SM16	Sa Matta	cc	8.79	0.65	marble, hostrock
SM17	Sa Matta	cc	20.91	0.23	marble, hostrock
SM19	Sa Matta	dol	9.36	0.66	marble, hostrock
SM22	Sa Matta	dol	8.82	0.37	marble, talc zone
SM23	Sa Matta	cc	7.71	-1.10	marble, talc zone
SM25	Sa Matta	cc	6.34	-1.27	talc zone
SM26	Sa Matta	dol	6.68	1.07	marble, talc zone
SM28	Sa Matta	cc	6.98	0.32	marble, hostrock
SM52	Sa Matta	dol	9.33	-0.73	marble, hostrock
SV1	Su Venosu	cc	11.48	0.80	marble, hostrock
SV2h	Su Venosu	cc	8.68	-0.50	marble, hostrock
SV3	Su Venosu	cc	15.98	1.27	marble, hostrock
SV4	Su Venosu	cc	12.82	1.02	marble, hostrock
SV5	Su Venosu	cc	12.10	0.80	marble, hostrock
SV7	Su Venosu	cc	11.26	-9.52	talc zone
SV14	Su Venosu	cc	6.13	-9.41	talc zone
SM 20a	Sa Matta	qtz	9.437		non-chlor. granite
SM 33	Sa Matta	qtz	11.255		non-chlor. granite
SM 31	Sa Matta	qtz	10.197		chlor. granite
SM 20b	Sa Matta	qtz	10.911		chlor. granite
SM 44	Sa Matta	qtz	11.943		chlor. granite
SM 27	Sa Matta	qtz	8.095		talc zone
SM 48	Sa Matta	qtz	9.02		talc zone
SM 40 a	Sa Matta	qtz	3.756		with albit
SM 7 a	Sa Matta	qtz	4.529		with albit
SM 40 b	Sa Matta	alb	3.632		
SM 7 b	Sa Matta	alb	2.954		
SM 1	Sa Matta	qtz	14.551		with mica schist

Appendix C

Ion-chromatography

Sample	Mineral	Li	Na	K	Mg	Ca	F	Cl	Br	J	NO_3	SO_4	Na/Br	Cl/Br	Q+/Q-	remarks
unit		ppb	ppb	ppb	ppb	ppb	ppb	ppb	ppb	ppb	ppb	ppb	mol/mol	mol/mol		
Lassing																
LA2	cc	8.54	14739.79	647.44	4047.86	8911.67	3.27	29663.19	25.57	7.79	398.93	708.71	2003.66	2615.01	1.67	hostrock
LA4ges	cc	10.68	6621.17	606.65	4257.42	10174.54	2.66	17055.83	44.53	10.55	2061.85	422.96	516.81	863.37	2.22	hostrock
LA1a	dol	5.17	3260.38	355.99	18405.80	5639.04	8.17	7524.68	27.70	4.84	283.00	288.35	409.05	612.24	8.71	hostrock
LA1b	qtz	0.41	10745.65	1887.42	3172.13	1990.26	0.60	21258.79	68.93	6.50	n.a.	51.83	541.82	695.16	1.46	vein
LA3	cc	0.20	4613.56	439.73	3786.83	7215.85	2.99	8557.84	14.25	8.32	n.a.	227.54	1125.18	1353.55	3.58	hostrock
LA4a	qtz	0.40	10992.88	4019.72	2112.60	6401.80	1.59	25509.78	81.97	7.86	6.71	52.95	466.09	701.44	1.49	vein
LA4b	cc	2.63	10113.99	897.71	3479.64	11842.07	2.24	18944.35	47.62	8.61	n.a.	424.01	738.12	896.62	2.46	hostrock
LA5	qtz	0.17	5394.76	1798.79	363.55	2031.57	6.04	11389.06	60.61	5.07	1.98	50.21	309.33	423.50	1.27	vein
LA6	qtz	0.09	6451.89	1673.02	361.08	2191.82	32.21	12428.38	63.40	4.71	1731.78	40.95	353.67	441.83	1.21	vein
LA8	cc	0.93	7344.56	478.88	1224.84	9672.72	2.01	13831.75	20.90	6.46	n.a.	164.33	1221.33	1491.65	2.32	hostrock
LA11a	cc	0.17	6734.21	414.97	892.50	18666.55	23.86	13773.09	21.56	8.13	n.a.	434.95	1085.60	1439.92	3.23	vein
LA12	cc	1.22	6850.04	314.79	1618.18	11146.42	3.26	13177.18	15.77	4.66	n.a.	168.23	1509.38	1883.01	2.65	hostrock
LA9a	cc	1.40	5678.90	302.90	4125.68	9998.67	14.67	11771.86	17.95	7.02	n.a.	1266.78	1099.64	1478.28	3.04	hostrock
LA9b	cc	2.75	7842.61	406.40	3452.86	12272.10	11.50	18269.18	26.34	8.13	222.88	1355.31	1034.63	1563.03	2.28	hostrock
LAPR31	dol	12.09	4046.19	205.85	24752.35	11456.63	4.31	6994.40	59.14	8.12	n.a.	280.35	237.78	266.57	13.67	hostrock
LAPR33	mgs	16.64	4612.47	118.68	24531.44	8903.59	259.34	8700.17	89.15	6.54	n.a.	412.60	179.82	219.96	9.93	hostrock
LAPR48	dol	5.96	4476.76	187.98	24685.60	3575.84	5.79	8928.66	136.93	6.08	n.a.	164.67	113.62	146.97	9.37	hostrock
LAPR65	dol	3.38	3096.45	73.20	31742.08	9305.00	27.38	5468.88	24.35	6.43	n.a.	799.75	441.91	506.17	18.61	hostrock
LAPR85	dol	16.62	4794.93	135.22	22738.07	8007.96	3.25	9103.74	96.63	9.60	n.a.	290.21	172.46	212.35	9.40	hostrock
LAPR121	dol	1.14	3857.82	46.29	12150.07	5687.78	276.28	6963.30	14.00	6.19	n.a.	203.58	957.97	1121.37	6.74	hostrock
Veitsch																
VE2a	mgs	1.80	2945.78	183.45	21002.06	7022.65	12.17	4884.30	50.63	2.66	n.a.	505.66	202.20	217.43	14.79	hostrock
VE7a	dol	27.61	13898.30	740.64	25408.13	9203.67	1.25	24925.40	1191.27	3.64	n.a.	217.25	40.55	47.16	4.40	hostrock
VE9a	dol	28.25	10606.67	529.47	25034.25	9715.04	1.76	21263.02	816.25	3.42	n.a.	321.07	45.16	58.71	4.90	hostrock
VE14a	dol	25.63	6269.13	277.34	22689.40	9795.73	4.92	15982.99	433.98	3.32	n.a.	496.79	50.20	83.01	5.65	hostrock
VE14c	mgs	3.78	3707.35	160.04	20349.72	7198.21	10.20	8570.55	195.68	3.86	n.a.	840.15	65.84	98.72	8.39	hostrock
VE2b	dol	6.66	7789.85	336.38	21428.72	8950.31	4.47	13983.72	84.24	6.72	n.a.	214.47	321.36	374.12	6.39	vein
VE5c	mgs	15.73	7480.36	302.21	18100.02	8966.82	0.63	13545.93	114.75	6.95	n.a.	156.41	226.56	266.07	5.87	hostrock
VE5b	dol	15.53	12610.44	511.11	26263.21	10538.32	1.27	24613.28	108.01	7.62	n.a.	348.52	405.76	513.61	4.62	vein
VE5d	mgs	17.96	10677.42	461.00	22915.38	10160.86	1.05	19813.15	133.14	7.84	n.a.	261.37	278.72	335.42	5.07	hostrock
VE5a	mgs	1.60	5044.57	223.99	20179.85	4054.56	6.33	12128.75	222.00	4.63	208.04	232.55	78.97	123.14	5.91	hostrock
VE1f	qtz	0.25	3942.43	744.60	4540.35	2473.61	0.93	7078.67	121.93	10.22	n.a.	60.50	112.37	130.85	3.38	vein
VE5e	qtz	0.67	7261.25	2871.61	2822.29	1964.09	10.85	15952.18	88.97	6.59	n.a.	125.92	283.64	404.11	1.58	vein
VE7b	qtz	5.46	13645.28	3149.88	1390.53	5959.00	3.01	27156.88	157.08	6.07	n.a.	124.96	301.90	389.65	1.41	vein
VE9b	qtz	0.49	2364.39	456.49	356.46	1730.80	13.02	3066.82	29.69	2.34	704.00	72.33	276.80	232.84	2.19	vein
VE4c	qtz	2.22	7407.45	1800.56	670.74	2317.39	7.39	14737.94	142.18	4.36	n.a.	209.62	181.07	233.64	1.28	vein
Wald a. S.																
WS12	mgs	4.17	7986.24	790.60	23734.89	6074.61	4.86	17161.82	226.34	6.55	n.a.	128.69	122.63	170.90	5.36	containing talc
WS9ca	mgs	4.63	6962.52	748.98	29605.79	6236.83	4.51	13648.45	99.66	8.97	n.a.	131.11	242.81	308.68	7.89	close to shearzone
WS9cb	mgs	1.63	4552.28	516.72	20566.48	3890.85	5.50	8523.27	54.68	5.69	409.52	106.95	289.32	351.30	8.38	close to shearzone
WS10ba	mgs	3.42	7485.18	762.17	21538.94	2033.60	6.91	18353.29	304.59	4.28	129.02	82.21	85.41	135.81	4.22	close to shearzone
WS1	dol	32.88	8915.76	1205.18	20471.52	8892.07	1.09	19579.25	337.12	6.49	n.a.	76.41	91.91	130.90	4.57	vein
WS2	mgs	6.48	8760.58	832.88	26573.17	3199.42	5.79	29283.39	735.82	5.83	49.24	84.33	41.38	89.70	3.28	no talc
WS3	mgs	19.43	11189.30	1490.48	28713.58	2831.39	6.64	29178.69	649.04	5.38	n.a.	81.27	59.92	101.33	3.64	containing talc
WS4	mgs	4.34	9069.90	948.38	23312.01	1824.52	3.55	24165.24	544.94	6.33	n.a.	133.54	57.84	99.95	3.51	no talc
WS9bg	mgs	0.85	5139.45	598.76	20561.92	5514.44	44.46	10037.16	94.13	6.87	n.a.	67.53	189.75	240.32	7.66	close to shearzone
WS11	mgs	1.99	6320.77	749.24	21321.58	2181.09	6.60	12983.49	213.01	6.29	n.a.	64.44	103.13	137.38	5.82	containing talc
WS20	mgs	6.43	5992.93	605.11	23062.06	5178.61	16.43	12176.37	183.33	6.10	n.a.	97.61	113.61	149.70	6.98	containing talc
WS21	mgs	2.75	8548.37	817.55	24278.88	1949.71	5.82	21440.38	380.66	6.41	166.30	78.10	78.05	126.95	4.05	containing talc
WS23d	mgs	12.82	8379.18	1009.63	21435.26	1176.13	4.23	16961.15	341.17	5.50	n.a.	83.74	85.36	112.05	4.57	no talc
WS23h	mgs	7.40	7908.30	970.01	22608.17	1454.47	3.22	16383.65	321.03	5.64	111.13	110.80	85.61	115.02	4.89	no talc
hostrocks																
SU 1	cc	1.70	3048.42	522.28	4126.79	8965.10	259.19	5399.78	14.47	73.77	n.a.	6177.31	732.06	840.94	3.16	marble hostrock
SU 2	cc	2.98	3177.33	110.28	2269.54	9368.84	63.55	5666.94	11.58	10.59	n.a.	440.84	953.51	1102.90	4.61	marble hostrock
WS 7	dol	0.33	1419.72	87.98	20702.93	7471.85	4.71	1773.80	7.90	3.84	n.a.	89.67	624.93	506.36	40.95	marble hostrock
WS 8	dol	1.44	2589.64	125.39	22451.13	8309.67	7.80	4872.30	15.24	4.49	n.a.	206.25	590.53	720.54	16.71	marble hostrock

Sample unit	Mineral	Li ppb	Na ppb	K ppb	Mg ppb	Ca ppb	F ppb	Cl ppb	Br ppb	J ppb	NO_3 ppb	SO_4 ppb	Na/Br mol/mol	Cl/Br mol/mol	Q+/Q-	remarks
Gemerska																
Poloma																
GP16	mgs	225.90	15662.98	1906.00	22899.01	1727.05	17.64	35564.86	731.18	3.7	312.9	219.6	74.45	109.63	2.67	hostrock
GP6	mgs	122.99	11259.90	1288.33	22961.12	1454.57	9.21	26223.32	518.85	4.5	260.3	200.5	75.43	113.91	3.31	hostrock
GP10	mgs	293.28	17645.87	2160.75	23803.83	1193.88	10.73	41237.83	848.75	5.1	233.6	184.7	72.26	109.50	2.44	hostrock
GP12	mgs	379.42	16898.64	2133.55	25623.25	3415.98	10.94	37587.60	706.90	4.9	n.a.	192.2	83.09	119.84	2.91	hostrock
GP17	dol	367.89	19969.46	1934.98	20775.74	9932.33	0.85	41307.09	806.28	5.6	n.a.	123.6	86.08	115.47	2.70	talc zone
GP9	dol	420.76	17692.28	2358.72	19220.01	9557.03	0.18	35742.93	653.11	5.6	n.a.	72.2	94.15	123.34	2.90	talc zone
GP42a	dol	580.53	22858.50	3038.97	25148.90	10972.07	0.42	43687.60	716.86	6.0	n.a.	203.8	110.83	137.35	3.03	talc zone
GP39	dol	427.15	16738.52	1808.34	24585.77	9816.97	0.90	32823.36	583.68	5.1	n.a.	143.6	99.67	126.74	3.58	talc zone
GP31b	qtz	31.91	20479.42	2567.58	180.66	1339.63	21.07	30556.54	452.62	3.0	n.a.	69.4	157.26	152.15	1.20	talc zone
GP42b	qtz	14.42	21137.44	1684.40	381.34	1901.09	6.15	34212.57	516.20	0.4	n.a.	68.2	142.32	149.38	1.12	talc zone
GP9	qtz	9.61	12026.89	1248.88	3422.94	3125.92	43.12	22068.01	376.26	1.6	827	75.4	111.09	132.19	1.54	talc zone

Sample	Mineral	Li	Na	K	Mg	Ca	F	Cl	Br	J	NO_3	SO_4	Na/Br	Cl/Br	Q+/Q-	remarks
unit		ppb	ppb	ppb	ppb	ppb	ppb	ppb	ppb	ppb	ppb	ppb	mol/mol	mol/mol		
Sa Matta																
SM3	cc	0.3	1397.5	858.9	867.7	12295.4	17.5	4647.6	124.1	0.4	n.a.	248.9	39	84	5.533468742	marble, talc zone
SM6	alb	0.7	2253.0	1794.4	2172.0	11049.3	83.4	14334.8	607.2	0.2	n.a.	120.2	13	53	2.087077229	albite
SM9	scc	5.9	2626.2	1437.0	2298.1	15719.8	1.9	15759.5	761.9	0.5	n.a.	102.0	12	47	2.466448625	talc zone
SM10	dol	42.4	9615.0	2577.6	26583.4	16236.0	2.4	51174.9	2260.3	0.5	n.a.	130.1	15	51	2.365390879	marble, hostrock
SM11	cc	117.1	24017.9	6934.3	29668.0	16794.6	5.5	120497.8	4869.9	1.2	n.a.	125.5	17	56	1.304875811	marble, hostrock
SM16	cc	1.2	783.4	837.0	1985.3	7567.2	48.6	2580.5	80.3	0.2	n.a.	125.1	34	72	7.556558491	marble, hostrock
SM17	cc	4.6	1047.5	5198.3	1049.6	7802.5	43.2	1651.0	44.1	0.3	n.a.	2271.5	83	84	6.773499532	marble, hostrock
SM19	dol	37.9	8319.4	2732.5	21318.1	17872.5	5.1	43068.2	1930.8	0.5	n.a.	187.5	15	50	2.480264386	marble, hostrock
SM20a	qtz	6.0	4373.5	7670.3	1140.5	3729.1	182.3	12385.9	487.4	0.2	n.a.	278.0	31	57	1.799217722	non-chl granite
SM20b	qtz	4.0	6699.9	4267.7	1189.6	4410.4	56.7	14850.5	551.6	0.2	n.a.	191.1	42	61	1.661813864	chloritised granite
SM22	dol	43.2	10691.6	3271.9	30102.1	14575.2	0.1	56855.9	2477.8	0.6	n.a.	152.9	15	52	2.295216483	marble, talc zone
SM23	cc	2.9	2532.8	1065.4	3397.3	12992.1	0.8	17824.3	500.6	0.5	n.a.	137.1	18	80	2.08182581	marble, talc zone
SM25	scc	2.2	2732.2	1091.5	2754.1	11856.8	1.7	14786.9	707.4	0.2	n.a.	58.1	13	47	2.25962648	talc zone
SM26a	scc	4.6	3749.0	1179.0	2726.1	13711.7	0.5	20379.4	913.4	0.3	n.a.	71.2	14	50	1.875670067	talc zone
SM26b	dol	0.6	579.0	387.3	2251.0	7474.7	59.6	1365.1	41.1	0.1	n.a.	51.4	49	75	13.72856014	marble, hostrock
SM27	qtz	1.0	4825.2	1078.4	1928.7	13385.8	1.7	21949.1	916.9	0.4	n.a.	70.0	18	54	1.683695956	talc zone
SM28	cc	0.5	1551.5	444.0	1665.7	8334.9	43.1	6288.7	259.8	0.3	n.a.	147.7	21	55	3.397800388	marble, hostrock
SM29	qtz	6.5	3101.7	14347.3	15009.9	7909.6	115.4	6584.1	161.9	0.2	n.a.	24.1	67	92	10.97515525	chloritised granite
SM31	qtz	4.3	4723.1	13635.9	4659.1	4406.9	190.3	11405.4	338.6	0.5	n.a.	105.9	48	76	3.424708874	chloritised granite
SM33	qtz	9.1	7387.7	7897.8	735.7	2012.1	81.4	14390.7	476.7	0.6	n.a.	258.9	54	68	1.626375183	non-chl granite
SM35	dol	56.6	16148.6	4559.2	24604.4	16232.0	0.1	77486.4	3402.8	0.7	n.a.	133.1	16	51	1.64136042	marble, hostrock
SM44	qtz	9.2	10323.3	1120.7	5139.9	11194.3	89.8	32605.8	672.2	0.3	n.a.	151.8	53	109	1.560491241	chloritised granite
SM51	qtz	8.0	17309.9	7242.9	4532.5	6632.0	621.6	7325.8	36.5	0.1	n.a.	430.4	1650	453	6.605605218	chloritised granite
SM48	qtz	10.8	8491.6	1149.6	9820.1	13968.3	344.3	27119.6	156.2	0.3	n.a.	326.5	189	391	2.406405412	talc zone
SM52	dol	6.6	14336.2	1819.2	21208.3	13223.1	0.2	40187.7	245.1	0.4	n.a.	287.4	203	370	2.692176037	marble, hostrock
Su Venosu																
SV1	cc	5.5	2421.6	1140.7	1918.1	8942.3	70.5	7248.0	187.9	4.1	n.a.	177.0	45	87	3.451548686	marble, hostrock
SV2	cc	1.2	731.1	553.4	1330.1	8972.1	24.7	1837.1	40.3	1.5	n.a.	81.1	63	103	10.90565361	marble, hostrock
SV3	cc	3.2	1484.3	543.4	1147.5	9205.7	18.5	6315.6	191.6	1.8	n.a.	70.1	27	74	3.457937367	marble, hostrock
SV4	cc	0.3	491.6	371.0	917.0	7615.5	17.7	1005.3	36.9	0.8	n.a.	94.6	46	61	15.3323914	marble, talc zone
SV5	cc	0.3	612.4	365.6	853.6	8123.3	16.7	1315.5	44.1	0.7	n.a.	136.7	48	67	12.36130343	marble, talc zone
SV6	qtz	14.6	36567.4	5439.6	2388.9	37681.4	0.3	126632.7	3214.2	20.8	n.a.	93.2	40	89	1.053843192	talc zone
SV7a	cc	0.5	1226.6	653.9	538.4	10024.3	20.3	2715.3	57.4	0.8	n.a.	161.6	74	107	7.519680987	marble, talc zone
SV10	qtz	7.6	31819.3	4969.4	5354.9	45782.9	8.4	121484.5	2591.8	3.2	n.a.	245.2	43	106	1.223091383	talc zone
SV14	scc	0.1	739.5	502.8	432.9	8846.8	12.8	879.6	39.5	0.2	n.a.	40.4	65	50	19.46491058	talc zone

Appendix D

(U-Th)/He anaylsis

sample	mineral	4-He (mol)	238-U (mol)	235-U (mol)	232-Th (mol)	147-Sm (mol)	Uncorr. Age (Ma)	Ft	Alpa-corr Age (Ma)	Mean age	stdev.	remarks
SM $20a_1$	apatite	3.67E-14	1.11E-12	8.21E-15	3.97E-13	1.27E-12	23.5	0.746	31.5			non-chl granite
SM $20a_2$	apatite	2.31E-14	6.38E-13	4.72E-15	2.69E-13	8.17E-13	25.4	0.717	35.4			non-chl granite
SM $20a_3$	apatite	3.59E-15	2.91E-14	2.16E-16	1.21E-13	9.96E-13	44.9	0.809	55.5*	33.4	2.8	non-chl granite
SM $20b_2$	apatite	9.98E-14	3.02E-12	2.24E-14	1.68E-12	4.80E-12	22.5	0.828	27.1			chlor. granite
SM $20b_3$	apatite	3.65E-14	1.09E-12	8.09E-15	4.18E-13	1.58E-12	23.6	0.736	32.0			chlor. granite
SM $20b_4$	apatite	1.63E-14	5.91E-13	4.37E-15	1.98E-13	7.88E-13	19.7	0.724	27.2	28.8	2.8	chlor. granite
SM 50_1	apatite	1.86E-14	5.68E-13	4.20E-15	7.60E-13	3.36E-12	19.0	0.864	21.9			chlor. granite
SM 50_2	apatite	1.81E-14	4.65E-13	3.44E-15	3.87E-13	2.82E-12	24.7	0.836	29.5			chlor. granite
SM 50_3	apatite	3.79E-15	1.36E-13	1.01E-15	1.99E-13	1.10E-12	15.7	0.796	19.7	23.7	5.1	chlor. granite
SM 31_2	apatite	3.96E-14	1.10E-12	8.16E-15	1.53E-12	1.23E-12	21.0	0.702	29.9			chlor. granite
SM 31_3	apatite	1.65E-14	3.65E-13	2.70E-15	3.83E-13	6.57E-13	27.9	0.704	39.6	34.8	6.9	chlor. granite
SM 33_1	apatite	3.30E-14	7.55E-13	5.59E-15	8.23E-13	1.79E-12	26.8	0.787	34.0			non-chl granite
SM 33_2	apatite	1.83E-14	4.24E-13	3.14E-15	4.16E-13	1.27E-12	26.9	0.724	37.2			non-chl granite
SM 33_3	apatite	5.46E-14	1.20E-12	8.85E-15	1.39E-12	2.40E-12	27.6	0.746	37.0	36.1	1.8	non-chl granite
SM $20a_1$	zircon	2.732E-12	3.178E-11	2.350E-13	7.082E-12	n.a.	62.97	0.84	74.89			non-chl granite
SM $20a_2$	zircon	8.792E-13	9.575E-12	7.082E-14	7.085E-12	n.a.	60.53	0.822	73.56			non-chl granite
SM $20a_3$	zircon	1.699E-12	2.198E-11	1.626E-13	9.651E-12	n.a.	54.14	0.789	68.53	72.32	3.35	non-chl granite
SM $20b_1$	zircon	4.158E-13	5.247E-12	3.881E-14	3.753E-12	n.a.	52.53	0.745	70.40			chlor. granite
SM $20b_2$	zircon	3.243E-13	5.102E-12	3.774E-14	2.466E-12	n.a.	44.16	0.737	59.83			chlor. granite
SM $20b_3$	zircon	5.152E-13	6.072E-12	4.491E-14	4.601E-12	n.a.	55.76	0.74	75.23	68.49	7.88	chlor. granite
SM 31_1	zircon	6.956E-13	7.433E-12	5.498E-14	4.122E-12	n.a.	63.97	0.767	83.27			chlor. granite
SM 31_3	zircon	6.196E-13	8.176E-12	6.047E-14	4.459E-12	n.a.	51.95	0.764	67.91	75.59	10.86	chlor. granite
SM 33_4	zircon	7.019E-13	8.884E-12	6.571E-14	8.144E-12	n.a.	50.40	0.753	66.84			non-chl granite